UNIVERSITY OF CALIFORNIA, .SAN DIEGO

Dynamics and Plasticity of Central Vestibular Nerve Synapses

A dissertation submitted in partial satisfaction of the

requirements for the degree Doctor of Philosophy

in

Neurosciences

by

Lauren E. McElvain

Committee in charge:

Professor Sascha du Lac, Chair
Professor Anirvan Ghosh, Co-Chair
Professor Hollis T. Cline
Professor Timothy Q. Gentner
Professor Richard J. Krauzlis
Professor Massimo Scanziani

2011

The Dissertation of Lauren E. McElvain is approved, and it is acceptable in quality and form for publication on microfilm and electronically:

Co-Chair

Chair

University of California, San Diego

2011

Happy is he who gets to know the reasons for things.

- Virgil

Table of Contents

List of Figures and Tables

Chapter 1

Chapter 2

Chapter 3

Chapter 4

Acknowledgments

I would like to thank my mentor, Sascha, for her support, guidance, and enthusiasm throughout my graduate career. Her rigor and creativity have been an inspiration, and I have benefited greatly from her thoughtful, first-principles approach to neuroscience. I also have deeply appreciated her kindness and encouragement over the years.

I also would like to thank all past and present members of the du Lac lab for creating an intellectually exciting and friendly lab environment. In particular, I'd like to thank: Kristine Kolkman for thoughtful advice, support, endless optimism, and a shared love of circuits; Aryn Gittis for her perspective, wealth of technical expertise, and good humor, as well as for teaching me to love ion channels; Ingrid von Welie for technical advice during my early days in the lab; Michael Faulstich for achieving the amazing feat of labeling the vestibular nerve for EM analysis and also for keeping the lab stocked with strong coffee, quirky humor, and a deep neuroethological perspective; and Richard Jacobs for collecting EM images. I'd particularly like to thank Martha Bagnall, my collaborator on the work presented in Chapter 2, for teaching me patch-clamp electrophysiology and encouraging me to study the long-neglected vestibular nerve synapse, as well as for her enthusiasm, kindness, and many thoughtful ideas. I'd also like to thank Seti Moghadam, Matthew Grivich, Stefani von Huben, Alex Sakatos, and Shiloh Guerrero for their good company and technical help over the years.

I thank my parents, Maureen and Jerry McElvain, for their endless support and understanding, as well as for encouraging me to simply follow my heart. I also thank

Doug and Lori McElvain for their support, encouragement, and willingness to humor me, as well as for learning to appreciate “GABA”, “glutamate” and “plasticity”. I also thank Owen McElvain for lots of laughs, good cheer, and, most of all, perspective.

Chapter 2 is a reprint of the material as it appears in Bagnall, M.W., McElvain, L.E., Faulstich, M., and du Lac, S. (2008). Frequency-independent synaptic transmission supports a linear vestibular behavior. Neuron *60*, 343-352 and is included with permission from all the manuscript’s authors.

Chapter 3 is original work in preparation as McElvain L.E., Faulstich M, Jeanne J.M, Moore J. du Lac S. Concerted functional and anatomical specializations mediate linear synaptic transmission and is included with permission from all the manuscript’s authors.

Chapter 4 is a reprint of the material as it appears in McElvain L.E., Bagnall M.W., Sakatos A., du Lac S. (2010). Bidirectional plasticity gated by hyperpolarization controls the gain of postsynaptic firing responses at central vestibular nerve synapses. Neuron *68*, 763-75 and is included with permission from all the manuscript’s authors.

Vita

2011 Ph.D., Neurosciences, University of California, San Diego

2003-2005 Research Assistant, Harvard Medical School

2003 Sc.B., Neuroscience, Brown University

Publications

McElvain L.E., Bagnall M.B., Sakatos A., du Lac S. (2010) Bidirectional plasticity gated by hyperpolarization controls the gain of postsynaptic firing responses at central vestibular nerve synapses. Neuron 68 (4): 763-775.

Bagnall M.W., McElvain L.E., Faulstich M., du Lac S. (2008) Frequency-independent synaptic transmission supports a linear vestibular behavior. Neuron 60(2): 343-52.

Wang J.T.*, McElvain L.E.*, Whelan S.P. (2007) Vesicular stomatitis virus mRNA capping machinery requires specific cis-acting signals in the RNA. J Virology 81(20): 11499-506.

Awards and Honors

2011 UCSD Leon Thal Award for Excellence in Graduate Research
2009-2010 Chapman Scholar, The Salk Institute for Biological Studies
2008-2009 Aginsky Scholar, The Salk Institute for Biological Studies
2003 *Magna cum laude* with Honors
2003 Brown University Award for Scholarship and Research in Neuroscience
2003 Sigma Xi
2002 HHMI Undergraduate Research Fellowship
2002 Phi Beta Kappa

ABSTRACT OF THE DISSERTATION

Dynamics and Plasticity of Central Vestibular Nerve Synapses

by

Lauren E. McElvain

Doctor of Philosophy in Neurosciences

University of California, San Diego, 2011

Professor Sascha du Lac, Chair

Professor Anirvan Ghosh, Co-Chair

The vestibular system is critical for postural balance, orientation, reflexive control of eye movements, and spatial cognition, yet compared with other sensory systems little is known about its cellular basis. Head motion signals are transduced in the inner ear and carried to brainstem vestibular nuclei by vestibular nerve afferents. The nature and quality of head motion information in the central nervous system depend on the capacity of vestibular nerve synapses to influence action potential firing in postsynaptic neurons. This dissertation examines the functional and molecular features of the vestibular nerve synapse that promote the faithful transmission of head motion signals. Experimental

results revealed that these synapses are specialized to provide postsynaptic neurons with unambiguous signals that linearly relate to head velocity. Extensive refinements of cellular machinery enable reliable, fast, linear synaptic transmission while still allowing for modifications of synaptic strength. Long-term depression and potentiation of vestibular nerve synapses linearly regulate the firing responses of postsynaptic neurons and are well suited to underlie cerebellum-dependent calibration of vestibular reflex strength.

Chapter 1: Introduction

Neural circuits differ markedly in how they process information, and this functional diversity is believed to reflect the specialized demands placed on each circuit by the animal behavior it subserves. The computational capacity of a neural circuit—how it transforms its inputs—arises from interactions among underlying neurons, and synaptic connections are critical determinants of circuit throughput (Abbott and Regehr, 2004). Over the past several decades, many studies have revealed the impressive functional and molecular heterogeneity of synapses. Notable differences across synapses include morphology, the molecular machinery of neurotransmitter release, short-term dynamics, the composition and regulation of postsynaptic receptors, and long-term plasticity mechanisms, among others (Atwood and Karunanithi, 2002; Cowan, 2001; Rollenhagen and Lubke, 2006). The assumption that synaptic refinements are tuned to optimize animal behavior has proven difficult to demonstrate at central synapses where the computational goals and behavioral function of individual synapses are difficult to specify.

Simple neural circuits offer unique opportunities to examine the functional roles of individual synaptic specializations within the context of defined circuit computations and behavioral outcomes. Among the simplest circuits in the mammalian nervous system are those underlying vestibular reflexes. These circuits produce motor responses that compensate for head motion in order to promote stable navigation and clear vision in mobile animals. The direct pathway that transforms head motion into compensatory movements comprises only two central synapses; vestibular nerve afferents synapse onto neurons in brainstem vestibular nuclei, which directly synapse onto motor neurons (Fig.

1.1). The excellent performance of the vestibular system is exemplified by behavioral analyses of the vestibulo-ocular reflex (VOR), which drives eye movements that accurately compensate for head motion over a nearly 40-fold range of head velocities (Fig 1.2). Decades of *in vivo* studies have identified the firing responses, functional connectivity, and computational properties of the participating cell types, making this circuit among the best characterized in the mammalian brain and thus exceptionally well suited for forging links between cellular machinery and animal behavior (du Lac et al., 1995).

Head motion is transduced by the three semicircular canals, the saccule, and the utricle in the inner ear. Hair cells in each of these structures synapse onto vestibular nerve afferents, which transmit head motion signals to the central nervous system. The sensory signals carried by these afferents are essential for the compensatory control of eye movements, as well as postural balance, coordination, and spatial cognition. Many properties of vestibular nerve afferents have been extensively examined, including the specificity of their hair cell synaptic inputs, biophysical and anatomical properties, and ion channel regulation (Eatock and Songer, 2011; Goldberg, 2000). However, surprisingly little is known about how nerve afferents transmit head motion signals to the central nervous system.

The work presented in this dissertation focuses on the first central synapse in the vestibular system: the vestibular nerve afferent synapse. This synapse conveys all vestibular signals to the central nervous system, and its cellular and molecular properties must be specialized to promote the excellent performance of vestibular behaviors. Previous studies on this synapse demonstrated only that it is glutamatergic and that

postsynaptic currents are mediated by both AMPA (α-amino-3-hydroxy-5-methyl-4-isoxazolepropionic acid) receptors and NMDA (N-Methyl-D-aspartic acid) receptors (Babalian et al., 1997; Doi et al., 1990; Kinney et al., 1994; Lewis et al., 1989; Straka et al., 1996; Takahashi et al., 1994). In contrast to the dearth of information on the cellular and molecular properties of this synapse, its behavioral demands are well defined: vestibular reflexes must be fast and accurate in order to precisely compensate for head motion. The vestibular system operates around high baseline firing rates, and vestibular nerve afferents fire ~50 Hz tonically and modulate from 5 to 125 Hz in the mouse (Bagnall et al., 2008; Lasker et al., 2008; Yang and Hullar, 2007). Firing rates in vestibular nerve afferents and postsynaptic vestibular nucleus neurons primarily code for head velocity, and their firing rates scale linearly with head movements (Fernandez and Goldberg, 1976; Highstein et al., 2005; Shimazu and Precht, 1965). The vestibular nerve synapse thus has a defined goal: the conversion of presynaptic nerve afferent firing rates into linear increases in postsynaptic firing rates.

Transmission dynamics of the vestibular nerve synapse

The vestibular system must use one of two solutions to promote linearity: either vestibular nerve synaptic transmission is non-linear and network dynamics in the vestibular nuclei—feedforward or feedback inhibition or excitation—offset the nonlinearity or, alternatively, transmission at the vestibular nerve synapse is linear in a manner not previously thought possible for central synapses. Setting the computation of the vestibular nerve synapse to match the linear computation performed by the overall circuit and behavior is conceptually appealing, but there are several biological obstacles

to this solution. The high firing rates of vestibular nerve afferents alone pose an extraordinary challenge for transmission machinery. Few central synapses have been shown to operate around similar firing rate ranges, and these include the cerebellar mossy fiber and Purkinje cell synapses, in addition to the end bulb and calyx of Held in the auditory brainstem (Oleskevich et al., 2000; Saviane and Silver, 2006; Telgkamp and Raman, 2002; von Gersdorff and Borst, 2002). Furthermore, the vestibular nerve synapse not only needs to be capable of high-rate transmission on occasion but must sustain high-rate transmission, because nerve afferents fire ~50 Hz tonically and never cease firing during the lifetime of an animal. On top of these demands, linearity would add the further requirement of exceptional precision.

At all previously studied central synapses, the strength of transmission depends on the rate and pattern of presynaptic activity. This creates enormous diversity in how individual synapses translate presynaptic firing codes into postsynaptic currents. While this filtering capacity of synaptic transmission has been proposed to contribute to neural computations (Abbott and Regehr, 2004), the waxing and waning of transmission in response to activity make synapses inherently non-linearly circuit elements. The process by which activity at a synapse transiently enhances or weakens synaptic strength for milliseconds to minutes is known as short-term synaptic plasticity. All central synapses display short-term depression and/or facilitation, whose magnitude and dependence on activity patterns vary dramatically across synapse types.

What causes synaptic strength to change in response to repeated activity? Synaptic transmission depends on three general steps: an action potential opens voltage-gated calcium channels, and calcium enters the presynaptic terminal; calcium binds the

calcium sensor and triggers vesicle fusion; and neurotransmitter diffuses across the synaptic cleft and binds postsynaptic receptors. Activity can transiently alter multiple mechanisms at each of these stages of synaptic transmission. First, every presynaptic action potential does not result in an identical concentration of calcium in the terminal. If an action potential has recently proceeded, the prior calcium influx can lead to calcium-dependent modifications of the calcium channel itself, and, depending on the terminal, the capacity of calcium buffers and extruders may be transiently exceeded such that calcium accumulates in the terminal (Catterall and Few, 2008; Neher and Sakaba, 2008). Moreover, at many synapses, repeated firing results in the progressive broadening of action potentials, creating the opportunity for enhanced calcium influx (Brody and Yue, 2000; Geiger and Jonas, 2000).

Second, the probability that a particular concentration of calcium actually causes vesicle fusion can change for multiple reasons, including mechanisms that are calcium-dependent, triggered by retrograde signals, or downstream of presynaptic auto-receptors (Zucker and Regehr, 2002). Third, maintaining a constant availability of fusion-ready vesicles at a release site is extraordinarily difficult at many synapses, because the clearing of a used vesicle and the translocation, docking, and priming of a new vesicle can be relatively slow. Even in the case of fast vesicle dynamics, the number of vesicles at the terminal can additionally limit transmission, particularly at high rates (Rizzoli and Betz, 2005; Sudhof, 2004).

Fourth, if released neurotransmitter does not have the opportunity to readily diffuse from the cleft, it must be efficiently taken up or broken down, or else the concentration of neurotransmitter in the cleft could vary following successive action

potentials (Tzingounis and Wadiche, 2007). Fifth, postsynaptic receptors desensitize following neurotransmitter binding, which diminishes their responsiveness to neurotransmitter and thus participation in transmission (Jones and Westbrook, 1996). Given the vast array of potential activity-dependent changes at synaptic connections, it is perhaps unsurprising that synaptic strength generally fluctuates in response to recent activity.

Could the vestibular nerve synapse be sufficiently specialized to mediate linear transmission and overcome common limitations in synaptic machinery? Alternatively, must behavioral linearity arise from slower network processing? Using whole-cell patch-clamp electrophysiological recordings in a slice preparation, we discovered that the vestibular nerve synapse exhibits exceptional rate-independent, linear transmission across the entire range of physiological presynaptic firing rates (5 - 125 Hz) and is thus perfectly suited to reliably relay head motion signals and support linear behaviors. In Chapters 2 and 3 of this dissertation, I define the features and requirements that underlie this synaptic linearity. Chapter 2 describes the basic properties of vestibular nerve synaptic transmission and its short-term plasticity dynamics in two distinct classes of vestibular nucleus neurons. This chapter also demonstrates that linear synaptic transmission is complemented by linear synaptic integration in vestibular nucleus neurons, which together provide a physiological basis for the linearity of vestibular reflexes.

Determinants of broadband synaptic linearity

The implementation of linear transmission at the vestibular nerve synapse must require a unique specialization or collection of specializations that avoid or offset typical

synaptic non-linearities. While other central synapses operate at high rates, they exhibit rate-dependent rundown caused by diminished release probability and/or postsynaptic receptor desensitization (Carter and Regehr, 2000; Saviane and Silver, 2006; Telgkamp and Raman, 2002; von Gersdorff and Borst, 2002; Wang and Manis, 2008). What makes the vestibular nerve synapse special? In Chapter 3 of this dissertation, I define the properties of the vestibular nerve synapse that underlie transmission and promote linearity across a wide range of presynaptic firing rates. The findings described in Chapter 3 include results from electrophysiology, pharmacology, electron microcopy, and computational modeling studies, all of which highlight a key strategy of the vestibular nerve synapse: greatly limiting the probability of neurotransmitter release minimizes the challenges of broadband linearity by allowing individual release sites to operate at low rates. The unreliable contribution of individual release sites, on account of their low probability of release, is offset by a large number of release sites at each synaptic terminal, which functionally "take turns". Thus, reliable transmission of head motion signals entering the vestibular system is not achieved through powerful individual connections but through the collective function of multiple release sites.

Long-term plasticity of vestibular nerve synapses

The performance of vestibular reflexes must be fast and accurate in order to promote postural stability and clear vision. The studies described above define several features of the vestibular nerve synapse that are well tuned to mediate fast and linear sensory-motor transformations. Excellent reflex performance also requires the appropriate calibration of the strength, or gain, of the reflex. Long-term plasticity in the

underlying circuitry must support such calibrations during development and following alterations to the body's periphery, such as changes in the optics of the eye or weakening of musculature as a result of aging. Central neural circuits must continually evaluate and re-optimize vestibular reflex performance throughout life.

The cerebellum plays an essential role in the calibration of vestibular reflexes, and the adaptation of the vestibulo-ocular reflex (VOR) is one of the best studied models of cerebellum-dependent motor learning. Lesions to the cerebellar cortex impair VOR adaptation, and most studies on its neural basis have focused on the putative contribution of Purkinje cells, the sole outputs of the cerebellar cortex (du Lac et al., 1995; Ito, 2002; Robinson, 1976). Purkinje cells directly inhibit vestibular nucleus neurons (Fig 1.1), and the highly influential Marr-Albus-Ito theory proposed that changes in the firing of Purkinje cells underlie the "memory" storage for VOR adaptation (Ito, 1984, 2002). In this model, LTD of the parallel fiber synapses onto Purkinje cells is the basis for their altered firing and thus the mechanism of VOR adaptation. While many experimental findings are consistent with this theory of motor learning, recent evidence has mounted against the possibility that parallel fiber LTD and Purkinje cell activity store the memory for VOR gain changes. Importantly, cerebellar inactivation does not impair learned gain changes, suggesting the long-term consolidation of VOR adaptation is downstream of Purkinje cells (Kassardjian et al., 2005; Shutoh et al., 2006). Moreover, an elegant series of experiments found VOR adaptation was normal in three types of transgenic mice in which cerebellar LTD was selectively blocked, demonstrating that the cerebellar LTD is not required for the either acquisition or the storage of VOR adaptation (Schonewille et al., 2011).

Thirty years ago, an alternative theory on VOR learning proposed that Purkinje cells were not the site of long-term storage of VOR adaptation, but rather changes in their firing pattern during learning induced memory storage in the vestibular nuclei (Miles and Lisberger, 1981). The Miles-Lisberger theory identified the vestibular nerve synapse as a putative site of memory storage for VOR adaptation and suggested that changes in the strength of this synapse would be optimally suited to underlie VOR adaptation. What had been missing from this theory, however, was a clear demonstration that activity could induce long-term plasticity at vestibular nerve synapses. Because Purkinje cells are GABAergic, mechanisms of VOR adaptation in the vestibular nuclei must be sensitive to hyperpolarization in order to be influenced by changes in Purkinje cell activity. Thus, synaptic plasticity at the vestibular nerve synapse would likely follow specialized induction rules.

The results in Chapter 4 of this dissertation demonstrate that the vestibular nerve synapse is capable of long-term, activity-dependent plasticity and that the direction of the plasticity is gated by hyperpolarization of postsynaptic vestibular nucleus neurons. Vestibular nerve LTD and LTP produce linear changes in the evoked firing responses of postsynaptic neurons. Thus, long-term plasticity at the vestibular nerve synapse controls the gain of linear synaptic transmission in a manner that is compatible with requirements for a cellular basis of VOR adaptation.

References

Abbott, L.F., and Regehr, W.G. (2004). Synaptic computation. Nature *431*, 796-803.

Atwood, H.L., and Karunanithi, S. (2002). Diversification of synaptic strength: presynaptic elements. Nat Rev Neurosci *3*, 497-516.

Babalian, A., Vibert, N., Assie, G., Serafin, M., Muhlethaler, M., and Vidal, P.P. (1997). Central vestibular networks in the guinea-pig: functional characterization in the isolated whole brain in vitro. Neuroscience *81*, 405-426.

Bagnall, M.W., McElvain, L.E., Faulstich, M., and du Lac, S. (2008). Frequency-independent synaptic transmission supports a linear vestibular behavior. Neuron *60*, 343-352.

Brody, D.L., and Yue, D.T. (2000). Release-independent short-term synaptic depression in cultured hippocampal neurons. J Neurosci *20*, 2480-2494.

Carter, A.G., and Regehr, W.G. (2000). Prolonged synaptic currents and glutamate spillover at the parallel fiber to stellate cell synapse. J Neurosci *20*, 4423-4434.

Catterall, W.A., and Few, A.P. (2008). Calcium channel regulation and presynaptic plasticity. Neuron *59*, 882-901.

Cowan, W.M., Südhof, T.C, and Stevens, C.F. (2001). Synapses.

Doi, K., Tsumoto, T., and Matsunaga, T. (1990). Actions of excitatory amino acid antagonists on synaptic inputs to the rat medial vestibular nucleus: an electrophysiological study in vitro. Exp Brain Res *82*, 254-262.

du Lac, S., Raymond, J.L., Sejnowski, T.J., and Lisberger, S.G. (1995). Learning and memory in the vestibulo-ocular reflex. Annu Rev Neurosci *18*, 409-441.

Eatock, R.A., and Songer, J.E. (2011). Vestibular Hair Cells and Afferents: Two Channels for Head Motion Signals. Annu Rev Neurosci.

Fernandez, C., and Goldberg, J.M. (1976). Physiology of peripheral neurons innervating otolith organs of the squirrel monkey. II. Directional selectivity and force-response relations. J Neurophysiol *39*, 985-995.

Geiger, J.R., and Jonas, P. (2000). Dynamic control of presynaptic Ca(2+) inflow by fast-inactivating K(+) channels in hippocampal mossy fiber boutons. Neuron *28*, 927-939.

Goldberg, J.M. (2000). Afferent diversity and the organization of central vestibular pathways. Exp Brain Res *130*, 277-297.

Highstein, S.M., Rabbitt, R.D., Holstein, G.R., and Boyle, R.D. (2005). Determinants of spatial and temporal coding by semicircular canal afferents. J Neurophysiol *93*, 2359-2370.

Ito, M. (1984). The modifiable neuronal network of the cerebellum. Jpn J Physiol *34*, 781-792.

Ito, M. (2002). Historical review of the significance of the cerebellum and the role of Purkinje cells in motor learning. Ann N Y Acad Sci *978*, 273-288.

Jones, M.V., and Westbrook, G.L. (1996). The impact of receptor desensitization on fast synaptic transmission. Trends Neurosci *19*, 96-101.

Kassardjian, C.D., Tan, Y.F., Chung, J.Y., Heskin, R., Peterson, M.J., and Broussard, D.M. (2005). The site of a motor memory shifts with consolidation. J Neurosci *25*, 7979-7985.

Kinney, G.A., Peterson, B.W., and Slater, N.T. (1994). The synaptic activation of N-methyl-D-aspartate receptors in the rat medial vestibular nucleus. J Neurophysiol *72*, 1588-1595.

Lasker, D.M., Han, G.C., Park, H.J., and Minor, L.B. (2008). Rotational responses of vestibular-nerve afferents innervating the semicircular canals in the C57BL/6 mouse. J Assoc Res Otolaryngol *9*, 334-348.

Lewis, M.R., Phelan, K.D., Shinnick-Gallagher, P., and Gallagher, J.P. (1989). Primary afferent excitatory transmission recorded intracellularly in vitro from rat medial vestibular neurons. Synapse *3*, 149-153.

Miles, F.A., and Lisberger, S.G. (1981). Plasticity in the vestibulo-ocular reflex: a new hypothesis. Annu Rev Neurosci *4*, 273-299.

Neher, E., and Sakaba, T. (2008). Multiple roles of calcium ions in the regulation of neurotransmitter release. Neuron *59*, 861-872.

Oleskevich, S., Clements, J., and Walmsley, B. (2000). Release probability modulates short-term plasticity at a rat giant terminal. J Physiol *524 Pt 2*, 513-523.

Rizzoli, S.O., and Betz, W.J. (2005). Synaptic vesicle pools. Nat Rev Neurosci *6*, 57-69.

Robinson, D.A. (1976). Adaptive gain control of vestibuloocular reflex by the cerebellum. J Neurophysiol *39*, 954-969.

Rollenhagen, A., and Lubke, J.H. (2006). The morphology of excitatory central synapses: from structure to function. Cell Tissue Res *326*, 221-237.

Saviane, C., and Silver, R.A. (2006). Fast vesicle reloading and a large pool sustain high bandwidth transmission at a central synapse. Nature *439*, 983-987.

Schonewille, M., Gao, Z., Boele, H.J., Vinueza Veloz, M.F., Amerika, W.E., Simek, A.A., De Jeu, M.T., Steinberg, J.P., Takamiya, K., Hoebeek, F.E*., et al.* (2011). Reevaluating the Role of LTD in Cerebellar Motor Learning. Neuron *70*, 43-50.

Shimazu, H., and Precht, W. (1965). Tonic and kinetic responses of cat's vestibular neurons to horizontal angular acceleration. J Neurophysiol *28*, 991-1013.

Shutoh, F., Ohki, M., Kitazawa, H., Itohara, S., and Nagao, S. (2006). Memory trace of motor learning shifts transsynaptically from cerebellar cortex to nuclei for consolidation. Neuroscience *139*, 767-777.

Straka, H., Debler, K., and Dieringer, N. (1996). Size-related properties of vestibular afferent fibers in the frog: differential synaptic activation of N-methyl-D-aspartate and non-N-methyl-D-aspartate receptors. Neuroscience *70*, 697-707.

Sudhof, T.C. (2004). The synaptic vesicle cycle. Annu Rev Neurosci *27*, 509-547.

Takahashi, Y., Tsumoto, T., and Kubo, T. (1994). N-methyl-D-aspartate receptors contribute to afferent synaptic transmission in the medial vestibular nucleus of young rats. Brain Res *659*, 287-291.

Telgkamp, P., and Raman, I.M. (2002). Depression of inhibitory synaptic transmission between Purkinje cells and neurons of the cerebellar nuclei. J Neurosci *22*, 8447-8457.

Tzingounis, A.V., and Wadiche, J.I. (2007). Glutamate transporters: confining runaway excitation by shaping synaptic transmission. Nat Rev Neurosci *8*, 935-947.

von Gersdorff, H., and Borst, J.G. (2002). Short-term plasticity at the calyx of held. Nat Rev Neurosci *3*, 53-64.

Wang, Y., and Manis, P.B. (2008). Short-term synaptic depression and recovery at the mature mammalian endbulb of Held synapse in mice. J Neurophysiol *100*, 1255-1264.

Yang, A., and Hullar, T.E. (2007). Relationship of semicircular canal size to vestibular-nerve afferent sensitivity in mammals. J Neurophysiol *98*, 3197-3205.

Zucker, R.S., and Regehr, W.G. (2002). Short-term synaptic plasticity. Annu Rev Physiol *64*, 355-405.

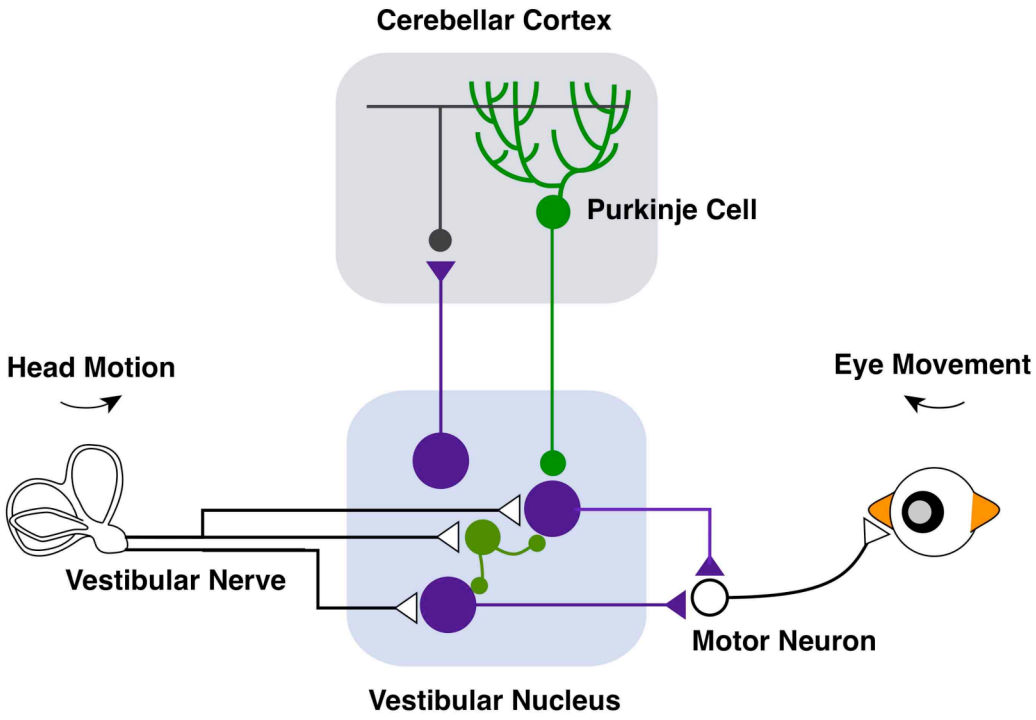

Fig. 1.1 Circuitry of the vestibulo-ocular reflex. The vestibular nerve transmits head motion signals from the vestibular apparatus to the central nervous system. Vestibular nerve afferents synapse onto vestibular nucleus neurons, which consist of projection neurons and local interneurons. The cerebellum plays a critical role in adapting the strength of vestibular reflexes. Cerebellar Purkinje cells directly inhibit a subset of neurons in the vestibular nucleus.

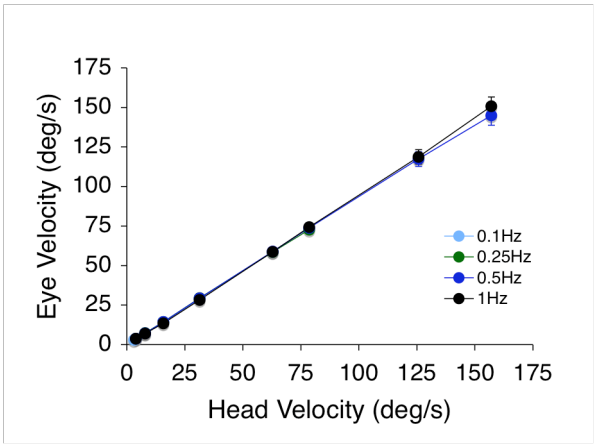

Fig. 1.2 Linear performance of the vestibulo-ocular reflex. Eve velocity was measured while mice were rotated sinusoidally in the horizontal plane at frequencies of 0.1, 0.25, 0.5, or 1 Hz. Eve movements are in the opposite direction of the head motion and stabilize the eyes in space. Figure adapted from Michael Faulstich.

Chapter 2. Frequency-independent synaptic transmission supports a linear vestibular behavior

Abstract

The vestibular system is responsible for transforming head motion into precise eye, head, and body movements that rapidly stabilize gaze and posture. How do central excitatory synapses mediate behavioral outputs accurately matched to sensory inputs over a wide dynamic range? Here we demonstrate that vestibular afferent synapses *in vitro* express frequency-independent transmission that spans their *in vivo* dynamic range (5 - 150 spikes/s). As a result, the synaptic charge transfer per unit time is linearly related to vestibular afferent activity in both projection and intrinsic neurons of the vestibular nuclei. Neither postsynaptic glutamate receptor desensitization nor saturation affect the relative amplitude or frequency-independence of steady-state transmission. Finally, we show that vestibular nucleus neurons can transduce synaptic inputs into linear changes in firing rate output, without relying on one-to-one calyceal transmission. These data provide a physiological basis for the remarkable linearity of vestibular reflexes.

Introduction

The nervous system serves to transform sensory inputs into motor outputs via cellular and synaptic processes that are specialized for the behaviors they support. In this study, we examine the transformation from presynaptic to postsynaptic firing rate in the well-defined brainstem circuit of the vestibular system to identify the physiological underpinnings of a fast, linear behavior.

Head movements trigger vestibular reflexes that produce rapid and precise compensatory movements of the eyes, head, and body. During the vestibulo-ocular reflex (VOR), the eyes are directed contraversive to head motion in order to maintain a stable retinal image. The VOR exhibits two remarkable characteristics: first, the latency from onset of head motion to onset of eye movement is < 10 ms (Huterer and Cullen, 2002; Minor et al., 1999); and second, eye velocity accurately compensates for head velocity over a broad dynamic range in a variety of species, including goldfish, frogs, rodents, cats, and primates (Faulstich et al., 2004; Furman et al., 1982; Pastor et al., 1992; Pulaski et al., 1981; Robinson, 1976; Straka and Dieringer, 2004).

These twin demands of speed and accuracy must be met by the supporting neuronal circuitry. The VOR relies on a trisynaptic pathway: information about head movement originates in the inner ear and is carried via vestibular nerve afferents to the brainstem vestibular nuclei; from there it travels to oculomotor nuclei (Fig. 2.1A). The brevity of this circuit keeps reflex times short. What qualities of the circuit ensure that eye velocity is precisely matched to head velocity over a wide dynamic range?

Vestibular afferents code primarily for head velocity (reviewed in Highstein et al., 2005), as do their postsynaptic targets, vestibular nucleus neurons (Beraneck and Cullen, 2007; Lisberger and Miles, 1980; Scudder and Fuchs, 1992). Given that the VOR operates accurately across a wide range of head velocities, transmission at the excitatory synapse from vestibular afferents onto vestibular nucleus neurons would be expected to be linear. However, transmission at most glutamatergic synapses is nonlinear: both the probability of transmitter release and the efficacy of postsynaptic response to that transmitter depend heavily on the recent history of the synapse (Zucker and Regehr,

2002). If the vestibular afferent synapse were to operate in this way, its ability to transmit precise signals about head velocity could be compromised.

We sought to determine whether synaptic transmission at the vestibular afferent synapse could succeed in linear information transfer. In this study, we record in voltage and current clamp from neurons in the vestibular nucleus while stimulating vestibular afferents in mouse brainstem slices. The results define the synaptic properties that produce a linear transformation from pre- to post-synaptic firing rates.

Methods

Behavioral testing

Linearity of the vestibulo-ocular reflex (VOR) was assessed in 6 C57/Bl6 mice at ages of 2-4 months as detailed (Faulstich et al., 2004). Mice were secured in a padded restraining tube with a post which had been affixed surgically to the head 3 days prior. The restraining tube was held in the middle of a turntable (Biomedical Engineering, NY, USA) such that the midpoint of the interaural axis was centered and tilted to align horizontal semicircular canals with earth horizontal (Calabrese and Hullar, 2006; Vidal et al., 2004). Eye movements were acquired with an infrared video camera mounted on the turntable which measured pupillary position and size and corneal reflection (RK-726I; Iscan). Pupil dilation was minimized with a 0.5% physostigmine solution applied 30-60 min prior to recordings. The VOR was evoked by rotating the turntable sinusoidally at a frequency of 1Hz with peak-to-peak amplitudes ranging from 1.25 to 50°, resulting in peak stimulus velocities from 3.9 to 157 °/s. Eye movements were evoked in complete darkness, sampled at 60 Hz, and calibrated as described (Stahl, 2002; Stahl et al., 2000).

Analyses of eye movements were performed in the velocity domain after digitally differentiating table and eye position traces, removing saccadic intrusions with a velocity threshold algorithm, and manually excluding traces with motion artifacts. Peak velocities were calculated from sinusoidal fits to table and eye velocity.

Physiology

Two transgenic lines of mice were used for synaptic physiology: YFP-16 (Feng et al., 2000), in which glutamatergic and glycinergic neurons in the MVN are fluorescently labeled; and GIN, in which a subset of GABAergic MVN neurons are fluorescently labeled (Bagnall et al., 2007; Oliva et al., 2000). Anatomical, physiological, and neurochemical evidence indicates that neurons labeled in the YFP-16 line are projection neurons, while neurons labeled in the GIN line are local neurons whose axons remain within the bilateral MVN (Bagnall et al., 2007; Epema et al., 1988; Holstein, 2000). Mice aged 15-25 days postnatal (mean, P21 ± 0.3) were deeply anesthetized with Nembutal and decapitated. After rapid dissection in ice cold Ringer's solution (in mM: 124 NaCl, 5 KCl, 1.3 $MgSO_4$, 26 $NaHCO_3$, 2.5 $CaCl_2$, 1 NaH_2PO_4), 250 - 400 µm thick slices were cut on a DSK DTK-1500E or Leica VT1000S vibratome and allowed to recover at 34 ºC for 30 min. Slices rested at room temperature before being transferred to a recording chamber and perfused with carbogenated Ringer's containing 1-10 µM strychnine and 100 µM picrotoxin at 34 ºC. All experiments were carried out in accordance with the standards of the Salk Institute IACUC.

Patch pipettes were pulled from flame-polished glass (Warner) with resistances of ~2-4 MΩ. Pipette internal solution contained (in mM) 140 K gluconate, 10 HEPES, 8

NaCl, 0.1 EGTA, 2 Mg-ATP, 0.3 Na_2-GTP. In the experiments involving application of γ-D-glutamyl glycine (γ-DGG), the K gluconate was replaced with Cs gluconate, and 1 mM QX-314 was added to the internal solution. Neurons were visualized with epifluorescence through a GFP filter as well as under infrared differential interference contrast illumination with Nomarski optics. A bipolar concentric stimulating electrode (FHC, Maine) was placed on the vestibular nerve lateral to the vestibular complex and controlled via two Isoflex stimulus isolation units (AMPI, Israel). A biphasic pulse, consisting of two 100 μs pulses of opposite polarity with a 100 μs interval, was delivered to the electrode to avoid charge build-up during high frequency trains.

Data were acquired with a Multiclamp 700B low-pass filtering at 6-10 kHz for voltage clamp and 10 kHz for current clamp. Data were digitized at 40 kHz with an ITC-16 or 18 (InstruTECH). House-written code in Igor 5 was used for acquisition and analysis. Recordings were discarded if series resistance, tested with a small hyperpolarizing square pulse, exceeded 20 MΩ. 5-10 sweeps (10-30 s interstimulus interval) of each stimulus train were averaged together. Neurons were usually held in current clamp between epochs of recording in voltage clamp; in two example traces (Fig. 2.5) a small (~25 pA) drift in holding current has been subtracted for display purposes.

Because vestibular nerve afferents are heterogeneous with respect to diameter and myelination, conduction velocities vary across the afferent population. As a result, in many EPSCs an inflection point was visible in the rise and/or decay, representing the arrival of several different synaptic currents at slightly different latencies. All such EPSCs were monosynaptic, based on their latency (< 2 ms) and on the fact that they did not disappear during manipulation of external divalent ions intended to eliminate

disynaptic activation (to 1 mM Ca^{2+}, 2.8 mM Mg^{2+}; or to 4 mM Ca^{2+}, 4 mM Mg^{2+}, data not shown). There was no clear relationship between stimulation intensity and the recruitment of these longer- or shorter- latency EPSC components. Because of the impossibility of studying these components systematically, we analyzed EPSC decay kinetics with a 90-10% or 80-20% fall time measure, rather than with exponential fits. During recordings, stimulation intensity was adjusted to produce a reliable EPSC, normally in the range of 1.5 - 3x the threshold intensity. During voltage clamp, the postsynaptic cell was clamped at -75 mV to isolate primarily an AMPA-mediated response. Firing rates are reported as the average of the reciprocal of the inter-spike interval, and were averaged across the entire 1 s of synaptic stimulation.

Statistical tests were done with KaleidaGraph 3.6 (Synergy Software) and are reported as mean ± SEM except as noted. Synthesized Cs gluconate was a gift of Dr. Court Hull. Chemicals were purchased from Sigma (St. Louis MO), with the exception of γ-DGG and cyclothiazide (Tocris, Bristol, UK) and EGTA-AM (Invitrogen). EGTA-AM was dissolved in DMSO (final concentration 0.05 - 0.1%). Following baseline trials, it was washed into the bath for 5 min prior to testing.

Naturalistic stimuli

Head velocity in freely locomoting mice was measured with a small head-mounted gyroscope which detected yaw velocity with bandwidth of 80 Hz (Analog Devices). Head movement signals were measured during 30 s epochs while mice were running in their home cages. The statistics of the head velocity data corresponded well with those reported during video analysis of mouse head movement (Beraneck et al.,

2008); head movements reaching velocities in excess of 100 °/s were observed less than 15% of the time, and epochs of these fast head movements lasted < 200 ms. A naturalistic stimulus was constructed by scaling a representative 5 s head velocity trace by 0.2, the average sensitivity of mouse regular and irregular type vestibular afferents, and assuming a baseline firing rate of 36 Hz, near the average for irregular afferents (Lasker et al., 2008; Yang and Hullar, 2007). This pattern was developed to maximize the possibility of uncovering nonlinearities of synaptic transmission in the low firing rate range.

Results

The performance of the VOR was assessed by rotating awake mice back and forth on a turntable in the dark while a video camera captured their eye movements. Eye motion was similar in amplitude and opposite in direction to head motion, as evident in sinusoidal plots of head and eye velocity (Fig. 2.1B). Remarkably, eye velocity was linearly matched to head velocity over a 40-fold range of peak head velocities, from 4 to 157 °/s (Fig. 2.1C). Across all head velocities tested, the VOR successfully compensated for 80% of head motion (in the light, visual reflexes compensate for the remainder (Faulstich et al., 2004)). The mouse VOR is therefore linear over a wide dynamic range of head motion.

The brainstem circuit for the VOR is outlined in Fig. 2.1A. Vestibular information about rotational head velocity, derived from fluid movement in the semicircular canals, is carried via fibers of the VIIIth nerve to neurons in the vestibular nuclei. The medial vestibular nuclei (MVN), which process head motion in the horizontal plane, control the muscles for horizontal eye movement via projections to the oculomotor and abducens

nuclei. Information about head velocity must be transformed into matched oculomotor responses through this circuit. How can head velocity be accurately converted into eye velocity across glutamatergic synapses, which are typically thought of as nonlinear elements (Abbott and Regehr, 2004)?

To address this question, we electrically stimulated vestibular afferents while recording from MVN neurons in slice preparation of the brainstem. Whole-cell patch clamp recordings were targeted to fluorescently labeled neurons in two transgenic mouse lines that label complementary neuronal distributions in the MVN: the YFP-16 line (Feng et al., 2000), which labels glycinergic and glutamatergic premotor projection neurons; and the GIN line (Oliva et al., 2000), which highlights a subset of local GABAergic neurons (Bagnall et al., 2007; Epema et al., 1988; Holstein, 2000; see also Experimental Procedures).

Stimulation of the vestibular nerve elicited synaptic currents in the majority of vestibular nucleus neurons, consistent with data suggesting that the vestibular nerve contacts most MVN neurons (Babalian et al., 1997; Goldberg and Fernandez, 1971; Lewis et al., 1989; Straka and Dieringer, 1996). Increases in stimulation intensity led to increases in excitatory postsynaptic current (EPSC) amplitude, indicating that each neuron receives input from multiple vestibular afferent fibers (Fig. 2.2A). The maximal synaptic currents elicited in YFP-16 neurons ranged as high as 6 nA, while those in GIN neurons were typically less than 1 nA (Fig. 2.2B; $p < 0.0001$, Wilcoxon unpaired test). In both YFP-16 and GIN neurons, EPSCs exhibited rapid rise and fall kinetics (Fig. 2.2C, 2.2D). These data demonstrate that MVN neurons receive multiple fast synaptic inputs,

with a larger maximum conductance in premotor than in local-projecting neurons, consistent with anatomical data (Huwe and Peterson, 1995; Sato and Sasaki, 1993).

In vivo, mouse vestibular afferents fire at ~30-70 spikes/s in the absence of head motion, and modulate above and below those firing rates during head motion (Lasker et al., 2008; Yang and Hullar, 2007). To evaluate the short-term dynamics of the synaptic response to repetitive activity, we stimulated presynaptic afferents with trains of 20 pulses at frequencies from 0.1 to 200 Hz. The paired-pulse ratio, measured as the ratio of the amplitude of the second EPSC to the first (Fig. 2.2E), was remarkably stable across these frequencies in both YFP-16 and GIN neurons. At the longest interval (10 s), no facilitation or depression was observed in either population; at intervals from 5 ms to 1 s, the paired-pulse ratio was ~0.85 in both types of neurons (Fig. 2.2F). This represents an unusual history-independent response, in contrast to the frequency-dependent transmission at many other types of synapses**.**

Over the course of 20-stimulus trains, EPSC amplitudes depressed during the first 5-10 stimuli and then reached a plateau of about 60% of their initial value for the remainder of the train (Fig. 2.3A, EPSCs recorded in a YFP-16 neuron during vestibular nerve stimulation at 20 and 100 Hz; Fig. 2.3B, the same for a GIN neuron). The number of stimuli, rather than the time course of their delivery, defined the rate of depression, as can be seen in plots of normalized EPSC amplitude relative to stimulus number (Fig. 2.3C). The absolute level of steady-state depression varied among neurons from 25-85%, but within any given neuron was constant across a wide range of stimulus frequencies (Fig. 2.3D). Therefore, in the steady state, EPSC amplitude is independent of afferent activity rates.

Given that the vestibular nerve fires action potentials at rates linearly related to head velocity (Highstein et al., 2005), the synaptic charge transfer over a given unit of time should be linearly related to the head motion signal, i.e. the presynaptic firing rate. A recent study on synapses from vestibular nucleus neurons onto cerebellar granule cells in anesthetized mice found a linear relationship between head velocity and charge transfer, over a range of EPSC frequencies from ~15-45 Hz (Arenz et al., 2008). To calculate charge transfer at the vestibular afferent synapse, EPSCs evoked during the plateau phase (pulses 11-20) were averaged, integrated and normalized to the integral of the first EPSC in the train. The resulting value for each stimulus was multiplied by the stimulus rate to obtain the total charge transfer during 1 s of steady-state activity. As shown in Fig. 2.3E, a linear relationship between the rate of stimulation and the total synaptic charge transfer per unit time was evident in both YFP-16 and GIN neurons, for frequencies ranging from 5 to 100 Hz (Fig. 2.3E).

Frequency-independent synaptic transmission must derive from one of two possibilities: either presynaptic release probabilities and postsynaptic glutamate sensitivity are constant across the relevant frequency domain; or nonlinearities of release are perfectly masked by corresponding nonlinearities of glutamate sensitivity. We tested in turn the two primary candidates for postsynaptic nonlinearities on this timescale, AMPA receptor desensitization and saturation (von Gersdorff and Borst, 2002).

At the homologous synapse in the auditory system, the endbulb of Held, postsynaptic AMPA receptor desensitization is responsible for some of the observed paired-pulse depression (Isaacson and Walmsley, 1996; Trussell et al., 1993; Yang and Xu-Friedman, 2008). Desensitization might conceal an increase in vesicular release from

vestibular afferents at higher rates of presynaptic activity (Wong et al., 2003). We tested this possibility by applying the desensitization antagonist cyclothiazide (100 μM) while recording EPSCs in the vestibular nuclei (Fig. 2.4A). Both decay times and peak amplitudes of synaptic currents were significantly increased by cyclothiazide (n = 6: decay time, mean 84 ± 27% increase; peak amplitude, 39 ± 11% increase; both $p < 0.05$, Wilcoxon paired test), while rise times were insignificantly lengthened (21 ± 9% increase) (Fig. 2.4C). However, steady-state synaptic depression was unaffected by cyclothiazide (Fig. 2.4B, 50 Hz data shown). These data indicate that AMPA receptor desensitization does not contribute to short-term plasticity at this synapse.

Receptor saturation is another possible cause of changes in postsynaptic glutamate sensitivity (Foster et al., 2002; Harrison and Jahr, 2003). We reduced saturation by applying the low-affinity glutamate receptor competitive antagonist γ-D-glutamyl glycine (γ-DGG, 2 mM; Fig. 2.4D) (Foster et al., 2005; Liu et al., 1999). As expected, γ-DGG reduced EPSC amplitude (to 28 ± 3% of original value, $p < 0.05$, Wilcoxon paired test, n = 6), while leaving synaptic kinetics intact (Fig. 2.4D, F). However, there was no change in the amplitude of steady-state depression (Fig. 2.4E, 50 Hz data shown). Together, these data demonstrate that neither saturation nor desensitization has a significant effect on frequency-independent steady-state depression at the vestibular afferent synapse, suggesting that postsynaptic receptor sensitivity to glutamate is stable across a wide range of presynaptic activity rates, and that the rate-invariance of this synapse is due to unusually stable presynaptic release probabilities.

In vivo, changes in head velocity are encoded as modulations of vestibular afferent firing rate. How is vestibular synaptic transmission affected by changes in

afferent activity rates? To examine whether the afferent steady-state depression exhibited any sensitivity to transitions between input frequencies, we stimulated the vestibular nerve with two patterns of trains: 20 stimuli at 10 Hz to achieve steady state transmission followed by 20 stimuli at 50 Hz, or vice versa. In the example neuron shown, EPSCs depressed to about half the initial amplitude during the first 20 stimuli, and did not recover or depress further when the stimulation rate was changed in either direction (Fig. 2.5A). These findings are reflected in the group data (Figs. 2.5B, C).

The data presented thus far suggest that during physiological head movements, each vestibular afferent action potential evokes a fixed amount of transmitter release and postsynaptic current. This was examined more directly by challenging vestibular afferents with a naturalistic pattern of stimuli derived from combining measurements of mouse head movement (Beraneck et al., 2008) with vestibular afferent firing rates and sensitivity to head motion (Lasker et al., 2008; Yang and Hullar, 2007; see also Experimental Procedures). In response to a 5 s naturalistic stimulus, shown in Fig. 2.5D, EPSC amplitudes depressed rapidly to a plateau of 60% of the initial value for the duration of the stimulus (Fig. 2.5E). Within the steady state, evoked EPSC amplitude did not depend on stimulus interval (Fig. 2.5F). These data stand in contrast to findings at the hippocampal CA3 to CA1 synapse, where physiological patterns of activity drive rapid synaptic facilitation, resulting in small EPSCs during periods of quiescence but large responses during bursts of activity (Klyachko and Stevens, 2006). Instead, during physiological modulation of vestibular afferent firing rates, synaptic amplitudes are rate-invariant.

Given the high constant firing rates of vestibular afferents, the responses to trains of constant and naturalistic stimuli indicate that afferent synapses operate within a regime of steady-state depression. If transmission were to recover rapidly from depression, EPSC amplitude would no longer be constant. To examine the timecourse of recovery from depression, vestibular afferents were stimulated with 20-pulse conditioning trains at 10, 50, or 100 Hz, followed by a test pulse some variable time later (Fig. 2.6A). At long intervals (> 200 ms), EPSC recovery was best fit by a single exponential with a time constant of ~2 s for all three conditioning trains (Fig. 2.6B). However, over shorter intervals (10-100 ms), EPSCs did not recover in amplitude (Fig. 2.6C; 50 Hz conditioning train). Furthermore, although EPSC recovery at many synapses includes a fast component that is diminished by additional slow Ca buffering (Dittman and Regehr, 1998; Yang and Xu-Friedman, 2008), application of 100 μM EGTA-AM had no effect on EPSC recovery at any interval (Fig. 2.6C, D).

The data presented thus far demonstrate that the synaptic charge transfer per unit time at the vestibular nerve synapse onto different types of vestibular nucleus neurons is linearly related to presynaptic activity rates. While it is known that the relationship between injected current and firing rate is linear in MVN neurons (du Lac and Lisberger, 1995; Fig. 2.7A), it is not known whether synapses are also capable of driving linear increases in firing rate in the face of changes in postsynaptic driving force. To evaluate the relationship between pre- and post-synaptic firing rates, responses of MVN neurons to 1 s of synaptic stimulation over a range of frequencies were recorded in current clamp. DC depolarizing or hyperpolarizing current was injected into MVN neurons to maintain a baseline firing rate of ~10 spikes/s, simulating the low end of *in vivo* firing rates

(Beraneck and Cullen, 2007). As shown in Fig. 2.7B for an example neuron, synaptic stimulation at 20 and 100 Hz for 1 s evoked increases in postsynaptic spiking, with the associated firing rates plotted in Fig. 2.7C. Over all afferent stimulation rates tested, this MVN neuron responded to increases in synaptic input frequency with linear increases in firing rate, up through presynaptic stimulation rates of 150 Hz (Fig. 2.7D).

Stimulation of vestibular afferents onto both YFP-16 and GIN neurons elicited highly linear firing rate responses across stimulation rates ranging from 20-150 Hz (YFP-16, median $R^2 = 0.948$; GIN, 0.978) (Fig. 2.7E). At 200 Hz, there was typically a slight to moderate drop in response amplitude, as predicted from the greater synaptic depression observed at that stimulation frequency in voltage clamp (Fig. 2.3D). The synaptic gain was variable across neurons, as expected due to differences in synapse amplitude, depression profile, and postsynaptic membrane properties (YFP-16, median = 0.17 spikes/Hz; GIN, 0.09; $p = 0.09$, Wilcoxon unpaired test) (Fig. 2.7F). Blocking NMDA receptors with APV had no effect on synaptic gain (post/pre = 1.04) or linearity (post/pre = 0.96; data not shown, n = 3 YFP-16 neurons). In all but one cell tested, the gain was less than 1, indicating that several EPSPs summed temporally in a linear fashion, regardless of the frequency of afferent stimulation. Thus, vestibular nerve activity can drive linear increases in firing rate in both GABAergic and nonGABAergic neurons without relying on one-to-one calyceal connections.

Discussion

This study demonstrates that the excellent performance of the VOR is supported by a linear transformation from presynaptic to postsynaptic firing rate at the first central

synapse in the vestibular system. Vestibular afferent stimulation evoked EPSCs in vestibular nucleus neurons that depressed rapidly to a maintained steady state amplitude which, within the behaviorally relevant range of afferent firing rates, did not depend on stimulus frequency or pattern. As a consequence, charge transfer across vestibular afferent synapses scaled linearly with stimulus frequency. The linearity evidenced at the synaptic level was preserved postsynaptically by linear current summation and spike generation. Neither postsynaptic sensitization nor receptor saturation affected the initial depression or steady-state transmission, pointing to a remarkable capacity for frequency-independent transmitter release by vestibular nerve afferent synapses.These results show that vestibular afferent synapses are well tuned to meet the demands of the stabilization system, in which head motion must be linearly matched by compensatory eye and body movement.

Rapid synaptic kinetics

The short latency of the VOR depends on rapid information transfer within a trisynaptic circuit. EPSCs from vestibular afferents exhibit swift rise and fall times (Fig. 2.2), resulting in no appreciable summation of synaptic currents arriving at intervals as brief as 10 ms (Figs. 2.2 and 2.3). The absence of effect of D-APV on postsynaptic firing responses to afferent stimulation indicates that NMDA receptor mediated current, which would broaden the EPSC, plays little role at mature ages. Thus, the majority of synaptic transmission at this site appears to be mediated by AMPA receptors. Rapid EPSC rise and fall times help keep postsynaptic depolarization brief, allowing for fast modulation of postsynaptic firing rate and rapid processing of sensory information.

Sustained history-independent release

Two features of the vestibular synaptic steady-state response are noteworthy: its sustained function even at high frequencies; and its fixed amplitude across a 30-fold range of firing rates. In the brainstem and cerebellum, baseline firing rates often exceed those of cerebral cortical regions, and several types of synapses exhibit the capacity for prolonged high-frequency transmission, such as the Purkinje cell output to target neurons in the deep cerebellar nuclei (Telgkamp and Raman, 2002) and the mossy fiber input to cerebellar granule cells (Saviane and Silver, 2006). At the Purkinje cell synapse, multiple release sites with low release probabilities permit robust transmission even at high frequencies (Telgkamp et al., 2004). Vestibular afferents may express similar specializations, although no studies have addressed this directly (Sato and Sasaki, 1993).

The finding that steady-state vestibular synaptic amplitudes are constant across a wide range of input frequencies contrasts with findings at excitatory cortical synapses, in which depression deepens as stimulation frequency increases (Abbott et al., 1997). What is the basis of this unusual property of vestibular transmission? We find that postsynaptic changes in glutamate sensitivity, in the form of AMPA receptor saturation and desensitization, contribute to neither the profile of short-term synaptic depression nor its frequency-independence (Fig. 2.4). Activity-dependent relief of polyamine block at calcium-permeable AMPA receptors (Rozov and Burnashev, 1999) is unlikely to contribute to depression because vestibular afferent synaptic properties are unchanged after ~1 hr patch recording without intracellular polyamines (data not shown). These results indicate that steady-state transmission derives from the ability of presynaptic terminals to release a constant quantity of transmitter following each action potential.

How does the range of frequency-independent release correspond to *in vivo* firing rates? Vestibular afferents encode head velocity via modulations around baseline firing rates (Goldberg and Fernandez, 1971). The high sensitivity and relatively low baseline firing rate of some mouse vestibular afferents make them susceptible to cutoff, or periods of no firing, during head movements that exceed 100 deg/s (Lasker et al., 2008; Yang and Hullar, 2007). However, estimations of head movement statistics in freely running mice from video (Beraneck et al., 2008) and gyroscopic (J. Moore, personal communication) analyses indicate that such rapid head velocities occur infrequently and typically last no more than 200 ms, equivalent to a rate of ~5 spikes/s. Although the most sensitive afferent fibers exhibiting the highest spontaneous rates could increase firing rates transiently up to 200 Hz during rapid head movements, firing rates of the majority of afferents would typically remain below 100 spikes/s. Thus, under behaviorally relevant conditions, the predominant firing rate range of vestibular afferents is 5 - 100 Hz, which matches the frequency-independent range of synaptic transmission.

Within the physiologically relevant regime of maintained afferent discharge, our results indicate that each action potential evokes the same amount of transmitter release. Multiple presynaptic factors control transmitter release, including magnitude of Ca^{2+} influx, sensitivity of the release machinery to Ca^{2+}, and vesicle availability (Zucker and Regehr, 2002). After prolonged periods of silence (which do not normally occur *in vivo*), presynaptic release exhibits a high initial amplitude, which then diminishes rapidly in the face of repeated stimuli. This short term depression could reflect changes in Ca^{2+} influx, Ca^{2+}-triggered biochemical changes, or depletion of a slowly-replenished pool of vesicles. Consistent with the latter hypothesis, synaptic amplitude recovers with a slow

timecourse after stimulus trains (Fig. 2.6). At both the climbing fiber synapse and the calyx of Held, recovery from depression is best described by a combination of fast and slow processes, with the fast process being sensitive to application of EGTA-AM (Dittman and Regehr, 1998; Yang and Xu-Friedman, 2008). In contrast, recovery from depression at the vestibular afferent synapse is well described by a single exponential and does not occur at all for short intervals of < 100 ms (Fig. 2.6). Furthermore, synaptic responses at all intervals were resistant to the effects of buffering residual Ca^{2+} with intracellular EGTA. In the simplest model for steady-state transmission consistent with our results, each afferent action potential triggers influx of a fixed amount of Ca^{2+}, which evokes a cycle of coordinated vesicle release and replenishment before being rapidly cleared from the presynaptic terminal. Given the maintained high firing rates at this synapse and the energetic costs of vesicle recycling, we suggest that vestibular afferents contain multiple release sites, each with low probability of release, such has been observed at Purkinje cell synapses (Telgkamp et al., 2004). Ultrastructural studies of the vestibular afferent synapse will be useful in evaluating this hypothesis.

Linear signal processing throughout the vestibular system

Eye movements compensate almost perfectly for head movements in the mouse (Fig. 2.1) as in other species (Robinson, 1981). Notably, each stage of vestibulo-ocular reflex processing examined thus far has been shown to be linear, including the transformation from head velocity to firing rates in both vestibular nerve and vestibular nucleus neurons (Goldberg and Fernandez, 1971; Shimazu and Precht, 1965), as well as between oculomotor neuronal activity and eye velocity (Skavenski and Robinson, 1973).

In primates, the firing range of vestibular afferents is double that in mice (Lasker et al., 2008; Yang and Hullar, 2007). Limitations in rate-invariant transmission might account for some of the nonlinearities observed in the primate VOR during rapid accelerations of the head (Minor et al., 1999).

Because our data provide a plausible physiological framework for linear synaptic transmission, we suggest that EPSC amplitudes may also be rate-invariant at other connections in the vestibular system, such as those from vestibular nucleus neurons to oculomotor neurons. Indeed, recent work supports this prediction at the vestibular nucleus neuron synapse onto granule cells in the cerebellum. At this synapse, EPSC frequency, but not amplitude, is modulated during head movement such that the total charge transfer is linearly related to head velocity (Arenz et al., 2008). Interestingly, the short term dynamics of mossy fiber synapses are affected by blockers of saturation and desensitization (Saviane and Silver, 2006), in contrast to the dynamics of primary afferent synapses onto vestibular nucleus neurons (Fig. 2.4). It remains to be determined whether these mechanistic differences compromise the ability of granule cells to fire linearly over a wide range of mossy fiber input rates, as we demonstrate in vestibular nucleus neurons (Fig. 2.7).

Ongoing activity promotes linearity

A salient property of vestibular circuits is that neurons fire continuously even in the absence of head motion. Operating around high baseline firing rates confers three advantages. First, sensory stimuli can be encoded as modulations in firing rate, providing a opportunity for bidirectional encoding of information--in this case, both increases and

decreases in head velocity. Second, postsynaptic neurons do not need to be depolarized from a hyperpolarized resting membrane potential, but instead are maintained in a voltage range close to threshold, minimizing the latency from synaptic input to postsynaptic firing. Third, silent neurons often exhibit nonlinearities in synaptic summation, because small inputs may not affect postsynaptic firing while large inputs may drive dendritic and somatic spiking (e.g., Carter et al., 2007; Gasparini and Magee, 2006). Maintaining high firing rates may be one measure by which vestibular circuit neurons avoid these nonlinearities.

Functional implications

At synapses that exhibit reliable transmission, such as auditory afferents or the neuromuscular junction, a flood of neurotransmitter release guarantees a successful postsynaptic spike. Vestibular afferents do not achieve linearity through one-to-one connections such as these, but instead rely on a combination of frequency-independent release and linear postsynaptic processing (Fig. 2.7). Why? We suggest that the major advantage of the vestibular solution is its flexibility. Calyceal transmission necessarily limits the prospects for modifiability. Vestibular nucleus neurons integrate information from visual and proprioceptive sources, in addition to direct and indirect vestibular sensory inputs (Angelaki and Cullen, 2008). Furthermore, the VOR is bidirectionally plastic throughout life, and one candidate locus of memory storage is the vestibular afferent input (Broussard and Kassardjian, 2004; Gittis and du Lac, 2006). It will be of great interest to determine whether the synaptic strengths of vestibular afferents can be altered without compromising their distinctive frequency-independence.

Acknowledgements

This chapter is a reprint of the material as it appears in Bagnall, M.W., McElvain, L.E., Faulstich, M., and du Lac, S. (2008). Frequency-independent synaptic transmission supports a linear vestibular behavior. Neuron *60*, 343-352 and is included with permission from all the manuscript's authors.

References

Abbott, L. F., and Regehr, W. G. (2004). Synaptic computation. Nature *431*, 796-803.

Abbott, L. F., Varela, J. A., Sen, K., and Nelson, S. B. (1997). Synaptic depression and cortical gain control. Science *275*, 220-224.

Angelaki, D. E., and Cullen, K. E. (2008). Vestibular system: the many facets of a multimodal sense. Annu Rev Neurosci *31*, 125-150.

Arenz, A., Silver, R. A., Schaefer, A. T., and Margrie, T. W. (2008). The contribution of single synapses to sensory representation in vivo. Science *321*, 977-980.

Babalian, A., Vibert, N., Assie, G., Serafin, M., Muhlethaler, M., and Vidal, P. P. (1997). Central vestibular networks in the guinea-pig: functional characterization in the isolated whole brain in vitro. Neuroscience *81*, 405-426.

Bagnall, M. W., Stevens, R. J., and du Lac, S. (2007). Transgenic mouse lines subdivide medial vestibular nucleus neurons into discrete, neurochemically distinct populations. J Neurosci *27*, 2318-2330.

Beraneck, M., and Cullen, K. E. (2007). Activity of vestibular nuclei neurons during vestibular and optokinetic stimulation in the alert mouse. J Neurophysiol *98*, 1549-1565.

Beraneck, M., McKee, J. L., Aleisa, M., and Cullen, K. E. (2008). Asymmetric recovery in cerebellar-deficient mice following unilateral labyrinthectomy. J Neurophysiol *100*, 945-958.

Broussard, D. M., and Kassardjian, C. D. (2004). Learning in a simple motor system. Learn Mem *11*, 127-136.

Calabrese, D. R., and Hullar, T. E. (2006). Planar relationships of the semicircular canals in two strains of mice. J Assoc Res Otolaryngol *7*, 151-159.

Carter, A. G., Soler-Llavina, G. J., and Sabatini, B. L. (2007). Timing and location of synaptic inputs determine modes of subthreshold integration in striatal medium spiny neurons. J Neurosci *27*, 8967-8977.

Dittman, J. S., and Regehr, W. G. (1998). Calcium dependence and recovery kinetics of presynaptic depression at the climbing fiber to Purkinje cell synapse. J Neurosci *18*, 6147-6162.

du Lac, S., and Lisberger, S. G. (1995). Membrane and firing properties of avian medial vestibular nucleus neurons in vitro. J Comp Physiol [A] *176*, 641-651.

Epema, A. H., Gerrits, N. M., and Voogd, J. (1988). Commissural and intrinsic connections of the vestibular nuclei in the rabbit: a retrograde labeling study. Exp Brain Res *71*, 129-146.

Faulstich, B. M., Onori, K. A., and du Lac, S. (2004). Comparison of plasticity and development of mouse optokinetic and vestibulo-ocular reflexes suggests differential gain control mechanisms. Vision Res *44*, 3419-3427.

Feng, G., Mellor, R. H., Bernstein, M., Keller-Peck, C., Nguyen, Q. T., Wallace, M., Nerbonne, J. M., Lichtman, J. W., and Sanes, J. R. (2000). Imaging neuronal subsets in transgenic mice expressing multiple spectral variants of GFP. Neuron *28*, 41-51.

Foster, K. A., Crowley, J. J., and Regehr, W. G. (2005). The influence of multivesicular release and postsynaptic receptor saturation on transmission at granule cell to Purkinje cell synapses. J Neurosci *25*, 11655-11665.

Foster, K. A., Kreitzer, A. C., and Regehr, W. G. (2002). Interaction of postsynaptic receptor saturation with presynaptic mechanisms produces a reliable synapse. Neuron *36*, 1115-1126.

Furman, J. M., O'Leary, D. P., and Wolfe, J. W. (1982). Dynamic range of the frequency response of the horizontal vestibulo-ocular reflex of the alert rhesus monkey. Acta Otolaryngol *93*, 81-91.

Gasparini, S., and Magee, J. C. (2006). State-dependent dendritic computation in hippocampal CA1 pyramidal neurons. J Neurosci *26*, 2088-2100.

Gittis, A. H., and du Lac, S. (2006). Intrinsic and synaptic plasticity in the vestibular system. Curr Opin Neurobiol *16*, 385-390.

Goldberg, J. M., and Fernandez, C. (1971). Physiology of peripheral neurons innervating semicircular canals of the squirrel monkey. I. Resting discharge and response to constant angular accelerations. J Neurophysiol *34*, 635-660.

Harrison, J., and Jahr, C. E. (2003). Receptor occupancy limits synaptic depression at climbing fiber synapses. J Neurosci *23*, 377-383.

Highstein, S. M., Rabbitt, R. D., Holstein, G. R., and Boyle, R. D. (2005). Determinants of spatial and temporal coding by semicircular canal afferents. J Neurophysiol *93*, 2359-2370.

Holstein, G. R. (2000). Inhibitory amino acid transmitters in the vestibular nuclei. In Neurochemistry of the vestibular system, A. J. Beitz, and J. H. Anderson, eds. (Florida, CRC Press), pp. 143-162.

Huterer, M., and Cullen, K. E. (2002). Vestibuloocular reflex dynamics during high-frequency and high-acceleration rotations of the head on body in rhesus monkey. J Neurophysiol *88*, 13-28.

Huwe, J. A., and Peterson, E. H. (1995). Differences in the brain stem terminations of large- and small-diameter vestibular primary afferents. J Neurophysiol *74*, 1362-1366.

Isaacson, J. S., and Walmsley, B. (1996). Amplitude and time course of spontaneous and evoked excitatory postsynaptic currents in bushy cells of the anteroventral cochlear nucleus. J Neurophysiol *76*, 1566-1571.

Klyachko, V. A., and Stevens, C. F. (2006). Excitatory and feed-forward inhibitory hippocampal synapses work synergistically as an adaptive filter of natural spike trains. PLoS Biol *4*, e207.

Lasker, D. M., Han, G. C., Park, H. J., and Minor, L. B. (2008). Rotational Responses of Vestibular-Nerve Afferents Innervating the Semicircular Canals in the C57BL/6 Mouse. J Assoc Res Otolaryngol.

Lewis, M. R., Phelan, K. D., Shinnick-Gallagher, P., and Gallagher, J. P. (1989). Primary afferent excitatory transmission recorded intracellularly in vitro from rat medial vestibular neurons. Synapse *3*, 149-153.

Lisberger, S. G., and Miles, F. A. (1980). Role of primate medial vestibular nucleus in long-term adaptive plasticity of vestibuloocular reflex. J Neurophysiol *43*, 1725-1745.

Liu, G., Choi, S., and Tsien, R. W. (1999). Variability of neurotransmitter concentration and nonsaturation of postsynaptic AMPA receptors at synapses in hippocampal cultures and slices. Neuron *22*, 395-409.

Minor, L. B., Lasker, D. M., Backous, D. D., and Hullar, T. E. (1999). Horizontal vestibuloocular reflex evoked by high-acceleration rotations in the squirrel monkey. I. Normal responses. J Neurophysiol *82*, 1254-1270.

Oliva, A. A., Jr., Jiang, M., Lam, T., Smith, K. L., and Swann, J. W. (2000). Novel hippocampal interneuronal subtypes identified using transgenic mice that express green fluorescent protein in GABAergic interneurons. J Neurosci *20*, 3354-3368.

Pastor, A. M., de la Cruz, R. R., and Baker, R. (1992). Characterization and adaptive modification of the goldfish vestibuloocular reflex by sinusoidal and velocity step vestibular stimulation. J Neurophysiol *68*, 2003-2015.

Pulaski, P. D., Zee, D. S., and Robinson, D. A. (1981). The behavior of the vestibulo-ocular reflex at high velocities of head rotation. Brain Res *222*, 159-165.

Robinson, D. A. (1976). Adaptive gain control of vestibuloocular reflex by the cerebellum. J Neurophysiol *39*, 954-969.

Robinson, D. A. (1981). The use of control systems analysis in the neurophysiology of eye movements. Annu Rev Neurosci *4*, 463-503.

Rozov, A., and Burnashev, N. (1999). Polyamine-dependent facilitation of postsynaptic AMPA receptors counteracts paired-pulse depression. Nature *401*, 594-598.

Sato, F., and Sasaki, H. (1993). Morphological correlations between spontaneously discharging primary vestibular afferents and vestibular nucleus neurons in the cat. J Comp Neurol *333*, 554-566.

Saviane, C., and Silver, R. A. (2006). Fast vesicle reloading and a large pool sustain high bandwidth transmission at a central synapse. Nature *439*, 983-987.

Scudder, C. A., and Fuchs, A. F. (1992). Physiological and behavioral identification of vestibular nucleus neurons mediating the horizontal vestibuloocular reflex in trained rhesus monkeys. J Neurophysiol *68*, 244-264.

Shimazu, H., and Precht, W. (1965). Tonic and kinetic responses of cat's vestibular neurons to horizontal angular acceleration. J Neurophysiol *28*, 991-1013.

Skavenski, A. A., and Robinson, D. A. (1973). Role of abducens neurons in vestibuloocular reflex. J Neurophysiol *36*, 724-738.

Stahl, J. S. (2002). Calcium channelopathy mutants and their role in ocular motor research. Ann N Y Acad Sci *956*, 64-74.

Stahl, J. S., van Alphen, A. M., and De Zeeuw, C. I. (2000). A comparison of video and magnetic search coil recordings of mouse eye movements. J Neurosci Methods *99*, 101-110.

Straka, H., and Dieringer, N. (1996). Uncrossed disynaptic inhibition of second-order vestibular neurons and its interaction with monosynaptic excitation from vestibular nerve afferent fibers in the frog. J Neurophysiol *76*, 3087-3101.

Straka, H., and Dieringer, N. (2004). Basic organization principles of the VOR: lessons from frogs. Prog Neurobiol *73*, 259-309.

Telgkamp, P., Padgett, D. E., Ledoux, V. A., Woolley, C. S., and Raman, I. M. (2004). Maintenance of high-frequency transmission at purkinje to cerebellar nuclear synapses by spillover from boutons with multiple release sites. Neuron *41*, 113-126.

Telgkamp, P., and Raman, I. M. (2002). Depression of inhibitory synaptic transmission between Purkinje cells and neurons of the cerebellar nuclei. J Neurosci *22*, 8447-8457.

Trussell, L. O., Zhang, S., and Raman, I. M. (1993). Desensitization of AMPA receptors upon multiquantal neurotransmitter release. Neuron *10*, 1185-1196.

Vidal, P. P., Degallaix, L., Josset, P., Gasc, J. P., and Cullen, K. E. (2004). Postural and locomotor control in normal and vestibularly deficient mice. J Physiol *559*, 625-638.

von Gersdorff, H., and Borst, J. G. (2002). Short-term plasticity at the calyx of held. Nat Rev Neurosci *3*, 53-64.

Wong, A. Y., Graham, B. P., Billups, B., and Forsythe, I. D. (2003). Distinguishing between presynaptic and postsynaptic mechanisms of short-term depression during action potential trains. J Neurosci *23*, 4868-4877.

Yang, A., and Hullar, T. E. (2007). The relationship of semicircular canal size to vestibular-nerve afferent sensitivity in mammals. J Neurophysiol.

Yang, H., and Xu-Friedman, M. A. (2008). Relative roles of different mechanisms of depression at the mouse endbulb of held. J Neurophysiol *99*, 2510-2521.

Zucker, R. S., and Regehr, W. G. (2002). Short-term synaptic plasticity. Annu Rev Physiol *64*, 355-405.

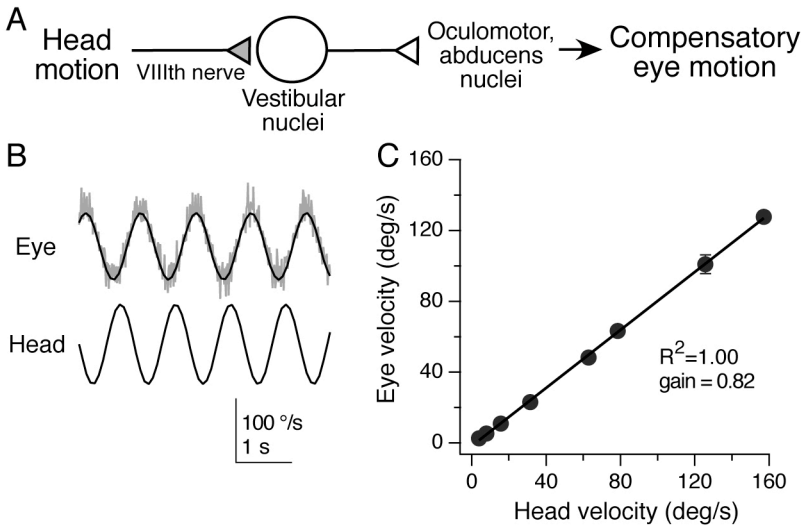

Fig. 2.1 Linear relationship between head velocity and compensatory eye velocity. A, The basic circuitry of the vestibulo-ocular reflex; the vestibular nerve afferent synapse onto vestibular nucleus neurons (shaded) is the focus of this study. B, In the dark, mice were rotated sinusoidally in the horizontal plane at a frequency of 1 Hz. Example of eye and head velocity in one mouse. Instantaneous eye velocity is shown in gray, with sinusoidal fit in black. C, Summary data for six mice showing that eye velocity was a linear function of head motion at 1 Hz over a wide range of velocities. Error bars represent SD and in most cases are smaller than the symbols.

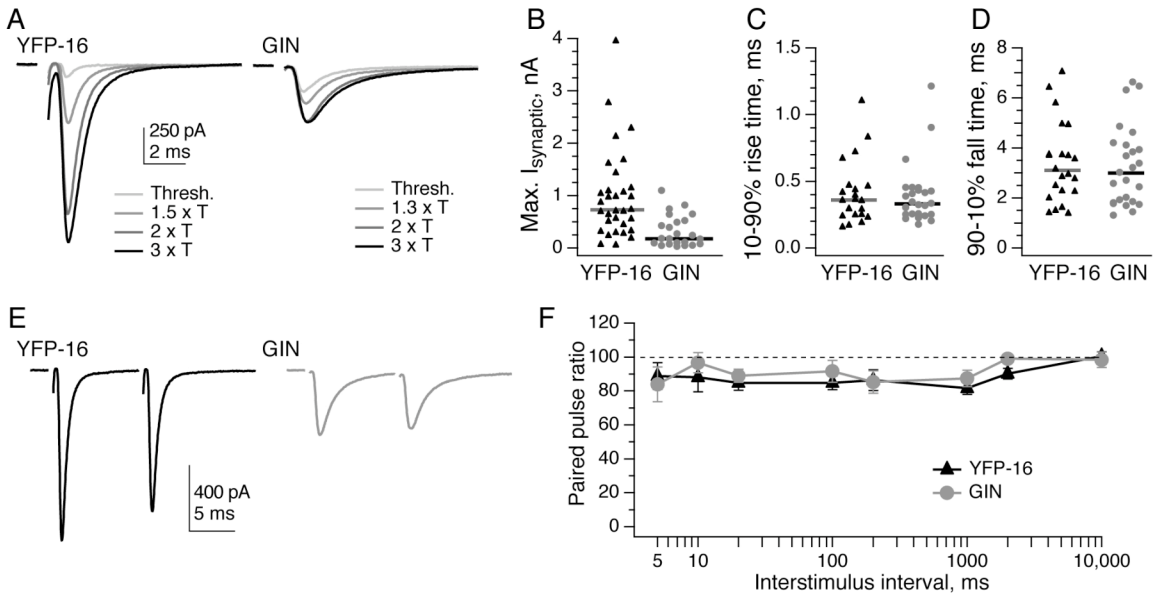

Fig. 2.2 EPSCs from vestibular afferents exhibit rapid kinetics and little paired-pulse modulation. A, Example EPSCs resulting from increasing stimulation intensities of the vestibular nerve in slice preparation, recorded from neurons labeled in the YFP-16 line (left) and the GIN line (right). Stimulation artifacts are blanked for clarity. T = threshold stimulation intensity. B, The maximum EPSC amplitude that could be elicited in YFP-16 neurons was 3-fold higher than that in GIN neurons ($p < 0.0001$). Two YFP-16 neurons had maximal EPSCs of 5-6 nA (not shown for graphical clarity). C, EPSC 10-90% rise times are rapid both in YFP-16 neurons and GIN neurons. D, EPSC 90-10% decay times (see Experimental Procedures) are also swift in YFP-16 and GIN neurons. Kinetics were usually measured at 1.5-3x the threshold stimulation intensity. Horizontal bars represent medians. E, Paired pulse. Examples of EPSCs elicited at a 10 ms interval in a YFP-16 (left) and GIN (right) neuron. F, Summary of paired-pulse ratios (100*EPSC2/EPSC1) across interstimulus intervals from 5 ms to 10 s. EPSCs in both YFP-16 and GIN neurons depressed to ~85% of their original values at stimulus intervals from 5 ms to 1 s, with no history dependence visible at intervals of 10 s. N = 3-10 cells per data point. Data are shown as mean ± SEM in this and subsequent figures.

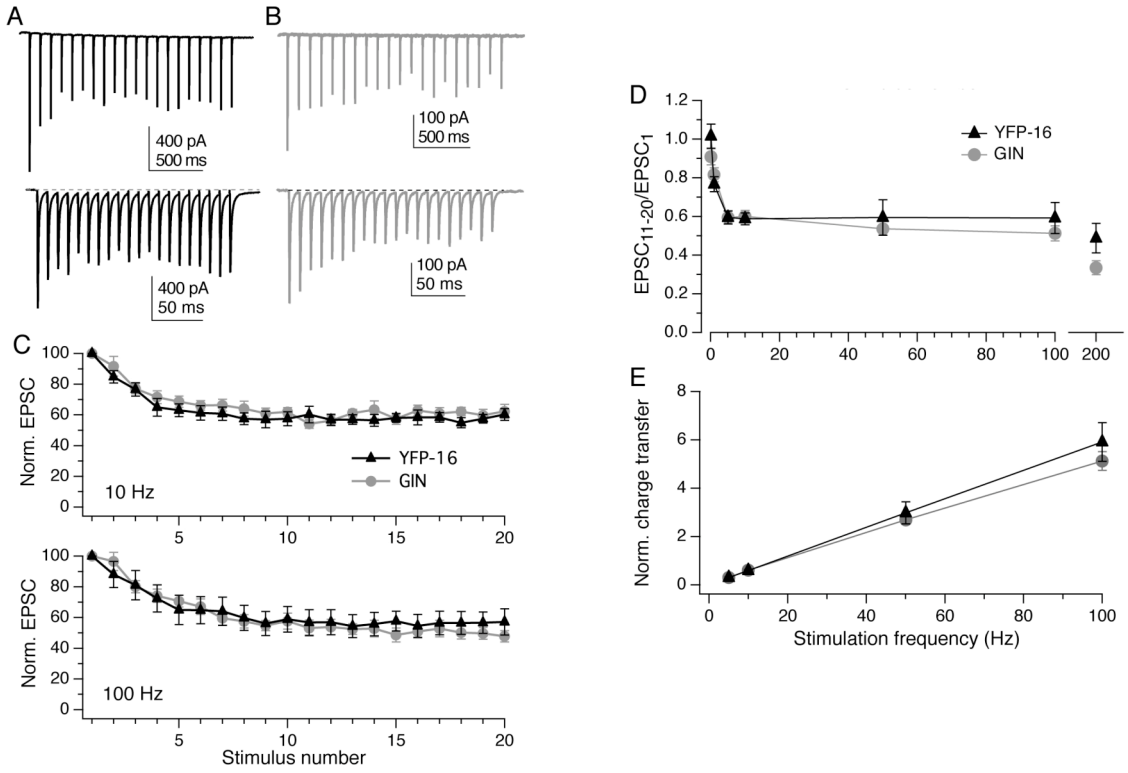

Fig. 2.3 Trains of stimuli evoke frequency-independent steady-state depression. A, EPSCs measured in a YFP-16 neuron during vestibular nerve stimulation at 10 Hz (top) or 100 Hz (bottom). B, Same as A, GIN neuron. In both examples, EPSCs rapidly achieve a steady-state plateau of ~60% of the initial value, regardless of stimulation frequency. C, Population data from both YFP-16 (n = 8) and GIN neurons (n = 11) with trains of 20 stimuli elicited at 10 Hz. D, Population data from YFP-16 (n = 7) and GIN neurons (n = 8) with trains of 20 stimuli elicited at 100 Hz. D, Summary of the magnitude of steady-state depression, defined as the average of $EPSC_{11\text{-}20}$ divided by $EPSC_1$, across stimulation frequencies from 0.1 to 200 Hz. In the steady state, EPSC amplitude does not depend on stimulation frequency from 5 to 100 Hz in either YFP-16 or GIN neurons. E, Total charge transfer per second during steady-state transmission increases linearly with increasing stimulation frequency ($R^2 = 1$ for both neuron types). Charge transfer was calculated as the average integrated area under the EPSC in steady state ($EPSC_{11\text{-}20}$), normalized to initial EPSC amplitude, and multiplied by the rate of stimulation.

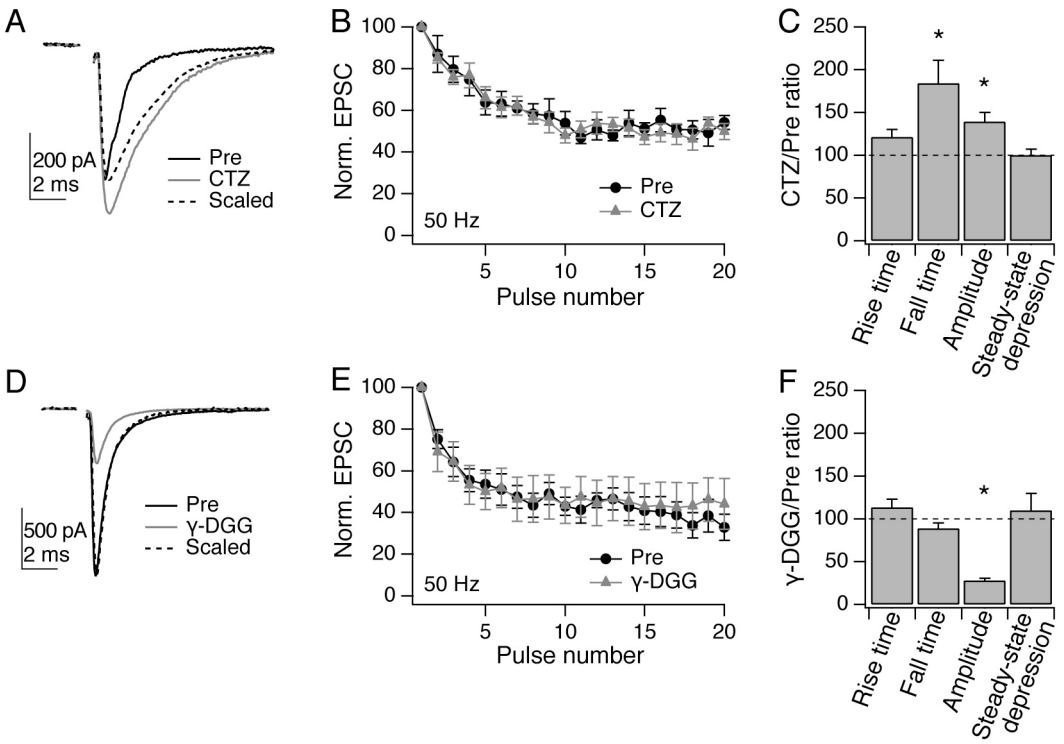

Fig. 2.4 Postsynaptic receptor desensitization and saturation do not affect short-term plasticity. A, Example EPSC elicited by vestibular nerve stimulation in a YFP-16 neuron (black). Cyclothiazide (100 μm; gray) increased EPSC amplitude and slowed its decay, as is evident in the experimental trace peak-scaled to control (dotted line). B, No difference is seen in steady-state depression of synaptic currents in the presence of cyclothiazide at 50 Hz (shown) or other frequencies tested (n = 6). C, Summary of kinetics and steady-state depression across the population. The peak EPSC amplitude and the 80-20% decay time were both significantly increased by cyclothiazide (n = 6; $p < 0.05$). Steady-state depression, quantified as EPSC11-20/EPSC1, was unaffected. D, Example EPSC elicited in a YFP-16 neuron. γ-DGG (2 mM; gray) reduced EPSC amplitude without significantly affecting kinetics (scaled trace, dotted line). E, Reducing receptor saturation does not affect short-term depression at 50 Hz (shown) or other frequencies tested (n = 6). F, Summary of kinetics and steady-state depression across the population. EPSC amplitude was significantly reduced ($p < 0.05$) while other parameters were unaffected.

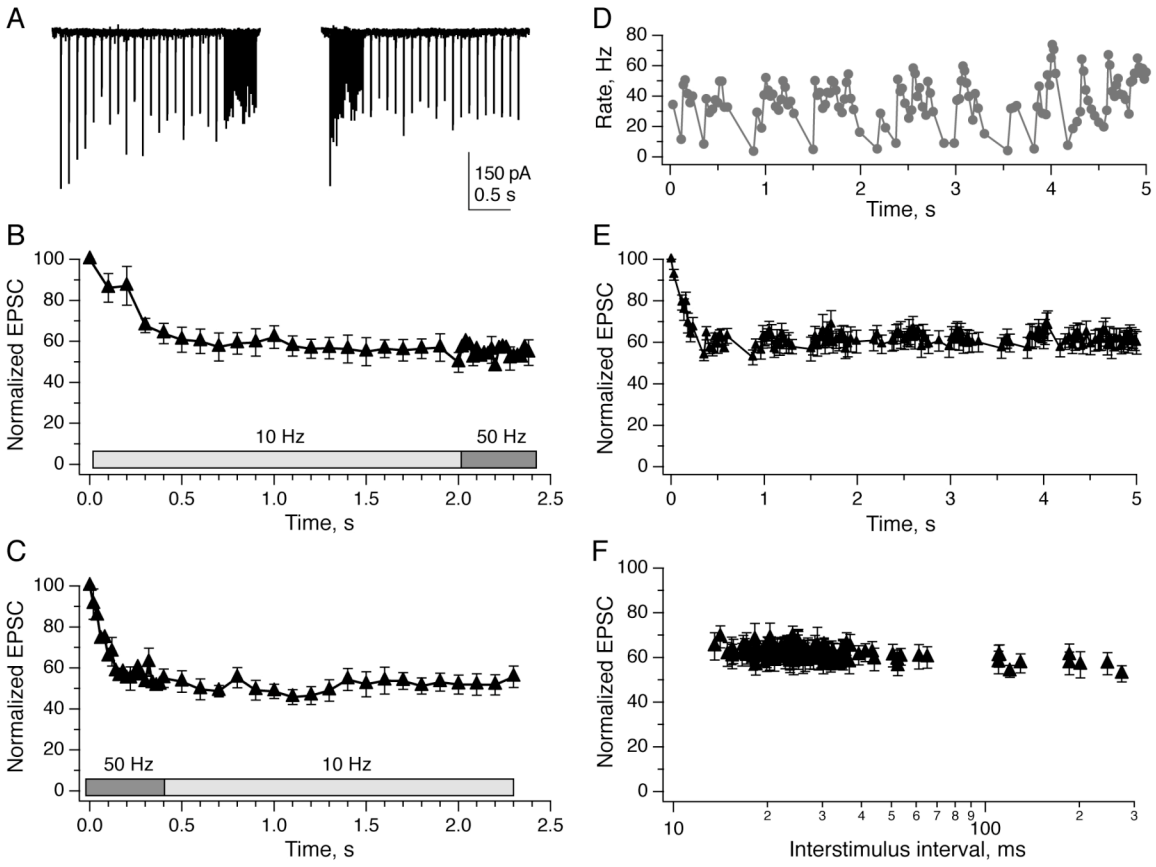

Fig. 2.5 The amplitude of steady state transmission is not affected by changes in stimulation rate. A, Example EPSCs recorded in a YFP-16 neuron during vestibular afferent stimulation with 20 pulses at 10 Hz followed by 20 pulses at 50 Hz (left) and 50 Hz followed by 10 Hz (right). Group data indicate that EPSC amplitudes were not affected by stimulus shifts from 10 Hz to 50 Hz (B, n=8) or from 50 Hz to 10 Hz (C, n=9). D, Naturalistic stimulus train, displayed as instantaneous rate vs time, that approximates the firing pattern of a typical mouse vestibular afferent firing during head movements (see Experimental Procedures). E, Average EPSC responses to the naturalistic stimulus shown in D (n = 7). EPSC amplitude decreased rapidly to a steady state level that was not affected by instantaneous variations in stimulus rate. F, Replotting the data from E demonstrated that EPSC amplitude did not depend on interstimulus interval. The responses to the first five stimuli have been omitted from this plot for clarity.

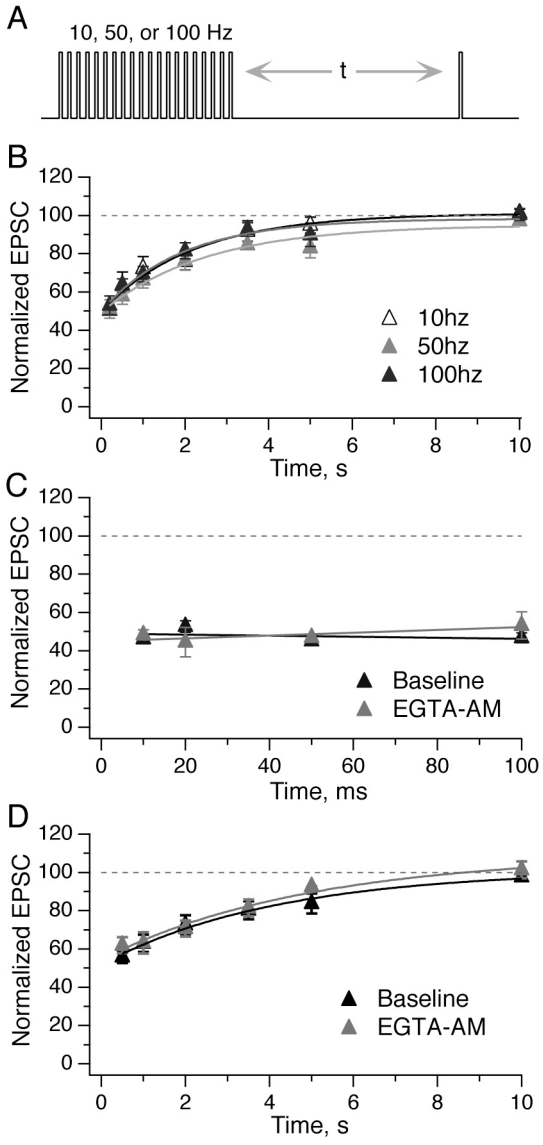

Fig. 2.6 Recovery of EPSC amplitudes from depression is slow and monoexponential. A, Vestibular afferents were stimulated with conditioning trains of 20 pulses at 10, 50, or 100 Hz, followed by a test pulse at a variable time afterwards. B, Recovery from depression was best fit with a single exponential. The tau of recovery was similar across the three conditioning frequencies of 10, 50, and 100 Hz (2.2, 2.5, and 1.9 s respectively; n = 5). C, EPSCs did not recover in amplitude during shorter intervals (10-100 ms, all tested with 50 Hz conditioning train). Application of 100 µM EGTA-AM for 5 min had no effect on recovery (n = 4). D, EGTA-AM had no effect on the timecourse of recovery for longer test intervals (conditioning train, 50 Hz; n = 7).

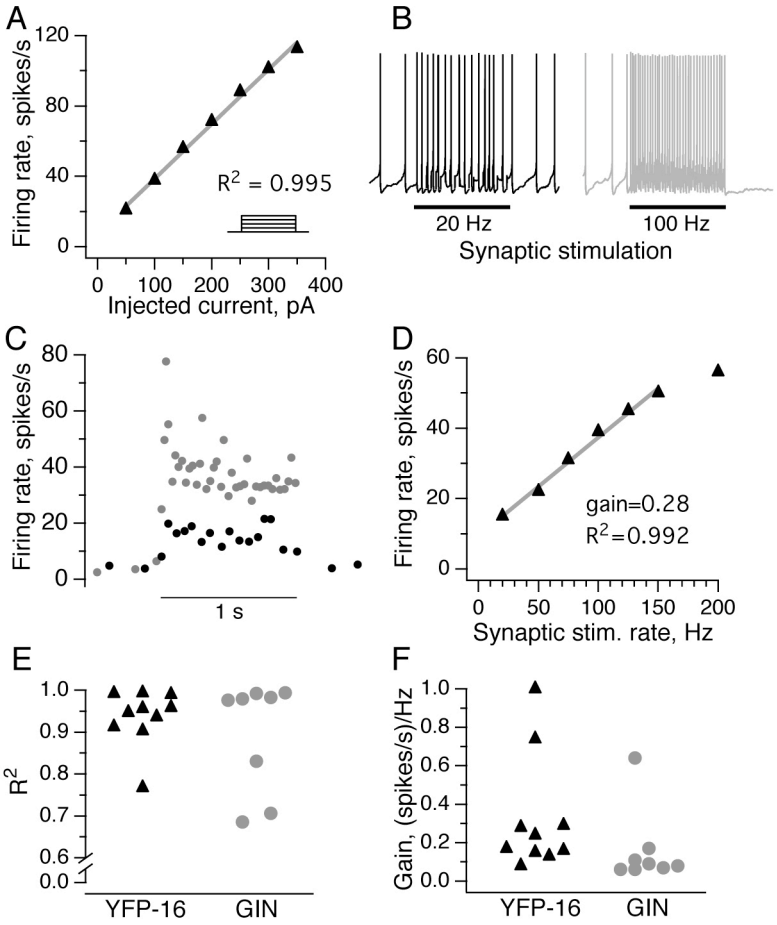

Fig. 2.7 Injected and synaptic currents can each drive linear increases in MVN firing rates. A, The firing rate of an example YFP-16 neuron during 1 s steps of depolarizing somatic current injection of varying amplitudes (inset). Neuronal firing rates, averaged over the 1 s step, were linearly related to injected current. B, Synaptic stimulation for 1 s drives increases in firing rate in the same neuron shown in A. Somatic current injection was used to maintain a stable baseline firing rate of ~5 Hz. C, The postsynaptic firing rate in this neuron at the two synaptic stimulation rates shown (20 and 100 Hz). D, Linear input to firing rate relationship for the neuron shown in C. The slope is less than 1, indicating the linear synaptic summation of input currents over time. E, Summary of goodness of linear fits in response to stimuli that ranged from 20 to 150 Hz rates in the population of YFP-16 and GIN neurons. F, Summary of firing response gains across the same population. Of the 8 GIN and 10 YFP-16 neurons tested, only one fired action potentials with every presynaptic stimulus (gain = 1).

Chapter 3: Concerted functional and anatomical specializations mediate linear synaptic transmission

Abstract

Synapses exhibit great diversity in their molecular and functional properties, which are hypothesized to correspond to their behavioral functions. However, limited knowledge of the precise behavioral and computational goals of individual synapses in the central nervous system has hindered efforts to link synaptic properties with functional outcomes. Here, we investigate the functional role of individual synaptic specializations at a synapse with well-defined behavioral and computational functions. The vestibular nerve synapse conveys head motion signals to the central nervous system and drives vestibular reflexes that stabilize the eyes, head, and body in space. Vestibular reflexes are fast, accurate, and, in the case of the vestibulo-ocular reflex (VOR), linear. The linear transformation of head movements into eye movements underlies clear vision during self-motion. Each aspect of the supporting circuitry examined thus far has been shown to be linear, including the first central synapse in the system: the vestibular nerve synapse. To identify how this synapse is specialized to mediate fast, linear transmission, we used whole-cell patch clamp recordings and pharmacology in mouse brainstem slices, electron microscopy, and computational modeling. This study demonstrates that the concerted function of multiple synaptic properties produce linear synaptic transmission that spans the behaviorally relevant range.

Introduction

Neural circuits are precisely wired to transform and relay behaviorally relevant signals. Circuit function is largely sculpted by the properties of underlying synaptic connections, whose performance is though to be specialized to meet the goals of animal behavior (Abbott and Regehr, 2004). Synaptic transmission is dynamic, and recent activity at a synapse can profoundly modify the strength of transmission for milliseconds to minutes, a process known as short-term synaptic plasticity (Zucker and Regehr, 2002). The extent and rate-dependence of short-term depression or facilitation vary across different synapse types and endow each with specialized computational features that regulate the ability of presynaptic neurons to influence their targets. Multiple synaptic properties are known to influence short-term plasticity, including postsynaptic receptor sensitivity, neuotransmitter release, and synapse anatomy (Fioravante and Regehr, 2011; Jones and Westbrook, 1996; Xu-Friedman and Regehr, 2004). What remains unknown, however, is how such properties subserve the behavioral goals of neural circuits and the extent to which goal-directed synaptic performance is determined by an individual property versus the ensemble function of multiple specializations. The limited ability to connect central synapses to defined functional and computational goals has hindered progress on linking synaptic mechanisms to behavioral functions. Here, we investigated the molecular and cellular basis of synaptic computation at a synapse that mediates a defined behavioral function and performs the simplest computation in the central nervous system: linear scaling of pre- to postsynaptic firing rates.

The vestibular nerve afferent synapse transmits primary sensory signals about head motion to neurons in brainstem nuclei, which target motor neurons and drive

reflexive movements. To stabilize the eyes, head, and body in space, this brief reflex circuit must generate motor responses that are well matched to sensory inputs, and in the case of the vestibulo-ocular reflex (VOR), eye movements are perfectly linear in relation to head movements across a wide range of conditions (Bagnall et al., 2008; Robinson, 1981). Head motion drives linear changes in the firing rates of both vestibular nerve afferents and vestibular nucleus neurons *in vivo* (Goldberg and Fernandez, 1971; Shimazu and Precht, 1965). Vestibular nerve synapses onto nucleus neurons exhibit exceptional broadband linear transmission (Bagnall et al., 2008). This linearity is achieved not through a lack of short-term synaptic plasticity but rather through the precise implementation of rate-independent short-term depression across the entire range of behaviorally relevant rates. In this study, we sought to identify the unique properties of the vestibular nerve synapse that promote linear transmission across the wide range of *in vivo* presynaptic firing rates (5 – 125 Hz). The results demonstrate that synaptic linearity requires the specialized function and concerted interaction of each pre- and postsynaptic property.

Methods

Electrophysiology

Oblique coronal brainstem slices were prepared from C57BL/6 mice aged 18-28 days postnatal. Mice were deeply anesthetized with Nembutal and then decapitated. The brain was dissected in 4 ºC artificial cerebrospinal fluid (ACSF, in mM: 124 NaCl, 5 KCl, 1.0 $MgSO_4$, 26 $NaHCO_3$, 2.5 $CaCl_2$, 1 NaH_2PO_4, and 11 dextrose) bubbled with 95% O_2/5% CO_2. 300-µm slices were cut on a DSK DTK-1500E, Leica VT1000S, or

Leica VT1200S vibratome and allowed to recover in 34 ºC ACSF for 30 min. Slices rested at room temperature before being transferred to a recording chamber and perfused with 34 ºC ACSF containing a near physiological calcium concentration (1.5 mM $CaCl_2$), 1-10 µM strychnine, and 100 µM picrotoxin. All experiments were carried out in accordance with the standards of the Salk Institute IACUC.

Neurons were visualized under IR-DIC on an Olympus BX51W1 microscope. Patch pipettes (2-5 MΩ) were pulled from flame-polished glass (Warner) and filled with internal solution contained (in mM): 140 K gluconate, 20 HEPES, 8 NaCl, 0.1 EGTA, 0.1 Spermine, 2 Mg-ATP, 0.3 Na_2-GTP. The vestibular nerve tract was identifiable under 10X magnification, and afferents were stimulated with a bipolar concentric stimulating electrode (FHC, Maine) controlled with two Isoflex stimulus isolation units (AMPI, Israel). Stimulating electrodes were localized to the vestibular nerve lateral to the vestibular complex (approximate location: 6-6.4 mm caudal to bregma, 4.4 mm ventral to the horizontal plane passing through bregma and lambda, and 1.7-1.8 mm lateral to the midline). A biphasic pulse, consisting of two 100 µsec pulses of opposite polarity with a 100 µsec interval, was delivered to the electrode to avoid charge buildup. Series resistance was monitored continuously with small hyperpolarizing square pulses, and experiments showing a series resistance above 16 MΩ were excluded.

Data were acquired with a Multiclamp 700B (Axon Instruments) with low-pass filtering at 4-10 kHz for voltage clamp and 10 kHz for current clamp. Data were digitized at 40 kHz with an ITC- 18 (InstruTECH). House-written code in Igor 6 (Wavematrics) was used for acquisition and analysis. Data are reported as mean ± SEM, and statistical significance was evaluated with paired (where possible) or unpaired Wilcoxon signed-

rank tests in KaleidaGraph 3.6 (Synergy Software). Stimulus artifacts were blanked in figures for clarity in all figures. Chemicals were purchased from Sigma (St. Louis MO), except for dl-TBOA (Tocris, Bristol, UK), γ-DGG and TEA (Ascent Scientific, Bristol, UK).

Estimation of quantal parameters

Quantal parameters were estimated using multiple probability fluctuation analysis (MPFA; Silver, 2003). EPSCs were recorded under 4-5 different extracellular Ca^{2+} concentrations (0.5 – 4mM), while the divalent concentration was maintained by varying the extracellular Mg^{2+} concentration. Stable epochs were delimited by Spearman rank-order analysis, and an average of 80 ± 6 EPSCs were recorded per condition.

The relationship between the mean EPSC amplitude (I) and the variance of the EPSC amplitude (σ^2) at each synapse was approximated by the function

$$\sigma^2(I) = \left[IQ_P - \frac{Q_P I^2 (1+\alpha)}{I + NQ_P \alpha} \right] \left(1 + CV_{QII}^2\right) + Q_P I CV_{QI}^2 \qquad (1)$$

where Q_P is the quantal size, N is the number of release sites, CV_{QI}^2 is the coefficient of variation in EPSC amplitude due to intrasite variability, CV_{QII}^2 is the coefficient of variation in EPSC amplitude due to intersite variability, and α is a measure of the nonuniformity of release probability across release sites (Silver, 2003).

The total nonuniformity in Q_P was estimated from coefficient of variation of the mean postsynaptic response to a single quantum of transmitter. Q_P was estimated from asynchronous EPSCs evoked following the substitution of Ca^{2+} with Sr^{2+}(5 mM). The

total nonuniformity in Q_P was found to be 0.56±0.08 (n=5). The inter- and intrasite variability were assumed to contribute equally to the total variability.

Data were fit to equation (1) using nonlinear least-squares regression. Errors in estimates of the variance were determined using h-statistics, which provide unbiased estimators for central moments of distributions, and the fit for each synapse was evaluated using the chi-square goodness-of-fit test (Saviane and Silver, 2006a; Silver, 2003). Only fits with $p \geq 0.05$ accepted for further analysis. Three cells were rejected on account of the maximal $P_R < 0.5$, and an additional cell was excluded because the relationship between mean and variance was best modeled by a linear rather than a quadratic relationship. Given that MPFA could not be applied to these four cells, which presumably had quite low P_R, the estimates in this study may slightly overestimate the average P_R.

Estimates of the number of release sites (N) and the quantal size (Q_P) for each synapse were computed from equation (1). Estimates of the release probability (P_R) were then computed from the binomial model

$$I = NP_R Q_P. \quad (2)$$

In 6 of the cells used for MPFA analyses, changes in the quantal parameters during 10 Hz train stimulation were estimated using coefficient of variation (CV) analysis of EPSC amplitude (Saviane and Silver, 2006b, 2007). The CV was calculated for each pulse in 20-30 pulse trains. Using the estimate of N from MFPA, P_R was estimated for each pulse using:

$$CV = \frac{\sigma}{I} = \sqrt{\frac{(1 - P_R)(1 + CV_{QII}^2) + CV_{QI}^2}{NP_R}} \quad (3)$$

Q_P was then calculated for each pulse using equation (2).

Models of short-term synaptic transmission

Short-term plasticity at the vestibular nerve synapse was modeled by a two pool system of vesicle dynamics. At each of N terminals, vesicles transitioned between two pools: "reserve" and "readily-releasable". A maximum of two vesicles could be in the readily-releasable pool (RRP) at any one time at each terminal. Vesicles moved from the reserve pool to the RRP with Poisson statistics, such that the probability that k vesicles transition to the RRP within a time interval dt has the distribution

$$P_{\text{Reserve}\rightarrow\text{RRP}}(k) = \frac{\left(\frac{dt}{\tau_{RRP}}\right)^k e^{-\left(\frac{dt}{\tau_{RRP}}\right)}}{k!} \quad (4)$$

where τ_{RRP} is the time constant of transition to the RRP. All terminals were considered to be statistically independent of each other.

Upon arrival of an action potential at the terminal, a RRP vesicle is released with probability, Pr(t). Consistent with experimental findings, a maximum of one vesicle per terminal could be released per action potential. The release probability of each vesicle is a function of recent activity at the terminal. Upon initial transition to the RRP, the release probability of each vesicle is set to $Pr_{\text{Steady-state}}$. The release probability is constant unless more than 500ms has elapsed since the arrival of the last action potential. After 500ms, the release probabilities increased according to the differential equation

$$\frac{d\Pr(t)}{dt} = -\tau_{prime}\left(\Pr(t) - \Pr_{Max}\right) \quad (5)$$

such that the probability of release of a docked vesicle increases asymptotically to Pr_{Max}, with a time constant of τ_{prime}. In its initial state, the release probability of each vesicle is set to Pr_{Max} to reflect the lack of nerve activity in the *in vitro* preparation. The short-term dynamics thus result from the limited initial supply of vesicles with high release probability. As long as activity in the nerve occurs at frequencies above 2Hz, release probabilities remain constant at $Pr_{Steady\text{-}state}$.

Parameters were set based on several experimental findings. $Pr_{Max} = 0.22$ and $N = 36$ were defined based on the MPFA analysis of the first pulse in each train. $Pr_{Steady\text{-}state}$ was set to $0.53 \times Pr_{Max}$, based the results from the CV analysis that indicated the short-term depression results from decreases in release probability and consistent with the observed magnitude of short-term depression. $\tau_{prime} = 2.67$s was set to the slow time constant of recovery from vesicle depletion. τ_{RRP} was fit to optimize the linearity of the steady state EPSC amplitudes at 10-100 Hz and to minimize the steady state EPSC amplitude at 300 Hz. Linearity of the model was determined by ratio of the steady-state response at 100 Hz versus at 10 Hz. Models were accepted as liniear if this ratio was greater than 0.96. For all the parameter values that yielded linearity at 10-100Hz, the value that minimized the EPSC amplitude at 300 Hz was chosen as optimal. This optimization yielded $\tau_{RRP} = 22$ ms when the RRP contained 2 vesicles and $\tau_{RRP} = 8$ ms when the RRP contained 1 vesicle.

Vesicle release was simulated for 20 repetitions of 50 action potential trains in the nerve at frequencies ranging from 0.1Hz to 300 Hz. Simulations were performed for 10

model synapses with identical parameters to obtain the average short-term dynamics. The number of vesicles released during each pulse across all terminals was summed for each pulse in the stimulus train and normalized by the number of vesicles released during the first pulse (Fig. 4.7, 4.8). Simulations of vesicle dynamics under high calcium concentrations (3.6mM) were conducted by elevating the release probability to the estimated value at that concentration (Pr_{Max} = 0.64).

Vestibular nerve labeling and EM analysis

Mice were deeply anesthetized with Ketamine/Xylazine (80 mg/kg and 10 mg/kg). The skull overlaying the cerebellum was exposed, and the interparietal plate was removed lateral to the midline. The cerebellum was then carefully aspirated, while avoiding major blood vessels, until the eigth nerve was exposed. Using a capillary glass pipette, a near-saturating solution of Texas red dextran (10,000 MW) in DI water was injected into the nerve where it exits the temporal bone of the scull. The exposed cavity was then filled with gelfoam soaked with lactated Ringer's, while the animal was kept anesthetized for 4-6 hours.

Mice were then anesthetized with Nembutal and transcardially perfused with PBS followed by 4% formaldehyde, 0.02% glutaraldehyde in PBS. The brain was removed and left in fixative until slicing. The brain was rinsed in cold PBS and the cerebellum and brainstem were cut into 50 μm slices on a vibratome. Slices were placed in a chamber and imaged on a fluorescence microscope to locate labeled vestibular neurons. Following imaging, slices were fixed in 2% glutaraldehyde in 0.1 M sodium cacodylate buffer, rinsed, postfixed in 1% osmium tetroxide and 1% potassium ferrocyanide, rinsed,

en bloc stained in 1% uranyl acetate, dehydrated with glycol methacrylate and flat embedded in Epon. The slices were blocked and mounted onto Epon stubs for sectioning parallel to the plane of imaging. Ultrathin sections (~60 nm) were cut on an ultramicrotome, collected onto formvar-coated slot grids and stained with 2% uranyl acetate and 0.2% lead citrate. The sections were examined in a JEOL 100CXII transmission electron microscope equipped with a digital camera. Neurons identified by the electron microscope were matched to the fluorescent images on the basis of morphology and location. Serial images of individual terminals were aligned and analyzed with Reconstruct software. Eight boutons were three-dimensionally reconstructed; each spanned 45-86 sections. Seven boutons arose from thick afferents, but the one arising from a thin afferent was not unique (volume: 17.95 μm^3; release sites: 16; active zone area: 0.14 ± 0.02 μm^2). Release sites were identified based on a presynaptic cluster of vesicles opposed to a postsynaptic density.

Results

We investigated the mechanisms underlying linear synaptic transmission by recording vestibular nerve synaptic currents in medial vestibular nucleus neurons. Experiments were conducted at 34°C and in ACSF containing 1.5 mM Ca^{2+}, so that synaptic transmission was near physiological. During 50-pulse stimulus trains to the vestibular nerve, the peak EPSC amplitude depressed progressively during the first ~10-15 stimuli and then reached a sustained, steady-state amplitude of ~55% relative to the first EPSC (Fig. 3.1A,B). The steady-state amplitude was independent of stimulation rate from 10 to 100 Hz (Fig. 3.1C). Thus, short-term depression is implemented at the

vestibular nerve synapse to produce postsynaptic currents that depress rapidly and then are maintained at a fixed steady-state value, which contrasts with the rate-dependent short-term plasticity observed at all previously studied central synapses (Zucker and Regehr, 2002). The rate-independence of the EPSC amplitude in the steady-state translated into linear changes in postsynaptic charge transfer per second (R^2 = 0.998, n=10, Fig. 3.1D). This profile of short-term depression is remarkably similar to that obtained previously under conditions of higher extracellular Ca^{2+} (2.5 mM) (Bagnall et al., 2008).

What prevents rate-dependent enhancement of short-term depression? How does the vestibular nerve synapse precisely sustain transmission at high-rates without vesicle depletion or postsynaptic receptors desensitization? Given the reliability of vestibular nerve synaptic transmission, one might expect its morphological correlate to be a calyceal or glomerular structure. To determine whether the synapse architecture provides clues on the basis of vestibular nerve synapse function, we examined the ultrastructure of nerve afferent boutons, which we labeled with fluorescent dextrans injected into the nerve *in vivo* (see Methods; Fig. 3.2A). We made three-dimensional reconstructions of eight boutons: six opposing dendrites and two opposing somata. All were exceptionally large, with an average volume of 15.8 ± 4.7 μm^3, and each bouton contained multiple discrete active zones (14 ± 6, Fig. 3.2B-E). Individual active zones were also large, 0.17 ± 0.09 μm^2, and, in some instances, quite close to one another, with a mean nearest-neighbor distance of 0.43 ± 0.24 μm . How does the presence of multiple active zones contribute to reliable, high-rate transmission? Does each site operate reliably with a high probability of

release? Otherwise, does transmission depend on alternating release from the multiple sites, which would allow individual release sites to operate less reliably?

To determine whether the multiple active zones identified by EM at each bouton correspond to functional release sites and to estimate their probability of release, we performed fluctuation analyses. EPSCs were elicited at low rates (either 0.067 or 0.2 Hz) and their peak amplitudes were measured under 4-5 release probability conditions, imposed by varying external [Ca^{2+}] and [Mg^{2+}] while a constant total divalent concentration was maintained (Fig 3.3A). The relationship between the mean and variance of the peak EPSC amplitude was fit with the multinomial model of release, multiple-probability fluctuation analysis (MPFA)(Silver, 2003; see Methods; Fig. 3.3B). MPFA indicated that the vestibular nerve synapse comprises multiple functional release sites (36 ± 6; Fig. 3.3C).

Although short-term depression typically occurs at synapses with a high initial release probability (Zucker and Regehr, 2002), individual release sites at the nerve synapse exhibited low release probabilities (P_R = 0.22 ± 0.04; Fig. 3.3C). The mean quantal size estimated with the MPFA method (Q_P= -28.4 ± 5.5 pA; Fig 3.3C) was similar to that determined through strontium-induced asynchronous release (-24.9 ± 2.0 pA, n = 5, p = 0.80). Thus, while the performance of vestibular reflexes is accurate and reliable, the system receives vestibular signals though a synapse whose individual release sites are inconsistent due to low P_R. Reliable signal transmission can be achieved by offsetting the low P_R with multiple release sites functioning in parallel.

To examine what synaptic properties change with repeated activity and underlie the progressive depression during the initial ~10-15 stimuli, we paired MPFA analysis

with CV analysis in 6 experiments, in which we stimulated the nerve with 20-pulse trains rather than single pulses (see Methods). MPFA was applied to the first EPSC in the train to determine N. Assuming the number of release sites (N) cannot change, we tracked P_R and Q during the train with CV analysis. P_R reliably decreased during the train to 53.3 ± 5.5% of the first pulse P_R (Fig. 3.3D; $p = 0.03$, 1^{st} pulse vs. steady-state), whereas Q_P did not significantly change (1^{st} pulse: -16.5 ± 3.0 pA, steady-state: -20.5 ± 3.8 pA, $p = 0.16$). Thus, decreases in P_R underlie short-term depression, corresponding to an average decrease from P_R= 0.22 to P_R= 0.12. Because vestibular nerve afferents are continuously active *in vivo*, this steady-state P_R is predicted to correspond to the *in vivo* P_R. Therefore, presynaptic afferent firing rates of 5 - 125 Hz predict average release rates of only 0.6 - 15 Hz at each release site *in vivo*.

This exceptionally low P_R distinguishes the vestibular nerve synapse from other well-studied, fast synapses (Meyer et al., 2001; Oleskevich et al., 2000; Saviane and Silver, 2006b; Telgkamp et al., 2004). Does low P_R contribute to broadband linearity? To examine the role of P_R, external $[Ca^{2+}]$ was increased to 2.5 mM ($P_R = 0.39 \pm 0.05$), but this did not impair synaptic linearity ($R^2 = 0.999$, n = 6, Fig 3.4 A,B), as previously reported (Bagnall et al., 2008). In contrast, a further increase to 3.6 mM ($P_R = 0.64 \pm 0.16$, n =6) impaired rate-independent transmission within the behaviorally-relevant range, causing significantly greater depression in response to 100 Hz versus 10 Hz stimulation (Fig. 3.4 A,B). Thus, limiting P_R plays a critical role in determining the range of synaptic linearity.

The low P_R at the vestibular nerve synapse might correspond to release machinery that is intrinsically less sensitive to Ca^{2+} influx. Alternatively, minimizing Ca^{2+} influx

might be an efficient strategy for limiting P_R because it would simultaneously minimize the demands on Ca^{2+} buffers. Given that fast-inactivating K^+ channels limit action potential duration in postsynaptic neurons, we hypothesized that similar currents in vestibular nerve afferents might minimize action potential duration and subsequently restrict Ca^{2+} influx and P_R. To test for the presence of fast repolarization currents, we bath applied TEA (1 mM) to block Kv3 and BK channels. TEA application increased EPSC amplitude to 265 ± 37% of the baseline value (n = 6, p = 0.03; Fig. 3.4 C,D) and decreased the paired-pulse ratio (20 ms interval) from 1.34 ± 0.14 to 0.94 ± 0.09 (p = 0.03). TEA also enhanced the absolute amplitude of steady-state EPSCs during train stimulation at all rates (5 - 125 Hz, n = 6; Fig. 3.4E) but dramatically impaired the rate-independence and corresponding linearity of transmission (Fig. 3.4F). Thus, linearity at the vestibular nerve synapse depends on the active control of P_R by coordinated K^+ and Ca^{2+} currents. In addition to the role of K^+ currents in limiting P_R at other synapses (Geiger and Jonas, 2000; Sabatini and Regehr, 1997), these results demonstrate their role in synaptic computation.

Why does increasing P_R cause EPSC rundown at high rates? Does enhanced release result in AMPA-R desensitization and/or vesicle depletion? We blocked postsynaptic receptor desensitization and saturation by applying the competitive AMPA-R antagonist γ-DGG (2 mM) (Wong et al., 2003). Under normal P_R conditions, the steady-state EPSC amplitude at 100 Hz is identical to that at 10 Hz (100 Hz EPSC/10 Hz EPSC = 1.00 ± 0.05), and γ-DGG had no effect on the rate-independence of transmission (1.05 ± 0.04, n = 5, p =0.53), indicating postsynaptic receptor properties do not normally contribute to short-term depression. In the presence of TEA, the steady-state EPSC

amplitude at 100 Hz was significantly smaller than that at 10 Hz (100 Hz EPSC/10 Hz EPSC = 0.66 ± 0.08), and γ-DGG had no effect on the magnitude of rundown at 100 Hz (0.69 ± 0.10, n = 5, p = 1.0). Therefore, non-linear transmission in high P_R conditions is caused by rate-dependent glutamate release, which is not accompanied by changes in postsynaptic receptor sensitivity.

When P_R is high, readily releasable vesicle pools are prone to depletion, and vesicle availability becomes limiting. Rate-dependent release in high P_R but not low P_R suggests that the vesicle dynamics at the nerve synapses are well-tuned to the combination of physiological firing rates and P_R. The EM of the nerve synapse showed large vesicle pools (Fig. 3.2 B, D), with each bouton containing ~12,000 vesicles. The vesicle clusters associated with release sites often extended >1 μm beyond the release site. How quickly can these vesicles be readied for release by synapse machinery? To determine the rate of vesicle reloading and to estimate the size of the reserve vesicle pool, we performed vesicle depletion experiments (Saviane and Silver, 2006b; Schneggenburger et al., 1999). Sustained stimulation at 100 Hz for 1 minute is non-physiological and eventually resulted in synaptic failures due to vesicle pool depletion at 7 of 8 synapses (Fig. 3.5 A). Following depletion of the vesicle pool, transmission depends exclusively on vesicle reloading, and thus the rate of release then directly reflects the rate of reloading. The rate of release (vesicles/s per release site) in the post-depletion state can be calculated from the cumulative EPSC slope (EPSC/s), divided by the average vesicle size and number of terminals (Q_P *N) underlying transmission (Fig. 3.5B). This analysis indicated the rate of reloading was 7.1 ± 1.7 vesicles/s per release site. Assuming the rate of reloading is constant throughout the stimulus, additional

released vesicles during the protocol must have originated from the reserve pool, which averaged 233 ± 93 vesicles, as calculated though back-extrapolation. Thus, both fast vesicle reloading and large vesicle pools make the vestibular nerve synapse exceptionally well suited to mediate sustained transmission at high rates.

To assess the dynamics of recovery from short-term depression, we applied 50-pulse trains at 10, 100, or 300 Hz followed by test pulses at discrete intervals from 10 ms – 10 s. Following train stimulation at either 10 or 100 Hz, the EPSC amplitude showed no recovery from the steady-state amplitude for ~500 ms and then exhibited a slow monoexponential recovery with a tau of 2.9 s (10 Hz) or 2.5 s (100 Hz) (Fig. 3.5 C,D). Stimulation at 300 Hz, however, exceeded the linear capacity of transmission, and EPSC amplitude fell below the steady-state value evoked at 10 and 100 Hz. Following cessation of 300 Hz train, the EPSC amplitude rapidly jumped to the steady-state value, which persisted for hundreds of milliseconds before recovering to baseline with a time course identical to that following slower trains (tau = 2.7 s, Figure 3.5 C, D). Thus, once the EPSC is depressed, the dynamics of recovery occur with two distinct kinetics: one fast and the second slow relatively to typical activity intervals. While entry into depression is governed by the number of stimuli and not time or rate, recovery from depression depends entirely on time.

During high rates of neurotransmitter release, spillover between release sites occurs at many synapses and can advantageously offset rundown (Carter and Regehr, 2000; DiGregorio et al., 2002; Telgkamp et al., 2004). Given rate-independent release, however, spillover would compromise linear transmission. Preventing spillover during sustained, high-frequency activity requires tight control of extracellular glutamate. Fast

EPSC rise (0.44 ± 0.04 ms) and decay (3.01 ± 0.21 ms, n = 15) kinetics suggest that the vestibular nerve synapse efficiently avoids spillover, which is further supported by the lack of effect of γ-DGG on short-term depression. The blockade of all glutamate transporters (EAAT1-5) with 200 μM dl-TBOA resulted in the accumulation of a large tonic current (Fig. 3.6A). Remarkably, even in the presence of pooling glutamate, the evoked phasic EPSC response remained rate-independent, indicating the lack of saturation and desensitization of AMPA-Rs (Fig. 3.6C). Blocking glutamate uptake dramatically increased the effect of transmission of postsynaptic firing, however, and evoked firing was no longer well timed with respect to the presynaptic input (Fig. 3.6D-F). Dl-TBOA thus degraded the history independence of transmission and converted the synapse from a linear filter into an integrator. dl-TBOA did not alter the kinetics or amplitude of the first EPSC (Fig. 3.6B), indicating that transmitter release and AMPA-R properties dictate EPSC kinetics, while the role of active glutamate uptake is to prevent glutamate pooling in order to ensure temporal fidelity. Under normal conditions, glutamate clearance at the nerve synapse is exceptionally efficient and paired with rate-independent release ensures faithful signal transmission between pre- and post-synaptic neurons.

To examine the contribution of individual synaptic specializations to broadband, linear transmission, we tested a simple model of short-term plasticity based on our experimental results (Fig. 3.7A). The model incorporated estimates of the number of release sites and release probability from MPFA and CV analyses (Fig. 3.3), vesicle pool size and reloading rate (Fig. 3.5), and the kinetics of recovery from depression (Fig. 3.5). The free parameter, the rate of vesicle translocation, docking, and priming was optimized

for linearity and implemented as 22 ms (see Methods). The model of the vestibular nerve synapse predicted extremely well the short-term depression of the vestibular nerve synapse and the rate-independence from 10 to 100 Hz (Fig. 3.7B). The average steady-state responses (pulses 30-50) from the model and from experimental data demonstrate the capacity of the model to predict the magnitude of the depression and the range of rates over which transmission is constant (Fig. 3.7C). The rate-independence of the synaptic response in the model corresponds to linear charge transfer (Fig. 3.7D).

Using this model, we were able to test the functional significance of individual synaptic properties. Raising the P_R to 0.64 dramatically impaired the rate-independence of transmission by causing rate-dependent rundown (Fig. 3.8A, D), as was observed experimentally (Fig. 3.4). The elevated P_R manipulations demonstrate that P_R is a critical determinant of the upper bound of the range of rates over which transmission is linear.

To test the role of recovery dynamics, we removed the 500 ms delay between the fast phase of recovery (22 ms) and the slow phase (2.7 s) and maintained all other model parameters. Removing this window between the recovery phases dramatically impaired the rate-independence of transmission (Fig. 3.8B, D). Without the delay, the slow recovery process opposes the short-term depression at low rates of activity and thus limits the lower bound of the linear range.

To identify how the parallel functioning of multiple release sites influences synapse function, we reduced the number of sites in the model from 36 to 5. Under this condition, the average computation of the synapse was identical to the model with 36 release sites (Fig. 3.8D), however the variability of the response dramatically increased (Fig. 3.8C). Because the release sites of the vestibular nerve synapse operate

independently, their main role is to promote trial-to-trial consistency that cannot be achieved with a small number of release sites given the variability produced by the low P_R.

Two additional models were tested in which only one vesicle was docked. One model contained only a reserve pool of vesicles, whereas the other additionally contained an intermediate pool. These models were also able to account for linear transmission, but both required the rate of vesicle translocation, docking, and priming to exceed 8 ms, which is 30 % faster than previously reported for a central synapse (Saviane and Silver, 2006b). Comparing all three models highlights the two possible solutions to vesicle availability: multiple docked vesicles per release site or extremely fast docking kinetics.

These models demonstrate that a precise coordination of synaptic properties—the number of release sites, the regulation of P_R, vesicle number and dynamics, and recovery dynamics—all interact to promote linear synaptic transmission across the physiological range. Two key principles of linear synaptic transmission emerge from these investigations. First, in order to establish a range of activity across which synaptic strength does not change, it is not necessary for underlying synaptic processes to be static. Rather, processes can simultaneously change as long as their kinetics are either fast or slow relative to transmission rates. Second, synaptic transmission and linearity are extended to high rates by limiting P_R. Interestingly, the active dampening of connection strength is a well-described principle in the design of linear electronic amplifiers.

Discussion

This study demonstrates that broadband linear transmission at the vestibular nerve synapse emerges from the coordinated function of multiple synaptic specializations. Vestibular nerve synapses limit P_R at the earliest stage of transmission by restricting Ca^{2+} influx. The low-probability contribution of individual release sites is offset by a large number of release sites at each synaptic terminal. This strategy reduces the challenge of sustaining transmission at high rates by allowing each site to participate in transmission in an alternating manner. Simultaneously, the synapse promotes vesicle availability through fast vesicle reloading, large vesicle pool, and efficient vesicle docking. Active glutamate uptake and consistent postsynaptic receptor sensitivity translate rate-invariant release into postsynaptic currents of constant amplitude. Thus, the reliable transmission of head motion signals entering the vestibular system is achieved through the collective function of multiple independent release sites and refinement at each stage of synaptic transmission.

Rate-independent release from presynaptic terminals

Transmission at the vestibular nerve synapse is distinctive in its constant steady-state amplitude across a nearly 30-fold range of presynaptic firing rates. Estimates of the quantal properties of transmission revealed that the vestibular nerve synapse has an exceptionally low release probability of 0.12 under steady-state conditions (Fig. 3.3). Thus, the firing range of nerve afferents *in vivo*, 5 – 125 Hz, corresponds to a rate of release of only 0.6 – 15 Hz at each release site. Because postsynaptic AMPA-Rs do not desensitize, vesicle availability is the critical determinant of the upper limit of linearity.

The relative speed of vesicle dynamics and the rate of release must thus complement one another to support linear transmission. Although low P_R reduces the demands on release machinery, the vast majority of central synapses would not sustain constant vesicle availability under the conditions faced by the vestibular nerve synapse. When the afferent fires at 100 Hz, a release site will release at 12 Hz on average. However, the stochastic nature of release will require the terminal to occasionally release at much higher rates. For example, during a 100 Hz train, 12% of the release events will occur at a 10 ms interval.

To sustain vesicle availability, the vestibular nerve has two specializations: large vesicle pools and fast vesicle dynamics (Fig. 3.5). The model of transmission predicts the rate of vesicle translocation, docking, and priming to be particularly fast. If only one vesicle is docked, linearity would require the rate to be at least 8 ms, which is ~30% faster than has been described for a central synapse (Saviane and Silver, 2006b). Alternatively, readying multiple vesicles in parallel would allow this rate to be much slower: 22 ms, which we implemented in the model (Fig 3.7). It is notable how similar the vesicle properties are to those at the cerebellar mossy fiber synapse, which suggests both synapses may rely on the same molecular machinery (Hallermann et al., 2010). It would be interesting to determine whether such fast dynamic arise from rapid replenishment from the reserve vesicle pool and "full-collapse fusion" or whether these dynamics in part reflect "kiss-and-run" or "flicker-fusion" modes of exocytosis (Smith et al., 2008) .

The model predicts the strength of transmission to depend on rate when P_R is high (P_R = 0.64; Fig. 3.8A), which corresponds to the experimental findings in 3.6 mM Ca^{2+}

and TEA (Fig. 3.4). Blocking AMPA-R saturation and desensitization with γ-DGG did not alter the rate-dependence under high P_R conditions. Thus, the progressive, rate-dependent rundown of transmission in high P_R reflects presynaptic limitations. Interestingly, while the cerebellar mossy fiber synapse has fast vesicle dynamics and large vesicle pools, it differs from the vestibular nerve synapse in its higher release probability (P_R = ~0.6) and rate-dependence (Saviane and Silver, 2006b).

The CV analysis indicated the average P_R of the vestibular nerve synapse decreases from 0.22 to 0.12 during train stimulation (Fig. 3.3). This analysis also showed that the size of Q_P is constant, which is consistent with the observed lack of desensitization and saturation of postsynaptic AMPA-Rs. Thus, the CV analysis identified the decrease in P_R as the cause of the short-term depression. What underlies this decrease in P_R during repeated simulation? At some synapses, a lack of fusion-ready vesicles can cause short-term depression, but this is unlikely at the vestibular nerve synapse given the impressive size of the vesicle reserve pool and fast vesicle dynamics. A more plausible scenario is that the decrease in P_R reflects a decrease in Ca^{2+} infux or in the Ca^{2+}-sensitivity of release machinery. One attractive theory is that the P_R of a vesicle ramps up over time when there is no firing in the terminal. Once firing resumes, those vesicles would be released, and newly readied vesicles would have a lower release probability. Evidence for a slow enhancement of P_R has been found at other synapses (Muller et al., 2010; Rollenhagen and Lubke, 2006).

The recovery from steady-state depression follows a time course that is not influenced by the previous firing rate (Fig. 3.5C,D). This slow process (2.7 s) follows a delay of ~500 ms. Because recovery processes oppose depression, the time course of

recovery plays a central role in determining the lower end of the linearity range. *In vivo,* the firing rates of vestibular afferents do not drop below 5 Hz, which means firing never pauses for long enough for the EPSC to recover from the steady-state amplitude *in vivo.* When vestibular nerve synapses are stimulated at non-physiologically high rates, a second fast phase of recovery (22 ms) is revealed, but the delay before the slow phase is maintained (Fig. 3.5C,D). The lack of an intermediate recovery process creates a temporal window of ~500 ms between the fast and slow phases that is essential for linearity. Eliminating this delay forces recovery and depression to oppose one another in a rate-dependent fashion, which impairs linearity at low rates (Fig. 3.8B). Most synapses do not exhibit such distinctive temporal separations between recovery dynamics, which must contribute to non-linearities at other synapses.

Model assumptions and calcium dynamics

The model of synaptic transmission used here relies on two key assumptions that have not been experimentally tested. The first is that the action potential duration and resultant Ca^{2+} influx do not depend on firing rate. In postsynaptic nucleus neurons, action potential width is known to be remarkable constant over a much wider range of firing rates (Gittis and du Lac, 2007; Sekirnjak and du Lac, 2002), and pharmacological results presented here indicate that the same potassium channels that regulate spike width in postsynaptic neurons are also expressed in the presynaptic terminals (Fig 3.3C-F). Given the size of vestibular afferent boutons, direct patch clamp recording from the boutons could allow for direct measurements of action potential consistency.

The second key assumption is that Ca^{2+} does not accumulate in the presynaptic terminal. While afferents express a high amount of the fast Ca^{2+} buffer parvalbumin (Eatock and Songer, 2011), it remains possible that Ca^{2+} might to some extent accumulate. If this occurred, the vestibular afferent terminal would need to express an extraordinarily precise offset for this accumulation. Future improvements in Ca^{2+} indicators may make direct measurements of the calcium dynamics possible.

What do our results imply about the nature of the Ca^{2+} sensor at the vestibular nerve synapse? The relationship between the internal Ca^{2+} concentration and vesicle fusion vesicle is known to be highly cooperative at central synapses (Schneggenburger and Neher, 2005). However, one interesting observation from the MPFA analysis was that the relationship between P_R and external Ca^{2+} scales linearly from 0.5 – 4 mM (R^2= 0.99). It is unclear how this relationship could arise unless presynaptic Ca^{2+} buffering were very efficient and the Ca^{2+} sensor atypical. Peripheral sensory synapses in the auditory, visual, and vestibular systems express Ca^{2+} sensors with a linear dependence on Ca^{2+}, and it is possible some of these specializations might be expressed in the central nervous system (Beurg et al., 2010; Dulon et al., 2009; Keen and Hudspeth, 2006; Thoreson et al., 2004).

Additional requirements for linearity

The capacity of the vestibular nerve synapse to transform glutamate release into fast, rate-invariant EPSCs depends on constant postsynaptic receptor sensitivity and efficient glutamate uptake. AMPA-Rs at vestibular nerve synapses are remarkably resistant to desensitization. In TEA, EPSC amplitudes were nearly tripled (Fig. 3.4C,D),

however application of γ-DGG did not reduce short-term depression. This indicates that AMPA-Rs did not desensitize even when exposed glutamate concentrations nearly 3-fold higher than physiological. Similarly, blocking active glutamate uptake with dl-TBOA resulted in glutamate pooling without altering the responsiveness of AMPA-Rs. The constant sensitivity of AMPA-Rs at the vestibular nerve synapse may be conferred by their composition of subunit isoforms and/or auxiliary proteins (Mosbacher et al., 1994; Nicoll et al., 2006; Partin et al., 1996; Priel et al., 2005).

While glutamate transporters are not required to protect AMPA-Rs from desensitization, they play a central role in preserving temporal fidelity at the vestibular nerve synapse. The blockade of glutamate uptake by dl-TBOA had a dramatic effect on the time course of transmission and transformed the synapse from a linear filter into an integrator (Fig. 3.6D-F). The concentration of dl-TBOA presented here (200 μM) blocks the five excitatory amino acid transporters (EAAT1-5). Bath application of 50 μM dl-TBOA (data not shown) to block EAAT2-5 had minimal effects on transmission, identifying the glial high-affinity transporter EAAT1 as the essential subtype at the vestibular nerve synapse.

Contribution of multiple release sites

Many fast synapses release transmitter from multiple discrete sites to optimize their influence on postsynaptic neurons (DiGregorio et al., 2002; Meyer et al., 2001; Telgkamp et al., 2004; von Gersdorff and Borst, 2002). Because the release sites at the vestibular nerve synapse operate independently, the number of sites does not influence the average computation performed by the synapse (Fig 3.8 D). Rather, the function of

multiple release sites at the vestibular nerve synapse is to minimize the jitter in trial-to-trial transmission (Fig 3.8C). Vestibular reflexes require reliable circuit performance, but synapses typically sacrifice reliability when P_R is low. Even with multiple release sites, vestibular nerve synapses demonstrate a fair amount of variability, and it is notable that the model captures this aspect (Fig 3.7B). Because postsynaptic neurons do not immediately fire in response to single EPSPs but rather integrate multiple before firing an action potential, postsynaptic neurons have some capacity to minimize the functional impact of variability in synaptic currents. The convergence of multiple afferent onto individual vestibular neurons and further convergence of vestibular nucleus neuron synapses onto motor neurons likely promote the precision of the system. The number of release sites estimated by MPFA (36 ± 6, Fig. 8.3C) exceeds the average number of active zones per bouton observed by EM (14 ± 6). This difference is consistent with anatomical evidence that single vestibular afferents often provide multiple collaterals to a single postsynaptic target (Hauglie-Hanssen, 1968; Ishizuka et al., 1982).

Principles of biological linearity

The excellent performance of the VOR exemplifies the capacity of the vestibular system to linearly transform head motion into compensatory movements (Bagnall et al., 2008; Robinson, 1981). Each stage of transmission examined thus far has been shown to be linear with respect to head motion, including the firing rates in vestibular nerve afferents and vestibular nucleus neurons (Goldberg and Fernandez, 1971; Shimazu and Precht, 1965). The cellular basis of this linearity in the central nervous system has been examined in vestibular nucleus neurons. Vestibular nucleus neurons transform current

injections into linear increases in firing rate (Sekirnjak and du Lac, 2002). Studies on the basis of intrinsic linearity have revealed basic requirements that share analogies with the requirements for synaptic linearity. Rather than allowing a cell or synapse to work near the limit of its capacity, linearity requires a mechanism that puts an active break on the cell or synapse to maintain operation in the middle of the dynamic range. For the vestibular nerve synapse, the coordination of fast action potential repolarization and Ca^{2+} channels minimizes Ca^{2+} influx and P_R. This sacrifice of synapse strength is necessary to ensure vesicle availability at high rates of activity. In postsynaptic neurons, the analogous break for intrinsic linearity is the potassium current that hyperpolarizes neurons between action potentials. This current opposes depolarizing inputs and dramatically limits the ability of the neuron to fire quickly (K.Kolkman, unpublished observations). This sacrifice in gain, however, promotes reliable sodium channel availability and is essential for extending the dynamic range of intrinsic linearity. Therefore, the implementation of linearity at each state of the vestibular system examined thus far relies on common cellular strategies.

Acknowledgements

Chapter 3 is original work in preparation as McElvain L.E., Faulstich M., Jeanne J.M,., and du Lac S. Concerted functional and anatomical specializations mediate linear synaptic transmission and is included with permission from all the manuscript's authors.

References

Abbott, L.F., and Regehr, W.G. (2004). Synaptic computation. Nature *431*, 796-803.

Bagnall, M.W., McElvain, L.E., Faulstich, M., and du Lac, S. (2008). Frequency-independent synaptic transmission supports a linear vestibular behavior. Neuron *60*, 343-352.

Beurg, M., Michalski, N., Safieddine, S., Bouleau, Y., Schneggenburger, R., Chapman, E.R., Petit, C., and Dulon, D. (2010). Control of exocytosis by synaptotagmins and otoferlin in auditory hair cells. J Neurosci *30*, 13281-13290.

Carter, A.G., and Regehr, W.G. (2000). Prolonged synaptic currents and glutamate spillover at the parallel fiber to stellate cell synapse. J Neurosci *20*, 4423-4434.

DiGregorio, D.A., Nusser, Z., and Silver, R.A. (2002). Spillover of glutamate onto synaptic AMPA receptors enhances fast transmission at a cerebellar synapse. Neuron *35*, 521-533.

Dulon, D., Safieddine, S., Jones, S.M., and Petit, C. (2009). Otoferlin is critical for a highly sensitive and linear calcium-dependent exocytosis at vestibular hair cell ribbon synapses. J Neurosci *29*, 10474-10487.

Eatock, R.A., and Songer, J.E. (2011). Vestibular Hair Cells and Afferents: Two Channels for Head Motion Signals. Annu Rev Neurosci.

Fioravante, D., and Regehr, W.G. (2011). Short-term forms of presynaptic plasticity. Curr Opin Neurobiol.

Geiger, J.R., and Jonas, P. (2000). Dynamic control of presynaptic Ca(2+) inflow by fast-inactivating K(+) channels in hippocampal mossy fiber boutons. Neuron *28*, 927-939.

Gittis, A.H., and du Lac, S. (2007). Firing properties of GABAergic versus non-GABAergic vestibular nucleus neurons conferred by a differential balance of potassium currents. J Neurophysiol *97*, 3986-3996.

Goldberg, J.M., and Fernandez, C. (1971). Physiology of peripheral neurons innervating semicircular canals of the squirrel monkey. I. Resting discharge and response to constant angular accelerations. J Neurophysiol *34*, 635-660.

Hallermann, S., Fejtova, A., Schmidt, H., Weyhersmuller, A., Silver, R.A., Gundelfinger, E.D., and Eilers, J. (2010). Bassoon speeds vesicle reloading at a central excitatory synapse. Neuron *68*, 710-723.

Hauglie-Hanssen, E. (1968). Intrinsic neuronal organization of the vestibular nuclear complex in the cat. A Golgi study. Ergeb Anat Entwicklungsgesch *40*, 3-105.

Ishizuka, N., Sasaki, S., and Mannen, H. (1982). Central course and terminal arborizations of single primary vestibular afferent fibers from the horizontal canal in the cat. Neurosci Lett *33*, 135-139.

Jones, M.V., and Westbrook, G.L. (1996). The impact of receptor desensitization on fast synaptic transmission. Trends Neurosci *19*, 96-101.

Keen, E.C., and Hudspeth, A.J. (2006). Transfer characteristics of the hair cell's afferent synapse. Proc Natl Acad Sci U S A *103*, 5537-5542.

Meyer, A.C., Neher, E., and Schneggenburger, R. (2001). Estimation of quantal size and number of functional active zones at the calyx of held synapse by nonstationary EPSC variance analysis. J Neurosci *21*, 7889-7900.

Mosbacher, J., Schoepfer, R., Monyer, H., Burnashev, N., Seeburg, P.H., and Ruppersberg, J.P. (1994). A molecular determinant for submillisecond desensitization in glutamate receptors. Science *266*, 1059-1062.

Muller, M., Goutman, J.D., Kochubey, O., and Schneggenburger, R. (2010). Interaction between facilitation and depression at a large CNS synapse reveals mechanisms of short-term plasticity. J Neurosci *30*, 2007-2016.

Nicoll, R.A., Tomita, S., and Bredt, D.S. (2006). Auxiliary subunits assist AMPA-type glutamate receptors. Science *311*, 1253-1256.

Oleskevich, S., Clements, J., and Walmsley, B. (2000). Release probability modulates short-term plasticity at a rat giant terminal. J Physiol *524 Pt 2*, 513-523.

Partin, K.M., Fleck, M.W., and Mayer, M.L. (1996). AMPA receptor flip/flop mutants affecting deactivation, desensitization, and modulation by cyclothiazide, aniracetam, and thiocyanate. J Neurosci *16*, 6634-6647.

Priel, A., Kolleker, A., Ayalon, G., Gillor, M., Osten, P., and Stern-Bach, Y. (2005). Stargazin reduces desensitization and slows deactivation of the AMPA-type glutamate receptors. J Neurosci *25*, 2682-2686.

Robinson, D.A. (1981). The use of control systems analysis in the neurophysiology of eye movements. Annu Rev Neurosci *4*, 463-503.

Rollenhagen, A., and Lubke, J.H. (2006). The morphology of excitatory central synapses: from structure to function. Cell Tissue Res *326*, 221-237.

Sabatini, B.L., and Regehr, W.G. (1997). Control of neurotransmitter release by presynaptic waveform at the granule cell to Purkinje cell synapse. J Neurosci *17*, 3425-3435.

Saviane, C., and Silver, R.A. (2006a). Errors in the estimation of the variance: implications for multiple-probability fluctuation analysis. J Neurosci Methods *153*, 250-260.

Saviane, C., and Silver, R.A. (2006b). Fast vesicle reloading and a large pool sustain high bandwidth transmission at a central synapse. Nature *439*, 983-987.

Saviane, C., and Silver, R.A. (2007). Estimation of quantal parameters with multiple-probability fluctuation analysis. Methods Mol Biol *403*, 303-317.

Schneggenburger, R., Meyer, A.C., and Neher, E. (1999). Released fraction and total size of a pool of immediately available transmitter quanta at a calyx synapse. Neuron *23*, 399-409.

Schneggenburger, R., and Neher, E. (2005). Presynaptic calcium and control of vesicle fusion. Curr Opin Neurobiol *15*, 266-274.

Sekirnjak, C., and du Lac, S. (2002). Intrinsic firing dynamics of vestibular nucleus neurons. J Neurosci *22*, 2083-2095.

Shimazu, H., and Precht, W. (1965). Tonic and kinetic responses of cat's vestibular neurons to horizontal angular acceleration. J Neurophysiol *28*, 991-1013.

Silver, R.A. (2003). Estimation of nonuniform quantal parameters with multiple-probability fluctuation analysis: theory, application and limitations. J Neurosci Methods *130*, 127-141.

Smith, S.M., Renden, R., and von Gersdorff, H. (2008). Synaptic vesicle endocytosis: fast and slow modes of membrane retrieval. Trends Neurosci *31*, 559-568.

Telgkamp, P., Padgett, D.E., Ledoux, V.A., Woolley, C.S., and Raman, I.M. (2004). Maintenance of high-frequency transmission at purkinje to cerebellar nuclear synapses by spillover from boutons with multiple release sites. Neuron *41*, 113-126.

Thoreson, W.B., Rabl, K., Townes-Anderson, E., and Heidelberger, R. (2004). A highly Ca2+-sensitive pool of vesicles contributes to linearity at the rod photoreceptor ribbon synapse. Neuron *42*, 595-605.

von Gersdorff, H., and Borst, J.G. (2002). Short-term plasticity at the calyx of held. Nat Rev Neurosci *3*, 53-64.

Wong, A.Y., Graham, B.P., Billups, B., and Forsythe, I.D. (2003). Distinguishing between presynaptic and postsynaptic mechanisms of short-term depression during action potential trains. J Neurosci *23*, 4868-4877.

Xu-Friedman, M.A., and Regehr, W.G. (2004). Structural contributions to short-term synaptic plasticity. Physiol Rev *84*, 69-85.

Zucker, R.S., and Regehr, W.G. (2002). Short-term synaptic plasticity. Annu Rev Physiol *64*, 355-405.

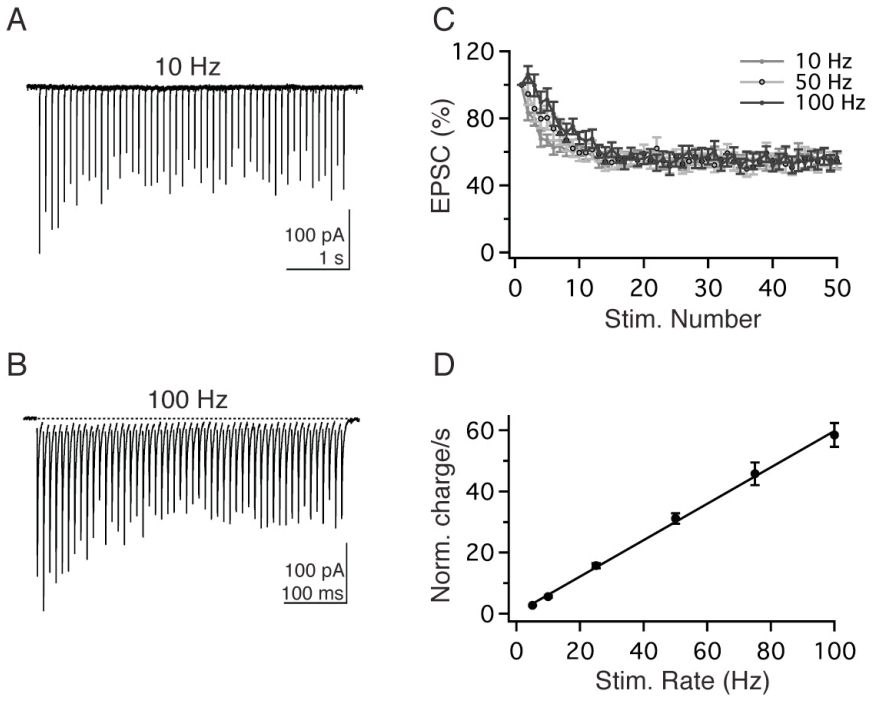

Fig. 3.1 Vestibular nerve synapses exhibit rate-independent short-term depression. (A) Example EPSC responses in a vestibular nucleus neuron to 50-pulse train stimulation of the nerve at 10 and (B) 100 Hz. EPSC amplitude decreases during the initial stimuli and then reaches a steady-state amplitude. (C) Normalized EPSC amplitudes evoked by 10, 50, and 100 Hz stimulus trains (n=11). (D) Total charge transfer per second during steady-state transmission ($EPSC_{30\text{-}50}$) increases linearly with increasing stimulation rate (R^2=0.999). Charge transfer was calculated as the integrated area under the average steady-state EPSC multiplied by rate of stimulation. In this and all subsequent figures, error bars = SEM.

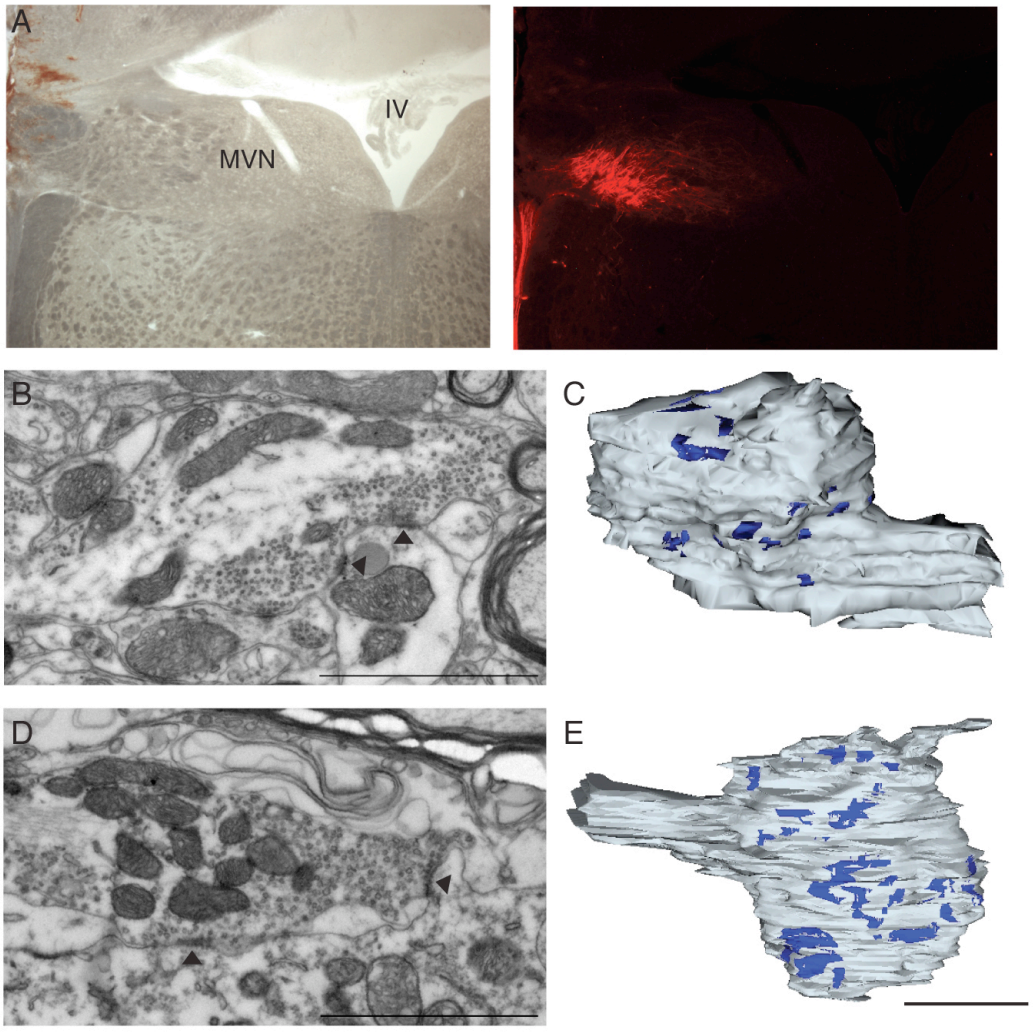

Fig. 3.2 Ultrastructure of vestibular nerve synapses. **(**A) A coronal brainstem section containing the fourth ventricle (IV), the medial vestibular nucleus (MVN), and the vestibular nerve imaged by light (left) and fluorescence (right) microscopy. The vestibular nerve was fluorescently labeled *in vivo* by stereotaxic dye injections into the nerve where it exited the temporal bone. (B) EM image of a vestibular nerve en passant bouton targeting the dendrite of a MVN neuron; arrowheads, active zones. Scale bar = 2 μm (C) Three-dimensional reconstruction of the example shown in B; grey = bouton, blue = active zones. (D) Ultrastructure and (E) reconstruction of a vestibular nerve terminal bouton targeting the soma of a MVN neuron. Scale bars = 2 μm.

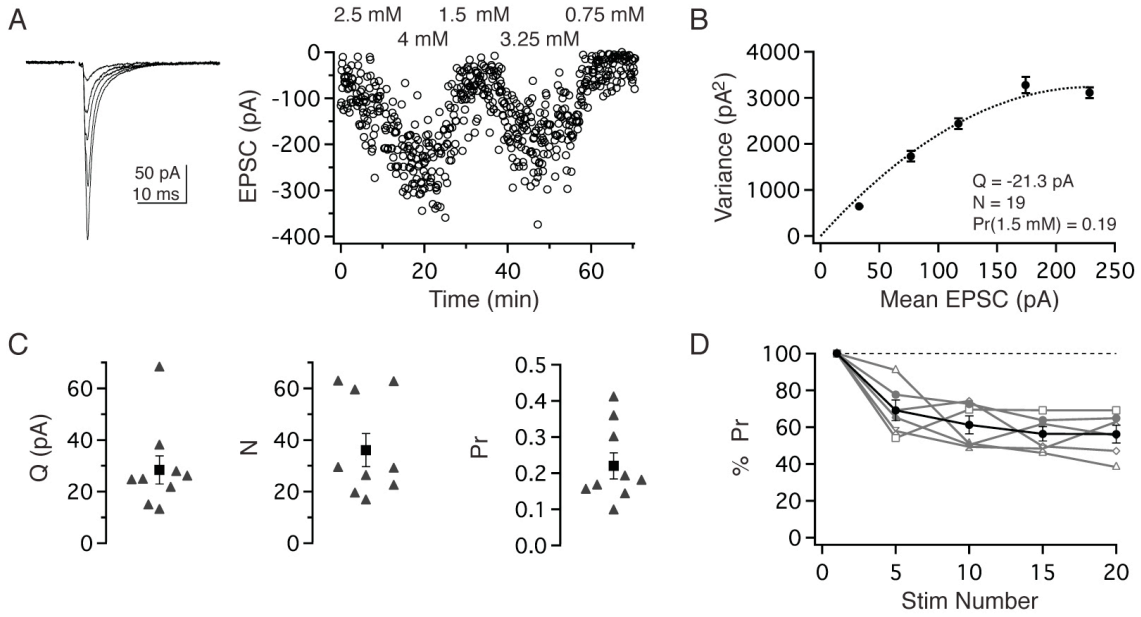

Fig. 3.3 Multiple release sites with low release probabilities mediate transmission. **(**A) Example average traces (left) and individual peak amplitudes (right) of EPSCs evoked in different extracellular Ca^{2+} concentrations. (B) Corresponding plot of the variance and mean of the peak EPSC amplitudes and fit from the multinomial model (see Methods). (C) Estimates of the quantal size, number of release sites, and release probability for nine vestibular nerve synapses. (D) Individual (grey) and average (black) percent changes in release probability during a 20-pulse stimulation train.

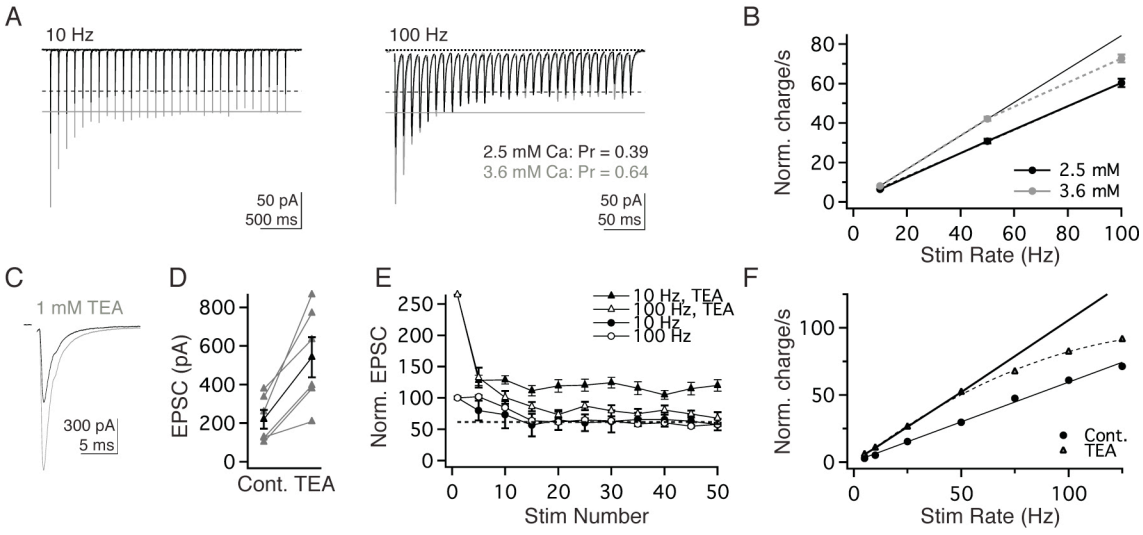

Fig. 3.4 Linear synaptic transmission depends on low release probability and fast presynaptic action potentials. **(**A) Example EPSC responses in an individual neuron to train stimulation at 10 Hz (left) and 100 Hz (right) in 2.5 mM (black) and 3.6 mM (grey) Ca^{2+}. (B) Normalized total charge transfer per second during steady-state transmission in 2.5 mM (black) and 3.6 mM (grey) Ca^{2+}. (C) Example EPSCs evoked under control conditions (black) and following the addition of 1 mM TEA (grey). (D) Individual (grey) and average (black) EPSC amplitudes before and after the application of TEA. (E) Normalized EPSC amplitudes in response to train stimulation at 10 and 100 Hz under control conditions (circles) and following application of TEA (triangles), normalized to first control EPSC. (F) Normalized total charge transfer per second during steady-state transmission under control conditions (circles) and with TEA (triangles). Solid lines are linear fits to data from train stimulation at rates ≤ 50 Hz.

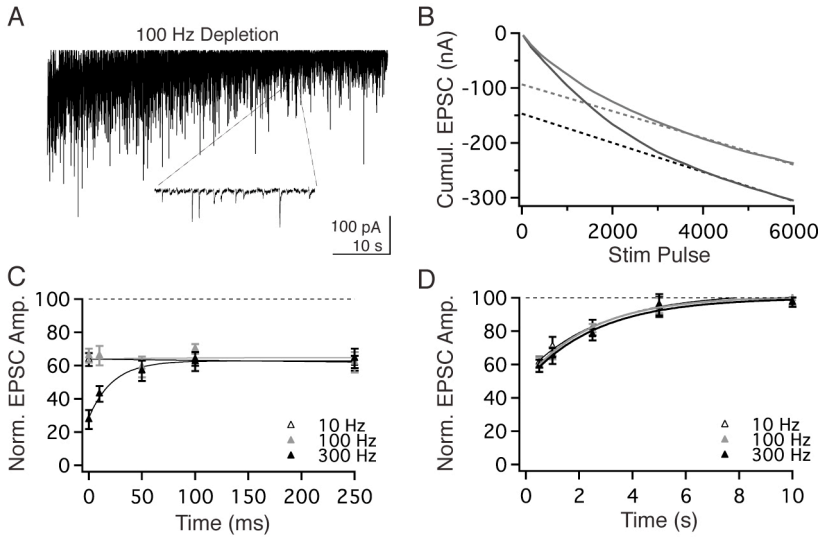

Fig. 3.5 Kinetics of vesicle pool dynamics and recovery from depression. **(**A) Example EPSC response to a depleting 6,000-pulse, 100 Hz train. Inset: blow up of 220-ms epoch showing occasional transmission failures. (B) Corresponding cumulative EPSC values to example train (black). A second application of the depleting stimulus was applied prior to full pool refilling (grey). Following reserve pool depletion (~pulse 3,000), the cumulative EPSC in both trials shows the same slope, which corresponds to the rate of vesicle reloading. Dashed lines indicate fits to last 20 s. (C) The vestibular nerve was stimulated with 50-pulse trains (10, 100, or 300 Hz), followed by a single test pulse at times 10 ms – 10 s. Stimulation at 300 Hz depressed EPSC amplitude beyond the steady-state, but recovery to the steady-state was rapid (tau = 0.22 ms). EPSCs did not recover from steady-state depression during short-intervals. (D) Recovery from steady-state depression after 500 ms was fit by a single exponential that did not depend of the rate of stimulation during the train.

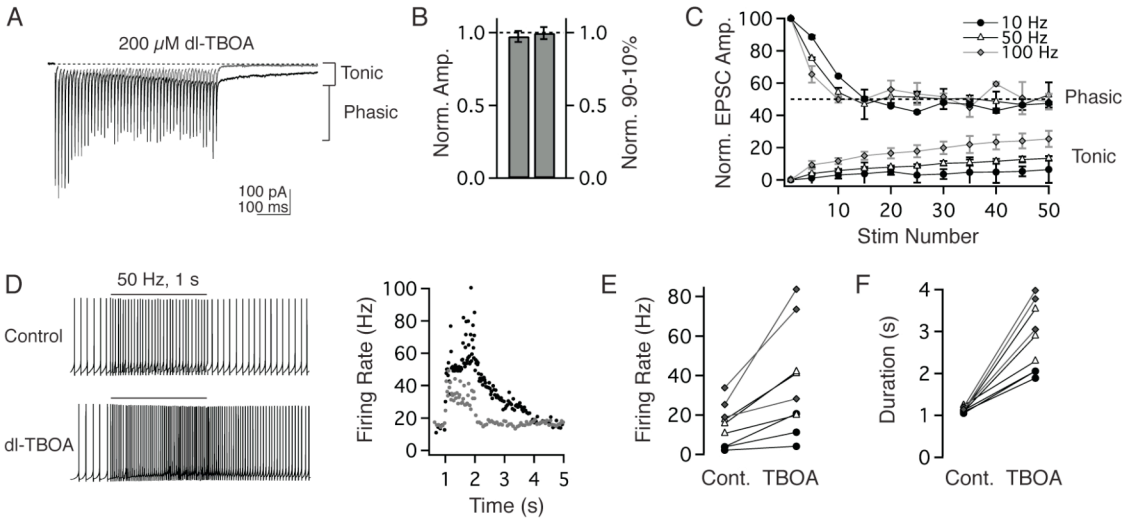

Fig. 3.6 Active glutamate uptake promotes temporal fidelity. (A) Example control EPSC responses to 100 Hz stimulation (grey) and following the addition of 200 μM dl-TBOA (black), which resulted in the accumulation of a tonic current underlying phasic EPSCs. (B) Effects of dl-TBOA on the amplitude and fall time of the first EPSC in the train. (C) Normalized phasic and tonic EPSC amplitudes in dl-TBOA in response to train stimulation at 10, 50, and 100 Hz. (D) Example evoked postsynaptic firing responses to a 1-s, 50 Hz train (top) and following dl-TBOA wash on (bottom); the instantaneous firing rates of these trials (right). (E) The effects of blocking glutamate transporters on the firing rate and (F) duration of postsynaptic responses to train stimulation.

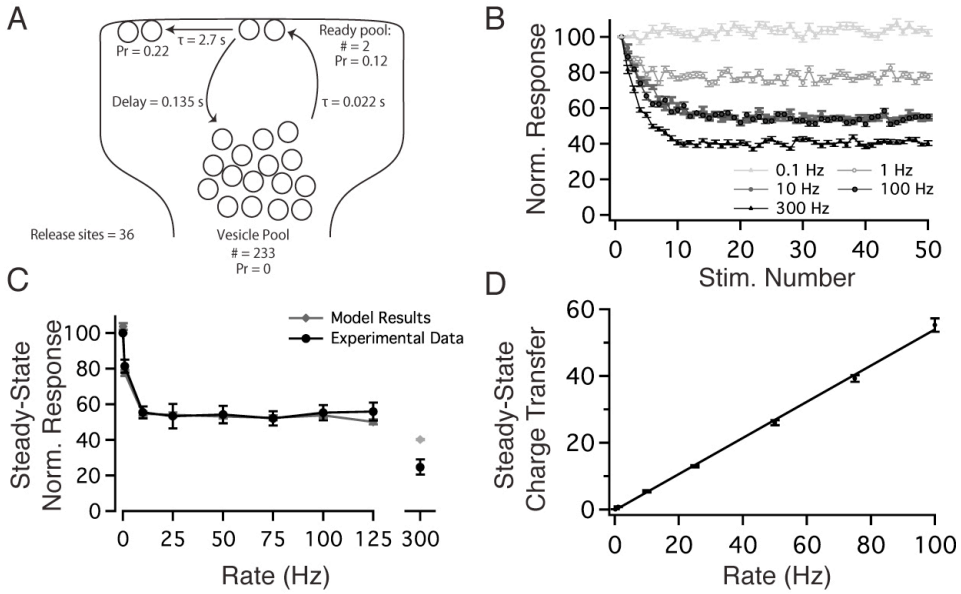

Fig. 3.7 Model of vestibular nerve synaptic transmission. **(**A) Schematic of vestibular nerve model constrained by experimentally-determined measurements (see Methods). (B) Model output for 50-pulse train stimulation at 0.1, 1, 10, 100, and 300 Hz, normalized to the response to the first pulse. (C) Normalized steady-state (pulses 30-50) responses from experimental data (black) and from the model (grey). (D) Corresponding linear total charge transfer for the responses of the model across the physiologically-relevant rates. Model results are the mean of 200 repetitions to correspond with 20 trials in 10 cells.

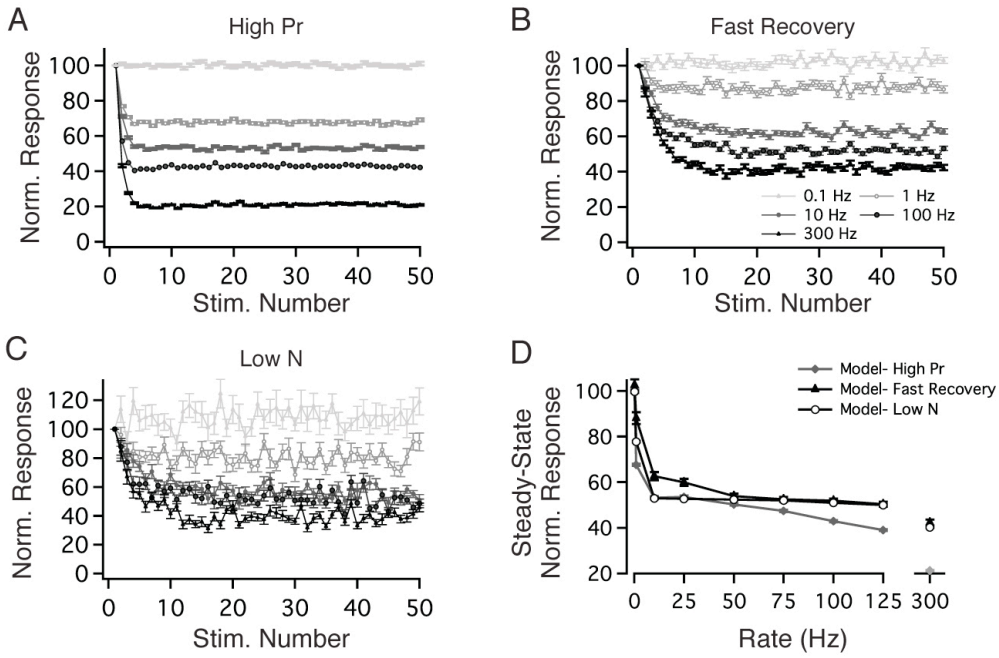

Fig. 3.8 Contribution of individual synaptic properties to rate-independent transmission. The normalized model output for 50-pulse train activity at 0.1, 1, 10, 100, and 300 Hz was assessed for three manipulations of model parameters. (A) Output from the model in which the initial P_R was increased from 0.22 to 0.64. (B) Output from the model after removing the 500-ms delay between the fast and slow phases of EPSC recovery. (C) Output from the model with only 5 release sites. (D) Normalized steady-state (pulses 30-50) responses from models with high release probability (grey), faster recovery (black), and few release sites (white). Model results are the mean 200 repetitions, except for the Low N results in D, which are the mean of 5000 repetitions.

Chapter 4. Bidirectional plasticity gated by hyperpolarization controls the gain of postsynaptic firing responses at central vestibular nerve synapses

Abstract

Linking synaptic plasticity with behavioral learning requires understanding how synaptic efficacy influences postsynaptic firing in neurons whose role in behavior is understood. Here we examine plasticity at a candidate site of motor learning: vestibular nerve synapses onto neurons that mediate reflexive movements. Pairing nerve activity with changes in postsynaptic voltage induced bidirectional synaptic plasticity in vestibular nucleus projection neurons: long-term potentiation relied on calcium-permeable AMPA receptors and postsynaptic hyperpolarization, while long-term depression relied on NMDA receptors and postsynaptic depolarization. Remarkably, both forms of plasticity uniformly scaled synaptic currents evoked by pulse trains, and these changes in synaptic efficacy were translated into linear increases or decreases in postsynaptic firing responses. Synapses onto local inhibitory neurons were also plastic but expressed only long-term depression. Bidirectional, linear gain control of vestibular nerve synapses onto projection neurons provides a plausible mechanism for motor learning underlying adaptation of vestibular reflexes.

Introduction

Activity-dependent changes in synaptic strength are assumed to underlie various forms of learning and memory, but connecting synaptic plasticity to behavioral consequences requires knowing both how plasticity affects the output of postsynaptic neurons and how those neurons influence behavior. The majority of behavioral circuits

comprise neurons that encode information in the patterns and/or rates of action potentials, and understanding how changes in synaptic strength affect postsynaptic firing is a critical step for linking cellular mechanisms of plasticity with learning. Most studies of synaptic plasticity, however, have focused exclusively on how activity alters synaptic currents in neurons within complex circuits where the relationship between neuronal firing and behavioral performance is poorly understood.

Here we investigate synaptic plasticity in a system that is exceptionally well suited for linking experience-dependent changes in synaptic strength with postsynaptic firing outputs and their consequences for learning and memory. Direct control of well-defined movements and simple circuitry make motor learning in the vestibulo-ocular reflex (VOR) a tractable model for assessing the behavioral consequences of cellular plasticity. The VOR generates eye movements that stabilize images on the retina during self-motion; motor learning in the VOR is triggered by persistent image motion during head movements and results in increases or decreases in the gain of evoked eye movements (Ito, 1984; Miles and Lisberger, 1981). Decades of studies in awake, behaving animals have provided the requisite information about how neuronal firing in vestibular and cerebellar circuits affects VOR performance and learning (du Lac et al., 1995; Hirata and Highstein, 2001). Remarkably, although the central vestibular nerve synapse has long been a candidate site of behavioral modification of the VOR (Miles and Lisberger, 1981), plasticity has not been demonstrated at this synapse.

Vestibular nerve afferents and postsynaptic medial vestibular nucleus (MVN) neurons fire tonically at high rates *in vivo,* and synaptic transmission at central vestibular nerve synapses drives remarkably linear increases in postsynaptic firing rates (Bagnall et

al., 2008). How might these constraints influence the existence and nature of plasticity at this synapse? The activity patterns required to modify synaptic efficacy in neurons that fire at high baseline rates differ from those that gate plasticity in quiescent circuits (Jorntell and Hansel, 2006; Pugh and Raman, 2009). Synaptic inhibition or hyperpolarization can induce long-lasting potentiation of intrinsic excitability in MVN neurons (Nelson et al., 2003) and can trigger synaptic plasticity in analogous deep cerebellar nucleus neurons (Pugh and Raman, 2006). Therefore, we reasoned that postsynaptic membrane potential might similarly influence vestibular nerve synaptic plasticity. In this study, we examine whether vestibular nerve synaptic activity in the presence or absence of postsynaptic hyperpolarization has long-term effects on both postsynaptic currents and evoked firing responses in MVN neurons. The results demonstrate that vestibular nerve synapses are bidirectionally plastic and the direction of plasticity depends on postsynaptic voltage. Long-term potentiation (LTP) and long-term depression (LTD) of postsynaptic currents are translated into linear changes in postsynaptic firing rates across a wide range of stimulus frequencies. Thus, plasticity at the vestibular nerve synapse functions as a cellular mechanism of linear gain control.

Methods

Tracer Injections

The oculomotor nucleus, thalamus, cerebellum, and medullary reticular formation were stereotaxically targeted for microinjection of Texas Red dextran crystals (3,000 molecular weight; Invitrogen) in mice aged 45-65 days postnatal. Animals were deeply anesthetized with isoflurane and then placed on a stereotaxic apparatus (Benchmark

Angle Two; http://MyNeuroLab.com). A custom-made injector needle (0.2 mm outer diameter, 0.1 mm inner diameter; Creative Instruments Development Company) was loaded with dextran crystals, and the tip was sealed with melted bone wax. The needle was lowered into the targeted brain region, and the interior plunger was repeatedly depressed (~100 μm) with calibrated air pressure (30 psi, 30 msec) to deliver the crystals into the tissue. After waiting 1-2 min, the needle was withdrawn and the skin was sutured. 4-6 days post injection, mice were anesthetized with Nembutal and perfused transcardially with phosphate buffered saline (PBS), followed by 4% paraformaldehyde in PBS (PFA) for 5 min. After removal of the brain from the skull, the tissue was postfixed for 30–60 min in PFA and then stored overnight at 4°C in 30% sucrose in PBS. 25 μm coronal sections were cut on a freezing microtome (Microm) and washed in PBS. Sections were then wet-mounted and coverslipped with 2.5% DABCO (1,4-diazabicyclo-[2.2.2]octane).

Anatomical analyses

Confocal images were acquired in 1.0 μm steps on a Olympus BX60 microscope using laser lines of 488 and 561 nm, with a 100x objective and 2.5x digital zoom. Fluoview software was used to z-stack images. Images were transferred to Adobe Photoshop (Adobe Systems) for whole-image brightness/contrast adjustment and image overlay. GFP/YFP expression and the presence of Texas Red in retrogradely labelled neurons were detected with fluorescein isothiocyanate and rhodamine filters, respectively. The presence of double-labeled neurons was assessed in 12-20 sections containing the rostral half of the MVN from each of 2-3 YFP-16 or GIN mice. The

presence of GIN+ terminals opposed to somata or proximal dendrites was assessed in at least 5 neurons retrogradely labeled from each target.

Physiology

Oblique coronal brainstem slices were prepared from YFP-16 (Feng et al., 2000) and GIN mice (Oliva et al., 2000), backcrossed 10 generations onto a C57BL/6 background. Mice aged 18-24 days postnatal were deeply anesthetized with Nembutal and then decapitated. The brain was dissected in ice cold Ringer's solution (in mM: 124 NaCl, 5 KCl, 1.3 $MgSO_4$, 26 $NaHCO_3$, 2.5 $CaCl_2$, 1 NaH_2PO_4, and 11 dextrose). 300-µm slices were cut on a DSK DTK-1500E or Leica VT1000S vibratome and allowed to recover in 34 ºC Ringer's for 30 min. Slices rested at room temperature before being transferred to a recording chamber and perfused with carbogenated Ringer's containing 1-10 µM strychnine and 100 µM picrotoxin at 34 ºC. All experiments were carried out in accordance with the standards of the Salk Institute IACUC.

Patch pipettes were pulled from flame-polished glass (Warner) with resistances of 2-4 MΩ. Pipette internal solution contained (in mM): 140 K gluconate, 20 HEPES, 8 NaCl, 0.1 EGTA, 0.1 Spermine, 2 Mg-ATP, 0.3 Na_2-GTP. Where indicated in the text, 1,2-bis(2-animophenoxy)ethane-N,N,N',N'-tetraacitic acid (BAPTA, 5 mM) replaced EGTA in the internal solution. For recordings of synaptic current-voltage relationships, the internal solution contained (in mM): 120 $CsMeSO_4$, 10 HEPES, 8 NaCl, 10 QX-314, 5 TEA-Cl, 5 BAPTA, 0.1 Spermine, 2 Mg-ATP, 0.3 Na_2-GTP. Membrane potential is corrected for measured junction potentials.

Neurons were visualized with epifluorescence through a GFP filter, as well as under infrared differential interference contrast illumination with Nomarski optics. The vestibular nerve tract was identifiable under 10X magnification and was confirmed by anterograde transport of fluorescently labeled dextran conjugates injected into the vestibular ganglion. Synaptic transmission at the nerve synapse was evoked by a bipolar concentric stimulating electrode (FHC, Maine) placed on the vestibular nerve lateral to the vestibular complex (approximate location: 6-6.4 mm caudal to bregma, 4.4 mm ventral to the horizontal plane passing through bregma and lambda, and 1.7-1.8 mm lateral to the midline) and controlled via two Isoflex stimulus isolation units (AMPI, Israel). A biphasic pulse, consisting of two 100 μsec pulses of opposite polarity with a 100 μsec interval, was delivered to the electrode to avoid charge buildup.

Data were acquired with a Multiclamp 700B low-pass filtering at 6-10 kHz for voltage clamp and 10 kHz for current clamp. Data were digitized at 40 kHz with an ITC-16 or 18 (InstruTECH). House-written code in Igor 6 was used for acquisition and analysis. Series resistance was monitored continuously with small hyperpolarizing square pulses, and experiments showing a series resistance above 16 MΩ or a change greater than 20% were excluded.

Neurons were held in current clamp between 200 msec voltage clamp epochs, when synaptic currents were measured. EPSCs were measured at -75 mV every 15 sec before and after induction protocols. EPSCs were normalized to the pre-protocol baseline, which lasted 10-12 min. EPSC changes reported in the text are the averages of minutes 10-20 post-protocol. Firing rates are reported as the average of the reciprocal of

the inter-spike interval. For LTP mechanism experiments, only neurons with intrinsic rebound were included for analysis and statistics.

Data are reported as mean ± SEM, and statistical significance was evaluated with paired (where possible) or unpaired Wilcoxon signed-rank tests in KaleidaGraph 3.6 (Synergy Software). Chemicals were purchased from Sigma (St. Louis MO), with the exception of D-APV (Tocris, Bristol, UK) and BAPTA tetrapotassium salt (Invitrogen).

Results

Projection neurons can be distinguished from local inhibitory neurons with transgenic mouse lines

The MVN contains two broad classes of neurons with different physiological, neurochemical, and anatomical properties (Bagnall et al., 2007; Straka et al., 2005). These complementary populations can be identified in transgenic mouse lines: glutamatergic and glycinergic neurons are fluorescently labeled in the YFP-16 line, and a subset of GABAergic neurons is fluorescently labeled in the GIN line (Bagnall et al., 2007; Feng et al., 2000; Oliva et al., 2000). To determine whether these distinct neuronal classes correspond to known MVN cell types or mediate different circuit functions, which would constrain the consequences of synaptic plasticity, we evaluated their projections to other brain areas. Fluorescent dextran conjugates were injected *in vivo* into previously identified targets of the MVN (Highstein and Holstein, 2006), including the oculomotor nucleus, thalamus, medullary reticular formation, and cerebellum. In YFP-16 mice, YFP-expressing neurons were retrogradely labeled from all targets (Fig. 4.1A-C). In contrast, GFP-expressing neurons in GIN mice were never retrogradely labeled from

injections targeted outside of the vestibular nuclei. GFP-positive synaptic terminals in GIN mice were, however, observed on the somata and proximal dendrites of neurons in the MVN retrogradely labeled from injections to the cerebellum, thalamus, and reticular formation (Fig. 4.1D). These results indicate that fluorescently labeled MVN neurons in the YFP-16 line are predominantly projection neurons, while those in the GIN line provide local inhibition within the bilateral MVN.

The vestibular nerve synapse is bidirectionally plastic

Vestibular nerve afferents provide the major excitatory drive to the MVN and synapse directly onto both YFP-16 and GIN neurons (Bagnall et al., 2008). We sought to determine whether these synapses were capable of activity-dependent plasticity that regulated postsynaptic firing responses and whether modifications of synaptic strength depended on postsynaptic cell type. To investigate whether vestibular nerve synapses were plastic, we devised two protocols based on those used to induce LTD (Zhang and Linden, 2006) and LTP (Pugh and Raman, 2006) at the analogous excitatory mossy fiber synapse onto deep cerebellar nucleus neurons. Because MVN neurons receive a tonic barrage of both excitatory and inhibitory synaptic inputs, the protocols mimic epochs of either enhanced excitation or inhibition. The "100 Hz stim" protocol comprised 30 repetitions of 550-msec vestibular nerve stimulation at 100 Hz, which elevated the firing rate of postsynaptic neurons (Fig. 4.2A). The "100 Hz stim plus hyperpolarization" protocol comprised 30 repetitions of 550-msec vestibular nerve stimulation at 100 Hz, paired with hyperpolarization of the postsynaptic neuron by ~15-25 mV for 250 msec to simulate strong, coincident inhibition (Fig. 4.2B).

We initially examined synaptic plasticity in projection neurons highlighted in the YFP-16 line. Fluorescent neurons were targeted for whole-cell patch recordings in oblique coronal brainstem slices. Neurons were recorded primarily in current clamp to enable spontaneous firing (11 ± 2 Hz) and physiological baseline Ca^{2+} dynamics. Electrical stimulation of the vestibular nerve elicited synaptic responses in most MVN neurons, as previously reported (Bagnall et al., 2008). EPSCs evoked by nerve stimulation were measured during brief voltage clamp epochs every 15 sec, and a stable 10 min baseline was established prior to protocol application. The 100 Hz stim protocol evoked postsynaptic firing that averaged 38 ± 10 Hz and induced a short-lasting post-tetanic depression, followed by a robust LTD of the vestibular nerve synapse that reduced the peak EPSC amplitude to 0.82 ± 0.06 of the baseline 15 mins post-protocol (Fig. 4.2A, n=11, p=0.03 vs. no-protocol control recordings: 0.98 ± 0.01, n=9). Thus, the vestibular nerve synapse displays activity-dependent, long-term strength modifications, and coincident pre- and post-synaptic activity results in LTD.

Given the extensive role of inhibition in the control of sensory processing and plasticity in the vestibular system (Buttner et al., 1992; Gittis and du Lac, 2006; Ito et al., 1970; Kato et al., 2003; Shimazu and Precht, 1966), we examined whether long-term synaptic efficacy was influenced by postsynaptic hyperpolarization. Remarkably, hyperpolarization of postsynaptic YFP-16 neurons during high-frequency vestibular nerve stimulation reversed the direction of long-term plasticity and resulted in LTP, which increased the peak EPSC amplitude to 1.31 ± 0.13 of the baseline (Fig. 4.2B, n=21, p=0.05 vs. no-protocol control; average hyperpolarization: -18.2 ± 1.3 mV). The stimulation patterns that induced synaptic plasticity did not induce concomitant changes

in the intrinsic properties of postsynaptic neurons (Table 4.1). These data show that the first central synapse in the vestibular system is capable of robust, bidirectional plasticity and that postsynaptic voltage controls the direction of plasticity.

Plasticity modulates the gain of evoked firing in projection neurons

What are the consequences of vestibular nerve synaptic plasticity for postsynaptic neuronal output? Although synaptic efficacy is typically assessed with either single stimuli or pairs of stimuli, vestibular nerve afferents fire at high baseline rates (~30-50 Hz *in vivo*) and rarely fall silent for extended periods (Hullar and Minor, 1999; Lasker et al., 2008). Consequently, we assessed the effects of synaptic plasticity by stimulating with trains of pulses at rates across the physiologically relevant operating range of the vestibular nerve.

At the vestibular nerve to MVN neuron synapse, stimulus trains evoke EPSCs that depressed rapidly, over the first ~10 pulses, to a steady-state amplitude that is independent of frequency (Bagnall et al., 2008). Neither the time course nor the relative magnitude of short-term synaptic dynamics were altered following the induction of LTD (n=9, p= 0.57) or LTP (n= 8, p= 0.08)(Fig. 4.3A, B). Importantly, a linear relationship between the rate of stimulation (5-100 Hz) and the normalized synaptic charge transfer was also preserved following the induction of LTD (R^2= 0.97 ± 0.01, n=11) and LTP (R^2= 0.99 ± 0.01, n= 8, Fig. 4.3C). These results demonstrate that LTD and LTP influenced EPSC amplitude uniformly across stimulus rates without affecting the short-term synaptic dynamics. Thus, vestibular nerve plasticity scales evoked postsynaptic

currents without altering the rate-independence of synaptic transmission and corresponding linear charge transfer.

For synaptic plasticity to have functional consequences, it must ultimately influence firing in postsynaptic neurons. The role of firing is exceptionally well characterized in the vestibular system, where head motion modulates the firing rate of MVN neurons. Applying stimulus trains to the vestibular nerve produced increases in MVN firing rates that were proportional to the stimulation rate (Fig. 4.4A, B*).* We quantified the firing response as synaptic gain: the slope of the relationship between postsynaptic firing rate and presynaptic stimulus rate. Firing responses varied considerably across neurons; baseline synaptic gains ranged from 0.11 to 0.87, corresponding to firing rates ranging from 17 to 102 Hz in response to 100 Hz stimulation.

To assess the effects of plasticity on firing, synaptic gain was measured in response to 25-100 Hz trains before and after induction of synaptic plasticity, while DC hyperpolarizing or depolarizing current was injected to maintain the baseline firing rate at ~ 7 Hz to facilitate comparisons across cells. Following the induction of LTD, firing responses to vestibular nerve stimulation decreased (Fig. 4.4B). Conversely, the induction of LTP resulted in increases in synaptic gain (Fig. 4.4C). Across the population, LTD decreased the synaptic gain to 0.83 ± 0.06 of the baseline gain (n=10, p=0.02), and LTP increased the synaptic gain to 1.49 ± 0.16 (n=10, p=0.004)(Fig. 4.4D). The linear relationship between postsynaptic firing and stimulation rate was preserved following plasticity induction (Fig. 4.4E). The baseline firing rate, from which increases in firing rate were evoked, was constant during LTD (Pre: 6.7 ± 0.9 Hz, Post: 6.7± 0.9

Hz) and LTP experiments (Pre: 7.2 ± 0.9 Hz, Post: 7.6 ± 0.9 Hz), and neither protocol altered the intrinsic excitability of postsynaptic neurons (Table 4.1), suggesting that changes in postsynaptic firing responses were driven completely by changes in synaptic strength. In control experiments, in which 30 repetitions of 250-msec hyperpolarizing steps were applied in the absence of synaptic stimulation, synaptic gain was unchanged (1.00 ± 0.02 of the baseline, n=5, p=0.42, data not shown).

The magnitude of the changes in firing rates produced by vestibular nerve synaptic plasticity varied across stimulation rates and neurons (Fig. 4.4D). The gain changes evoked by LTP corresponded to an average firing rate increase of 13.2 ± 3.3 Hz in response to 100 Hz stimulation, but an increase of 0.8 ± 1.6 Hz in response to 25 Hz stimulation. Similarly, gain changes following LTD decreased the average firing response by 7.2 ± 3.3 Hz during 100 Hz stimulation and by 1.8 ± 1.5 Hz during 25 Hz stimulation. Synaptic gain was unaffected in 2/10 neurons following LTP induction and in 4/10 neurons following LTD induction, despite accompanying changes in EPSC amplitude. The absolute changes in firing responses at any stimulus rate were not correlated with initial firing rate or baseline synaptic gain. These results indicate that although the relationship between synaptic strength and postsynaptic firing responses is influenced by several factors, plasticity at the vestibular nerve synapse functions as a bidirectional, linear gain control mechanism that regulates the strength of signal throughput.

Vestibular nerve synapses contain NMDA and calcium-permeable AMPA receptors

The induction of synaptic plasticity in many systems requires Ca^{2+} influx through postsynaptic receptors. Although several studies have indicated that vestibular nerve

synapses are glutamatergic and contain both NMDA and AMPA receptors (Babalian et al., 1997; Doi et al., 1990; Kinney et al., 1994; Lewis et al., 1989; Straka et al., 1996; Takahashi et al., 1994), relatively little is known about the Ca^{2+} permeability or voltage dependence of the postsynaptic receptors. We measured current-voltage (IV) relationships of the AMPA and NMDA receptors in YFP-16 neurons in the presence of specific pharmacological antagonists to identify receptor subtypes (Fig. 4.5A). The AMPA-R IV relationship strongly rectified (Rectification Index, +45 mV/-45 mV: 0.44 ± 0.06; range: 0.18-0.79, n=11) (Fig. 4.5B, D), suggesting the presence of GluA2-lacking, Ca^{2+}-permeable AMPA-Rs (CP-AMPA-Rs) (Bochet et al., 1994; McBain and Dingledine, 1993). The selective blocker of GluA2-lacking AMPA-Rs, Philanthotoxin-433 (PhTx-433, 10μM) reduced EPSC amplitude by 55.9 ± 10.1% (range: 7.4-86.9%, n=9, data not shown), indicating that vestibular nerve synapses onto projection neurons contain a composite of GluA2-lacking and GluA2-containing AMPA-Rs.

The NMDA-R contribution to vestibular nerve synaptic transmission was small relative to that of AMPA-Rs (NMDA +45 mV/AMPA -65 mV: 0.48 ± 0.10; range: 0.18-0.89, n=9) (Fig. 4.5E). The NMDA-R current duration, 104 ± 18 msec, and voltage dependence (Fig. 4.5A, C) suggested that NMDA-Rs predominantly contain the NR2A subunit (Cull-Candy and Leszkiewicz, 2004). These data show that two complementary Ca^{2+}-permeable glutamate receptors support vestibular nerve transmission: CP-AMPA-Rs, which pass Ca^{2+} maximally at relatively hyperpolarized postsynaptic membrane potentials, and NMDA-Rs, which pass Ca^{2+} maximally at relatively depolarized potentials.

LTD and LTP depend differentially on postsynaptic glutamate receptors

Given the presence of two distinct Ca^{2+}-permeable glutamate receptors at this synapse, we tested whether postsynaptic Ca^{2+} elevations were required for either type of long-term synaptic plasticity. Indeed, both LTD and LTP were blocked by the inclusion of the Ca^{2+} chelator BAPTA (5 mM) in the recording pipette (100 Hz stim protocol: 1.00 ± 0.03, n=7, p=0.03; 100 Hz stim plus hyperpolarization protocol: 0.98 ± 0.03, n=6, p=0.02, Fig. 4.5F, I).

Does Ca^{2+} influx through NMDA-Rs or CP-AMPA-Rs contribute to the induction of long-term plasticity at the vestibular nerve synapse? We first examined the role of NMDA-Rs. Blockade of NMDA-Rs via bath application of D-APV (100 μM) or intracellular inclusion of MK-801 (1 mM) abolished 100 Hz stim-induced LTD (1.01 ± 0.03, n=6, p=0.02, Fig. 4.5G), without blocking LTP (1.41 ± 0.13, n=9, p=0.19, Fig. 4.5J). Thus, postsynaptic NMDA-Rs are required for LTD, but not LTP, at the vestibular nerve synapse.

To test the role of CP-AMPA-Rs, we bath applied the specific blocker PhTx-433 (10 μM). In the presence of PhTx-433, LTD induced by 100 Hz stimulation was unaltered (0.79 ± 0.07, n=6, p=0.59, Fig. 4.5H). Interestingly, the 100 Hz stim plus hyperpolarization protocol resulted in synaptic depression (0.81 ± 0.10, n=5, p=0.008, Fig. 4.5K) in the presence of Phtx-433, rather than potentiation, indicating that CP-AMPA-Rs are required for LTP induction. The unmasked LTD indicates that the 100 Hz stim plus hyperpolarization protocol simultaneously recruits LTP and LTD mechanisms, with the balance in favor of LTP under normal conditions. Consistent with this interpretation, applying the 100 Hz plus hyperpolarization protocol in the presence of D-

APV resulted in enhanced LTP (Fig. 4.5J), while applying same protocol in the presence of reduced extracellular Mg^{2+} (0.3 mM) to augment Ca^{2+} influx via NMDA-Rs suppressed the induction of LTP (0.95 ± 0.4, n=5, data not shown). Thus, LTD and LTP at the vestibular nerve synapse operate in parallel and require distinct Ca^{2+}-permeable glutamate receptors.

To determine whether CP-AMPA-Rs are additionally expressed presynapically, 10 μM PhTx-433 was washed onto slices and the paired-pulse ratio (PPR) at the 20-msec interval was measured. The presence of PhTx-433 did not alter the PPR (Baseline: 93.1 ± 4.2%, PhTx-433: 96.9 ± 3.9%, p=0.20), suggesting that CP-AMPA-Rs predominantly exerted their effects on LTP postsynaptically. We conclude that LTP required postsynaptic Ca^{2+} passed by CP-AMPA-Rs and that LTD requires postsynaptic Ca^{2+} passed by NMDA-Rs. This complementary dependence on postsynaptic ionotropic glutamate receptors enables membrane voltage to gate the direction of synaptic plasticity.

Postinhibitory rebound depolarization contributes to LTP induction

What are the essential postsynaptic requirements for the induction of LTP? Postsynaptic hyperpolarization produces several distinct effects: it prevents firing, modulates the amplitude of voltage-dependent currents, and recruits low voltage-activated currents. Many neurons in the MVN exhibit rebound firing, a transient elevation in firing rate following relief from hyperpolarization, and the magnitude of rebound firing varies across individual neurons (du Lac and Lisberger, 1995; Sekirnjak and du Lac, 2002; Serafin et al., 1991). During the 100 Hz stim plus hyperpolarization plasticity protocol, 15 of 21 neurons (Fig. 4.2) exhibited rebound firing (42 ± 8 Hz), quantified as

the average firing rate increase over the spontaneous rate during the initial 300 msec post-hyperpolarization. LTP was induced in 11 of these 15 neurons (EPSC post-protocol: 1.45 ± 0.16, n=15, p=0.002 vs. control). In contrast, LTP was not induced in any of the remaining 6 neurons that did not exhibit rebound firing post-hyperpolarization (EPSC post-protocol: 0.95 ± 0.03, n=6, p=0.57 vs. control; Rebound vs. Non-rebound: p=0.004, Fisher Exact Test).

To assess whether rebound currents merely distinguished two subtypes of YFP-16 neurons or, additionally, played a causal role in LTP induction, we manipulated the timing of rebound relative to synaptic stimulation in the 100 Hz stim plus hyperpolarization. We first extended the duration of the hyperpolarization step to 550 msec, such that the rebound occurred immediately after, rather than during, the 550-msec stimulus train. This protocol induced LTP of 1.27 ± 0.12 (Fig. 4.6A, n=7, p=0.05), comparable to LTP induced by hyperpolarization lasting 250 msec (p=0.81). We then extended the hyperpolarization step duration to 1550 msec so that rebound followed synaptic stimulation by 1000 msec. This protocol, which temporally dissociated synaptic input and intrinsic rebound, did not induce LTP (Fig. 4.6B, 0.96 ± 0.09 of baseline, n=7, p=0.61 vs. control). These results suggest that intrinsic rebound is a critical component of LTP induction that must to be temporally linked to synaptic stimulation.

To test whether this rebound requirement was mediated by enhanced firing following synaptic stimulation, we applied the 100 Hz stim plus hyperpolarization protocol to neurons lacking intrinsic rebound firing and injected a 300 msec suprathreshold depolarizing current following hyperpolarization (Fig. 4.6C). The addition of this mimicked rebound was inadequate to induce LTP in non-rebounding neurons

(0.88 ± 0.07 of baseline, n=7, p=0.005 vs. 100 Hz stim plus hyperpolarization, Fig. 4.6C). Furthermore, the magnitude of EPSC potentiation did not correlate with the rate of rebound firing in YFP-16 neurons displaying intrinsic rebound (R^2=0.08). Thus, while rebound firing distinguishes two populations of YFP-16 neurons and is predictive of LTP induction, hyperpolarization offset and rebound currents contribute to LTP via mechanisms beyond simple increases in postsynaptic firing rate.

Vestibular nerve synapses onto GABAergic interneurons are plastic

Thus far we have focused on projection neurons. Are vestibular nerve synapses onto local inhibitory neurons (Fig. 4.1D) also plastic? To investigate this potential additional site of plasticity for head movement-driven behaviors, we applied the stimulus protocols that induced LTD and LTP in YFP-16 neurons to GIN neurons. The 100 Hz stim protocol evoked LTD in GIN neurons (0.74 ± 0.05 of baseline, n=6, p=0.001, Fig. 4.7A). The induction of LTD in interneurons was blocked by intracellular, postsynaptic BAPTA (5 mM) (0.99 ± 0.08, n=6, p=0.02), as well as by the NMDA-R antagonist D-APV (100 μM) (1.01 ± 0.07, n=6, p=0.02, Fig. 4.8A, B). These data demonstrate that LTD in vestibular nucleus interneurons requires Ca^{2+} influx through NMDA-Rs, as is the case for projection neurons (Fig. 4.5G).

In striking contrast, the stimulus protocol that induced LTP in projection neurons did not result in potentiation of synaptic strength onto interneurons but instead induced a weak LTD (0.90 ± 0.05 of baseline, n=9, p=0.08, Fig. 4.7B). Interestingly, blocking NMDA-Rs with bath application of D-APV during the 100 Hz stim plus hyperpolarization protocol unmasked an underlying synaptic potentiation (1.25 ± 0.11 of

baseline, n=7, p=0.04, Fig. 4.8C). This D-APV-unmasked LTP in interneurons was sensitive to PhTx-433 (0.95 ± 0.07, n=8, p=0.04, Fig. 4.8D). These results indicate that, as in projection neurons, CP-AMPA-R activation paired with postsynaptic hyperpolarization can induce LTP in interneurons, but LTP is typically masked by NMDA-R-mediated LTD.

Several factors might underlie LTD dominance in interneurons, including differential expression of glutamate receptors or post-hyperpolarization rebound currents. Indeed, the AMPA-R IV relationship in GIN neurons was less rectifying than that measured in YFP-16 neurons (Rectification Index GIN: 0.69 ± 0.06, n=13, p=0.01, Fig. 4.5D), while the NMDA/AMPA ratio in GIN neurons was not significantly different from YFP-16 neurons (GIN: 0.47 ± 0.09, n=13, p=0.67, Fig. 4.5E). The inclusion of a relatively smaller proportion of CP-AMPA-Rs at synapses onto GIN neurons may limit the recruitment of LTP. All GIN neurons exhibited post-hyperpolarization rebound firing, although its magnitude was less than half that of the YFP-16 neurons that rebounded (GIN: 20 ± 3 Hz, YFP-16: 42 ± 8 Hz, p=0.02). Thus, CP-AMPA-R and rebound currents are differentially expressed according to circuit function in the MVN, such that both are minimized in local inhibitory GIN neurons.

Discussion

This study demonstrates that the first central synapse in the vestibular system is bidirectionally plastic. Vestibular nerve synaptic plasticity is governed by non-Hebbian induction rules and produces linear changes in postsynaptic neuronal firing responses to vestibular nerve activity across a wide range of presynaptic rates. Vestibular nerve LTD

and LTP depend on Ca^{2+} influx through different postsynaptic ionotropic glutamate receptors: LTD requires activation of NMDA-Rs, while LTP requires activation of CP-AMPA-Rs. Although LTD can be induced by nerve afferent activity alone, the induction of LTP requires a specific temporal conjunction of vestibular nerve synaptic activity and post-synaptic hyperpolarization. Synapses onto both MVN projection neurons and local interneurons are plastic, and differences in synaptic and intrinsic conductances across cell types shape the balance of LTD and LTP. Given the powerful influence of the vestibular nerve on MVN neuronal firing, plasticity at this synapse is optimally suited to regulate the gain of vestibular behaviors while preserving the speed and computation of the underlying circuits.

Linear scaling of postsynaptic currents and firing rates via synaptic plasticity

Synaptic efficacy has typically been probed by measuring postsynaptic, subthreshold responses to stimuli consisting of either single shocks or pairs of shocks. Given that many synapses exhibit short-term plasticity (changes in efficacy as a function of recent activity), it is not possible to infer synaptic responses to multiple stimuli from responses to individual stimuli. For example, although LTP uniformly potentiates synaptic currents elicited by brief presynaptic bursts in hippocampal neurons (Pananceau et al., 1998; Selig et al., 1999), LTP expression depends strongly on stimulus rate and history in cortical neurons (Markram and Tsodyks, 1996). Our results demonstrate that at central vestibular nerve synapses, the induction of either LTD or LTP results in a uniform scaling of synaptic efficacy, such that steady-state synaptic transmission remains rate-invariant over a wide range of stimulus frequencies (Fig. 4.3). What mechanisms could

account for these proportionate changes in synaptic efficacy? Given that changes in the probability of transmitter release are typically accompanied by changes in short-term synaptic dynamics (Zucker and Regehr, 2002) and that postsynaptic properties do not contribute to short-term dynamics at the vestibular nerve synapse (Bagnall et al., 2008), our findings are most consistent with a postsynaptic locus of expression of vestibular nerve synaptic plasticity.

The effects of bidirectional synaptic plasticity on postsynaptic firing have not been previously reported. Several studies report how changes in synaptic strength translate into changes in postsynaptic firing (Bliss and Lomo, 1973; Fetz and Gustafsson, 1983; Mittmann and Hausser, 2007; Reyes and Fetz, 1993; Smith and Otis, 2005; Walter and Khodakhah, 2006), but none have probed responses over the entire range of behaviorally relevant stimulus rates. The transformation of synaptic inputs into action potentials is influenced by both active and passive dendritic processes as well as by somatic filtering, complicating the relationship between synaptic strength and resultant postsynaptic firing. Vestibular nucleus neurons differ markedly from the much more extensively studied pyramidal cells in the hippocampus and cortex, both in the rate-invariance of primary excitatory synaptic transmission (Bagnall et al., 2008) and in the wide range of firing rates over which spike generation remains linear (Sekirnjak and du Lac, 2002; Serafin et al., 1991). Whether synaptic plasticity produces scaling of postsynaptic firing responses in other neurons that exhibit linear spike generation—such as fast-firing hippocampal, cortical, and basal ganglia interneurons, as well as other brainstem and cerebellar neurons—remains to be examined.

Activity requirements and mechanisms of vestibular nerve synaptic plasticity

Distinct mechanisms and postsynaptic Ca^{2+} sources underlie LTD and LTP at the vestibular nerve synapse. LTD is induced by high-frequency synaptic activation paired with postsynaptic depolarization. The ability of BAPTA and D-APV to prevent LTD (Fig. 4.5) implies that LTD is triggered by Ca^{2+} influx through postsynaptic NMDA-Rs, whose Mg^{2+} sensitivity enables Ca^{2+} influx to reflect postsynaptic voltage. The NMDA-R component at the vestibular nerve synapse is relatively small (Fig. 4.5E) and contributes minimally to synaptically-evoked firing in postsynaptic neurons (Bagnall et al., 2008), suggesting a predominant function of NMDA-Rs at this synapse may thus be to regulate synaptic depression.

It is remarkable that the direction of plasticity induced by high frequency synaptic stimulation is reversed by postsynaptic membrane hyperpolarization (Fig. 4.2). The effects of BAPTA, PhTx-433, and delayed rebound indicate that LTP is triggered by a combination of Ca^{2+} influx through postsynaptic AMPA-Rs and signals which accompany the offset of hyperpolarization. The dependence of LTP and LTD on distinct glutamate receptors with complementary voltage dependences (Fig. 4.5B,C) enables postsynaptic membrane potential to bidirectionally bias the induction of plasticity.

Our findings indicate that the relative timing of synaptic activity and postsynaptic hyperpolarization is critical for the induction of LTP (Fig. 4.6B). The correlation between rebound firing and LTP suggests that underlying rebound currents may play an important role in LTP induction. Hyperpolarization affects several sources of Ca^{2+} that could contribute to both rebound and LTP induction, including low-voltage activated T-type Ca^{2+} channels (Aizenman and Linden, 1999; Alvina et al., 2009; Molineux et al., 2006;

Sekirnjak and du Lac, 2002; Zheng and Raman, 2009). Our results are consistent with a model in which Ca^{2+} influx via AMPA-Rs primes synapses and then subsequent Ca^{2+} influx during rebound triggers LTP.

Alternatively, hyperpolarization offset could influence LTP by restoring, rather than elevating, Ca^{2+} levels. In addition to recruiting low-voltage activated Ca^{2+} channels, hyperpolarization also deactivates high-voltage activated Ca^{2+} channels that are tonically active in spontaneously firing neurons (Nelson et al., 2003; Zheng and Raman, 2009). A recent study of the analogous mossy fiber to cerebellar nucleus synapse demonstrated that LTP induction there requires transient decreases in the baseline Ca^{2+} levels of postsynaptic neurons (Person and Raman, 2010). Further experiments are required to define both the critical currents modulated by hyperpolarization and the Ca^{2+} dynamics required for LTP induction at the vestibular nerve synapse.

Synaptic plasticity in brainstem and cerebellar circuits

Several forms of plasticity in brainstem and cerebellar circuits depend on inhibition (Pugh and Raman, 2009), including intrinsic excitability in the MVN (Nelson et al., 2003) and synaptic plasticity in the cerebellar nuclei (CN) (Pugh and Raman, 2008). Plasticity mechanisms in the MVN and CN are thought to be coordinated by the cerebellar cortex, which directly inhibits neurons in both nuclei. Interestingly, although the stimulus protocols that induced bidirectional plasticity in this study are quite similar to those that induce plasticity at the analogous mossy-fiber synapse in the CN, the underlying mechanisms differ. In CN neurons, high-frequency presynaptic activity paired with postsynaptic depolarization induces mGluR1-dependent LTD, whereas

presynaptic activity paired with postsynaptic hyperpolarization induces NMDA-R-dependent LTP (Pugh and Raman, 2006, 2008; Zhang and Linden, 2006). While the intrinsic firing properties of neurons in the cerebellar and vestibular nuclei are largely equivalent (Bagnall et al., 2007; Bagnall et al., 2009; Sekirnjak and du Lac, 2002; Uusisaari et al., 2007), the two nuclei are functionally distinct: vestibular nucleus neurons can influence motoneurons directly via projections to ocular motor and spinal nuclei, whereas CN neurons modulate motor and cortical function via multiple intervening synapses. Furthermore, vestibular nerve axons convey primary sensory signals, while most cerebellar mossy fibers convey signals that have already been processed extensively by central neurons. The finding that hyperpolarization gates potentiation of excitatory synapses similarly in the two different nuclei, albeit via distinct mechanisms, implies that such plasticity rules may be a general strategy used by spontaneously firing neurons in cerebellar and brainstem circuits.

The activity patterns and Ca^{2+} signals required to induce synaptic plasticity are thought to be inverted in the cerebellum relative to the hippocampus and cerebral cortex (Jorntell and Hansel, 2006), reflecting differing circuit functions and baseline firing rates. While vestibular nerve synaptic plasticity is similar to many forms of plasticity in cerebellar circuits in its non-Hebbian induction requirements, it differs in its Ca^{2+} dependence. Low intracellular BAPTA concentrations (0.1mM) had no effect on vestibular nerve LTD (0.80 ± 0.13, n=4) but interfered with LTP induction (0.98 ± 0.01, n=4, data not shown), suggesting that, as in forebrain synapses (Bear et al., 1987; Cummings et al., 1996; Hansel et al., 1997), LTP requires a higher postsynaptic Ca^{2+} concentration than does LTD. Thus, while the high baseline firing rates in cerebellar and

vestibular circuits constrain the activity patterns that induce synaptic plasticity, the underlying mechanisms are tuned specifically to each synapse.

Cell type specific regulation of synaptic plasticity

Although repeated high frequency stimulation elicits LTD at vestibular nerve synapses onto all MVN neurons, the addition of postsynatpic hyperpolarization induces LTP in YFP-16 neurons but not in GIN neurons (Figs 4.2, 4.7). Retrograde labeling experiments revealed that YFP-16 neurons, which are glutamatergic or glycinergic (Bagnall et al., 2007), are a major source of projections to motor, cerebellar, and thalamic targets (Fig. 4.1). In contrast, GIN neurons, which are GABAergic (Bagnall et al., 2007), do not appear to project outside of the vestibular nuclei but instead provide local and commissural inhibition of projection neurons (Fig. 4.1D). The differential recruitment of plasticity onto projection neurons and interneurons, coupled with extensively intermingled cell types within the vestibular nucleus, complicate drawing parallels with the extensive dataset on plasticity of field potentials evoked by synaptic stimulation within the vestibular complex (Grassi et al., 2009; Grassi et al., 2002; Grassi and Pettorossi, 2001; Grassi et al., 1996; Puyal et al., 2003). The cell-type specificity of LTP induction reported here highlights the importance of targeting recordings to identified neuronal populations (McBain, 2008; Tzounopoulos et al., 2004).

The mechanisms of bidirectional plasticity are conserved across YFP-16 and GIN neurons. Blockade of NMDA-Rs (Fig. 4.8C) revealed that synapses onto GIN neurons can be potentiated by pairing vestibular nerve stimulation with hyperpolarization but that concomitant depression typically masks this potentiation. The bias against LTP in

interneurons appears to be regulated by both intrinsic and synaptic mechanisms: rebound currents and CP-AMPA-Rs at the vestibular nerve synapse are both minimized in GIN interneurons relative to YFP-16 projection neurons. Thus, the balance of LTD and LTP at vestibular nerve synapses appears to be influenced by two distinct mechanisms that are both regulated according to cell type.

Functional Implications

The vestibular system, which is plastic throughout life, is critical for a wide range of functions, including stability during movement, spatial orientation, and autonomic regulation (Angelaki and Cullen, 2008). Our results demonstrate that vestibular signaling is plastic at the first stages of central transmission. The firing of MVN neurons influences several modifiable reflexes via projections onto ocular and spinal motor neurons, most notably the vestibulo-ocular reflex (VOR), which has long served as a model for cerebellar-dependent learning (Ito, 1984; Miles and Lisberger, 1981). Our results support the Miles-Lisberger hypothesis of learning in the VOR (Miles and Lisberger, 1981), which proposes that MVN firing responses to head movements could be regulated by plasticity of the primary sensory input onto a subset of vestibular nucleus neurons.

Motor learning in the VOR requires the cerebellum, but results of cerebellar inactivation experiments indicate that the expression of learned changes resides downstream of the cerebellar Purkinje cells, in the MVN (Kassardjian et al., 2005; Shutoh et al., 2006). Recordings from vestibular nucleus neurons, together with behavioral analyses of motor learning, indicate that parallel modifiable and unmodifiable

pathways mediate performance and adaptation of the VOR (Lisberger, 1984; Lisberger and Pavelko, 1986). The modifiable pathway includes neurons that are powerfully inhibited by cerebellar Purkinje cells and project to ocular motoneurons, and the faster, unmodifiable pathway is thought to include neurons that do not receive cerebellar inhibition but that also project to ocular motoneurons (Lisberger and Pavelko, 1988; Ramachandran and Lisberger, 2008; Scudder and Fuchs, 1992). Increases or decrease in the gain of the VOR are associated with bidirectional changes in the firing responses to head movements of MVN neurons receiving cerebellar inhibition. Our findings that bidirectional plasticity of vestibular nerve synapses can only be evoked in a distinct subset of projection neurons is consistent with the notion of modifiable and unmodifiable VOR pathways.

That the LTD and LTP demonstrated here cause bidirectional, linear changes in postsynaptic firing responses to vestibular nerve stimulation make them plausible candidate mechanisms for contributing to VOR learning. An attractive hypothesis is that the YFP-16 neurons which exhibit bidirectional plasticity comprise the modifiable pathway, and that the relative timing of Purkinje cell inhibition and vestibular nerve activity modulates the gain of the VOR via bidirectional vestibular nerve synaptic plasticity. Given direct projections to ocular motoneurons, LTP or LTD of the vestibular nerve synapse onto YFP-16 neurons would result in increases or decreases in VOR gain, respectively. Relating cellular mechanisms *in vitro* with behavioral function *in vivo*, however, requires extrapolation across different physiological conditions. The range of evoked firing rates in our study was lower than that observed in intact animals (Beraneck and Cullen, 2007; Lasker et al., 2008), reflecting limitations in the number of vestibular

afferents that can be stimulated in a viable brain slice and lower *in vitro* baseline firing rates. Given the remarkably wide range of linear spike generation in vestibular nucleus neurons that project to ocular motor neurons, however, it is likely that the linear scaling of synaptic currents observed in this study apply to the wider range of synaptic drive experienced by neurons *in vivo*.

Several types and loci of plasticity are likely to contribute to motor learning in the vestibular system. The robust depression onto interneurons described here is a regulatory site that could be utilized independently or in conjunction with plasticity at other sites to influence vestibular processing. Local inhibition in the MVN includes feedforward (Straka et al., 1997) and commissural connections (Bagnall et al., 2007; Malinvaud et al., 2010), whose specific roles in signal processing and circuit throughput are only beginning to be dissected (Biesdorf et al., 2008). Plasticity of the primary excitatory drive onto interneurons could regulate vestibular behaviors by modulating tonic inhibition of ipsi- or contralateral projection neurons. Behavioral evidence suggests that the learning of VOR gain increases and decreases may not be mediated by mechanisms that are direct opposites of one another (Boyden and Raymond, 2003; Miles and Eighmy, 1980), and the multiple forms and sites of synaptic plasticity described here provide the circuit with several potential regulatory mechanisms. The straightforward relationship between synaptic efficacy and postsynaptic firing responses, coupled with extensive knowledge of the functional significance of firing in identified cell types (Angelaki and Cullen, 2008; du Lac et al., 1995), makes linking synaptic plasticity with circuit and, ultimately, behavioral consequences tractable in the vestibular system.

Acknowledgments

This chapter is a reprint of the material as it appears in McElvain L.E., Bagnall M.W., Sakatos A., du Lac S.. Bidirectional plasticity gated by hyperpolarization controls the gain of postsynaptic firing responses at central vestibular nerve synapses. Neuron *68*, 763-75 and is included with permission from all the manuscript's authors.

References

Aizenman, C.D., and Linden, D.J. (1999). Regulation of the rebound depolarization and spontaneous firing patterns of deep nuclear neurons in slices of rat cerebellum. J Neurophysiol *82*, 1697-1709.

Alvina, K., Ellis-Davies, G., and Khodakhah, K. (2009). T-type calcium channels mediate rebound firing in intact deep cerebellar neurons. Neuroscience *158*, 635-641.

Angelaki, D.E., and Cullen, K.E. (2008). Vestibular system: the many facets of a multimodal sense. Annu Rev Neurosci *31*, 125-150.

Babalian, A., Vibert, N., Assie, G., Serafin, M., Muhlethaler, M., and Vidal, P.P. (1997). Central vestibular networks in the guinea-pig: functional characterization in the isolated whole brain in vitro. Neuroscience *81*, 405-426.

Bagnall, M.W., McElvain, L.E., Faulstich, M., and du Lac, S. (2008). Frequency-independent synaptic transmission supports a linear vestibular behavior. Neuron *60*, 343-352.

Bagnall, M.W., Stevens, R.J., and du Lac, S. (2007). Transgenic mouse lines subdivide medial vestibular nucleus neurons into discrete, neurochemically distinct populations. J Neurosci *27*, 2318-2330.

Bagnall, M.W., Zingg, B., Sakatos, A., Moghadam, S.H., Zeilhofer, H.U., and du Lac, S. (2009). Glycinergic projection neurons of the cerebellum. J Neurosci *29*, 10104-10110.

Bear, M.F., Cooper, L.N., and Ebner, F.F. (1987). A physiological basis for a theory of synapse modification. Science *237*, 42-48.

Beraneck, M., and Cullen, K.E. (2007). Activity of vestibular nuclei neurons during vestibular and optokinetic stimulation in the alert mouse. J Neurophysiol *98*, 1549-1565.

Biesdorf, S., Malinvaud, D., Reichenberger, I., Pfanzelt, S., and Straka, H. (2008). Differential inhibitory control of semicircular canal nerve afferent-evoked inputs in second-order vestibular neurons by glycinergic and GABAergic circuits. J Neurophysiol *99*, 1758-1769.

Bliss, T.V., and Lomo, T. (1973). Long-lasting potentiation of synaptic transmission in the dentate area of the anaesthetized rabbit following stimulation of the perforant path. J Physiol *232*, 331-356.

Bochet, P., Audinat, E., Lambolez, B., Crepel, F., Rossier, J., Iino, M., Tsuzuki, K., and Ozawa, S. (1994). Subunit composition at the single-cell level explains functional properties of a glutamate-gated channel. Neuron *12*, 383-388.

Boyden, E.S., and Raymond, J.L. (2003). Active reversal of motor memories reveals rules governing memory encoding. Neuron *39*, 1031-1042.

Buttner, U., Straube, A., and Kurzan, R. (1992). Oculomotor effects of gamma-aminobutyric acid agonists and antagonists in the vestibular nuclei of the alert monkey. Ann N Y Acad Sci *656*, 645-659.

Cull-Candy, S.G., and Leszkiewicz, D.N. (2004). Role of distinct NMDA receptor subtypes at central synapses. Sci STKE *2004*, re16.

Cummings, J.A., Mulkey, R.M., Nicoll, R.A., and Malenka, R.C. (1996). Ca2+ signaling requirements for long-term depression in the hippocampus. Neuron *16*, 825-833.

Doi, K., Tsumoto, T., and Matsunaga, T. (1990). Actions of excitatory amino acid antagonists on synaptic inputs to the rat medial vestibular nucleus: an electrophysiological study in vitro. Exp Brain Res *82*, 254-262.

du Lac, S., and Lisberger, S.G. (1995). Membrane and firing properties of avian medial vestibular nucleus neurons in vitro. J Comp Physiol A *176*, 641-651.

du Lac, S., Raymond, J.L., Sejnowski, T.J., and Lisberger, S.G. (1995). Learning and memory in the vestibulo-ocular reflex. Annu Rev Neurosci *18*, 409-441.

Feng, G., Mellor, R.H., Bernstein, M., Keller-Peck, C., Nguyen, Q.T., Wallace, M., Nerbonne, J.M., Lichtman, J.W., and Sanes, J.R. (2000). Imaging neuronal subsets in transgenic mice expressing multiple spectral variants of GFP. Methods *28*, 41-51.

Fetz, E.E., and Gustafsson, B. (1983). Relation between shapes of post-synaptic potentials and changes in firing probability of cat motoneurones. J Physiol *341*, 387-410.

Gittis, A.H., and du Lac, S. (2006). Intrinsic and synaptic plasticity in the vestibular system. Curr Opin Neurobiol *16*, 385-390.

Grassi, S., Frondaroli, A., Dieni, C., Scarduzio, M., and Pettorossi, V.E. (2009). Long-term potentiation in the rat medial vestibular nuclei depends on locally synthesized 17beta-estradiol. J Neurosci *29*, 10779-10783.

Grassi, S., Frondaroli, A., and Pettorossi, V.E. (2002). Different metabotropic glutamate receptors play opposite roles in synaptic plasticity of the rat medial vestibular nuclei. J Physiol *543*, 795-806.

Grassi, S., and Pettorossi, V.E. (2001). Synaptic plasticity in the medial vestibular nuclei: role of glutamate receptors and retrograde messengers in rat brainstem slices. Prog Neurobiol *64*, 527-553.

Grassi, S., Pettorossi, V.E., and Zampolini, M. (1996). Low-frequency stimulation cancels the high-frequency-induced long-lasting effects in the rat medial vestibular nuclei. J Neurosci *16*, 3373-3380.

Hansel, C., Artola, A., and Singer, W. (1997). Relation between dendritic Ca2+ levels and the polarity of synaptic long-term modifications in rat visual cortex neurons. Eur J Neurosci *9*, 2309-2322.

Highstein, S.M., and Holstein, G.R. (2006). The anatomy of the vestibular nuclei. Prog Brain Res *151*, 157-203.

Hirata, Y., and Highstein, S.M. (2001). Acute adaptation of the vestibuloocular reflex: signal processing by floccular and ventral parafloccular Purkinje cells. J Neurophysiol *85*, 2267-2288.

Hullar, T.E., and Minor, L.B. (1999). High-frequency dynamics of regularly discharging canal afferents provide a linear signal for angular vestibuloocular reflexes. J Neurophysiol *82*, 2000-2005.

Ito, M. (1984). The Cerebellum and Neural Control. (New York: Raven).

Ito, M., Highstein, S.M., and Fukuda, J. (1970). Cerebellar inhibition of the vestibulo-ocular reflex in rabbit and cat and its blockage by picrotoxin. Brain Res *17*, 524-526.

Jorntell, H., and Hansel, C. (2006). Synaptic memories upside down: bidirectional plasticity at cerebellar parallel fiber-Purkinje cell synapses. Neuron *52*, 227-238.

Kassardjian, C.D., Tan, Y.F., Chung, J.Y., Heskin, R., Peterson, M.J., and Broussard, D.M. (2005). The site of a motor memory shifts with consolidation. J Neurosci *25*, 7979-7985.

Kato, R., Iwamoto, Y., and Yoshida, K. (2003). Contribution of GABAergic inhibition to the responses of secondary vestibular neurons to head rotation in the rat. Neurosci Res *46*, 499-508.

Kinney, G.A., Peterson, B.W., and Slater, N.T. (1994). The synaptic activation of N-methyl-D-aspartate receptors in the rat medial vestibular nucleus. J Neurophysiol *72*, 1588-1595.

Lasker, D.M., Han, G.C., Park, H.J., and Minor, L.B. (2008). Rotational responses of vestibular-nerve afferents innervating the semicircular canals in the C57BL/6 mouse. J Assoc Res Otolaryngol *9*, 334-348.

Lewis, M.R., Phelan, K.D., Shinnick-Gallagher, P., and Gallagher, J.P. (1989). Primary afferent excitatory transmission recorded intracellularly in vitro from rat medial vestibular neurons. Synapse *3*, 149-153.

Lisberger, S.G. (1984). The latency of pathways containing the site of motor learning in the monkey vestibulo-ocular reflex. Science *225*, 74-76.

Lisberger, S.G., and Pavelko, T.A. (1986). Vestibular signals carried by pathways subserving plasticity of the vestibulo-ocular reflex in monkeys. J Neurosci *6*, 346-354.

Lisberger, S.G., and Pavelko, T.A. (1988). Brain stem neurons in modified pathways for motor learning in the primate vestibulo-ocular reflex. Science *242*, 771-773.

Malinvaud, D., Vassias, I., Reichenberger, I., Rossert, C., and Straka, H. (2010). Functional organization of vestibular commissural connections in frog. J Neurosci *30*, 3310-3325.

Markram, H., and Tsodyks, M. (1996). Redistribution of synaptic efficacy between neocortical pyramidal neurons. Nature *382*, 807-810.

McBain, C.J. (2008). Differential mechanisms of transmission and plasticity at mossy fiber synapses. Prog Brain Res *169*, 225-240.

McBain, C.J., and Dingledine, R. (1993). Heterogeneity of synaptic glutamate receptors on CA3 stratum radiatum interneurones of rat hippocampus. J Physiol *462*, 373-392.

Miles, F.A., and Eighmy, B.B. (1980). Long-term adaptive changes in primate vestibuloocular reflex. I. Behavioral observations. J Neurophysiol *43*, 1406-1425.

Miles, F.A., and Lisberger, S.G. (1981). Plasticity in the vestibulo-ocular reflex: a new hypothesis. Annu Rev Neurosci *4*, 273-299.

Mittmann, W., and Hausser, M. (2007). Linking synaptic plasticity and spike output at excitatory and inhibitory synapses onto cerebellar Purkinje cells. J Neurosci *27*, 5559-5570.

Molineux, M.L., McRory, J.E., McKay, B.E., Hamid, J., Mehaffey, W.H., Rehak, R., Snutch, T.P., Zamponi, G.W., and Turner, R.W. (2006). Specific T-type calcium channel isoforms are associated with distinct burst phenotypes in deep cerebellar nuclear neurons. Proc Natl Acad Sci U S A *103*, 5555-5560.

Nelson, A.B., Krispel, C.M., Sekirnjak, C., and du Lac, S. (2003). Long-lasting increases in intrinsic excitability triggered by inhibition. Neuron *40*, 609-620.

Oliva, A.A., Jr., Jiang, M., Lam, T., Smith, K.L., and Swann, J.W. (2000). Novel hippocampal interneuronal subtypes identified using transgenic mice that express green fluorescent protein in GABAergic interneurons. J Neurosci *20*, 3354-3368.

Pananceau, M., Chen, H., and Gustafsson, B. (1998). Short-term facilitation evoked during brief afferent tetani is not altered by long-term potentiation in the guinea-pig hippocampal CA1 region. J Physiol *508 (Pt 2)*, 503-514.

Person, A.L., and Raman, I.M. (2010). Deactivation of L-type Ca current by inhibition controls LTP at excitatory synapses in the cerebellar nuclei. Neuron *66*, 550-559.

Pugh, J.R., and Raman, I.M. (2006). Potentiation of mossy fiber EPSCs in the cerebellar nuclei by NMDA receptor activation followed by postinhibitory rebound current. Neuron *51*, 113-123.

Pugh, J.R., and Raman, I.M. (2008). Mechanisms of potentiation of mossy fiber EPSCs in the cerebellar nuclei by coincident synaptic excitation and inhibition. J Neurosci *28*, 10549-10560.

Pugh, J.R., and Raman, I.M. (2009). Nothing can be coincidence: synaptic inhibition and plasticity in the cerebellar nuclei. Trends Neurosci *32*, 170-177.

Puyal, J., Grassi, S., Dieni, C., Frondaroli, A., Dememes, D., Raymond, J., and Pettorossi, V.E. (2003). Developmental shift from long-term depression to long-term potentiation in the rat medial vestibular nuclei: role of group I metabotropic glutamate receptors. J Physiol *553*, 427-443.

Ramachandran, R., and Lisberger, S.G. (2008). Neural substrate of modified and unmodified pathways for learning in monkey vestibuloocular reflex. J Neurophysiol *100*, 1868-1878.

Reyes, A.D., and Fetz, E.E. (1993). Effects of transient depolarizing potentials on the firing rate of cat neocortical neurons. J Neurophysiol *69*, 1673-1683.

Scudder, C.A., and Fuchs, A.F. (1992). Physiological and behavioral identification of vestibular nucleus neurons mediating the horizontal vestibuloocular reflex in trained rhesus monkeys. J Neurophysiol *68*, 244-264.

Sekirnjak, C., and du Lac, S. (2002). Intrinsic firing dynamics of vestibular nucleus neurons. J Neurosci *22*, 2083-2095.

Selig, D.K., Nicoll, R.A., and Malenka, R.C. (1999). Hippocampal long-term potentiation preserves the fidelity of postsynaptic responses to presynaptic bursts. J Neurosci *19*, 1236-1246.

Serafin, M., de Waele, C., Khateb, A., Vidal, P.P., and Muhlethaler, M. (1991). Medial vestibular nucleus in the guinea-pig. II. Ionic basis of the intrinsic membrane properties in brainstem slices. Exp Brain Res *84*, 426-433.

Shimazu, H., and Precht, W. (1966). Inhibition of central vestibular neurons from the contralateral labyrinth and its mediating pathway. J Neurophysiol *29*, 467-492.

Shutoh, F., Ohki, M., Kitazawa, H., Itohara, S., and Nagao, S. (2006). Memory trace of motor learning shifts transsynaptically from cerebellar cortex to nuclei for consolidation. Neuroscience *139*, 767-777.

Smith, S.L., and Otis, T.S. (2005). Pattern-dependent, simultaneous plasticity differentially transforms the input-output relationship of a feedforward circuit. Proc Natl Acad Sci U S A *102*, 14901-14906.

Straka, H., Biesdorf, S., and Dieringer, N. (1997). Canal-specific excitation and inhibition of frog second-order vestibular neurons. J Neurophysiol *78*, 1363-1372.

Straka, H., Debler, K., and Dieringer, N. (1996). Size-related properties of vestibular afferent fibers in the frog: differential synaptic activation of N-methyl-D-aspartate and non-N-methyl-D-aspartate receptors. Neuroscience *70*, 697-707.

Straka, H., Vibert, N., Vidal, P.P., Moore, L.E., and Dutia, M.B. (2005). Intrinsic membrane properties of vertebrate vestibular neurons: function, development and plasticity. Prog Neurobiol *76*, 349-392.

Takahashi, Y., Tsumoto, T., and Kubo, T. (1994). N-methyl-D-aspartate receptors contribute to afferent synaptic transmission in the medial vestibular nucleus of young rats. Brain Res *659*, 287-291.

Tzounopoulos, T., Kim, Y., Oertel, D., and Trussell, L.O. (2004). Cell-specific, spike timing-dependent plasticities in the dorsal cochlear nucleus. Nat Neurosci *7*, 719-725.

Uusisaari, M., Obata, K., and Knopfel, T. (2007). Morphological and electrophysiological properties of GABAergic and non-GABAergic cells in the deep cerebellar nuclei. J Neurophysiol *97*, 901-911.

Walter, J.T., and Khodakhah, K. (2006). The linear computational algorithm of cerebellar Purkinje cells. J Neurosci *26*, 12861-12872.

Zhang, W., and Linden, D.J. (2006). Long-term depression at the mossy fiber-deep cerebellar nucleus synapse. J Neurosci *26*, 6935-6944.

Zheng, N., and Raman, I.M. (2009). Ca currents activated by spontaneous firing and synaptic disinhibition in neurons of the cerebellar nuclei. J Neurosci *29*, 9826-9838.

Zucker, R.S., and Regehr, W.G. (2002). Short-term synaptic plasticity. Annu Rev Physiol *64*, 355-405.

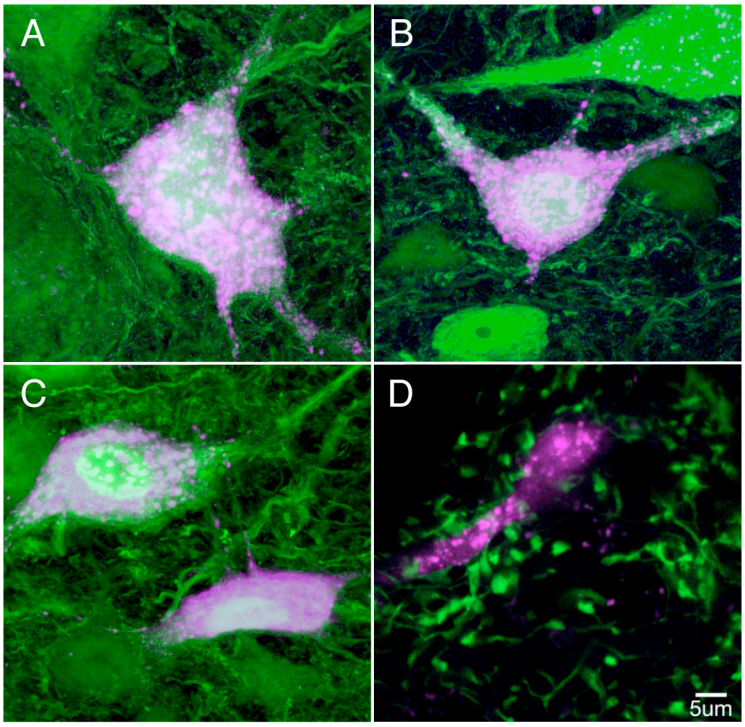

Fig. 4.1 Two transgenic mouse lines define populations of projection and interneurons in the MVN. A-C: Neurons expressing fluorescent protein in the YFP-16 mouse line (green) were retrogradely labeled from stereotaxic dye injections (purple) into the thalamic parafascicular nucleus (A), the medullary reticular formation (B), and the oculomotor nucleus (C). The neurons shown are representative cases; several neurons were double labeled in multiple sections from 2-3 injections in each target structure. In panel D, fluorescent terminals in the GIN mouse line are labeled in green and are in close apposition to the proximal dendrite of a neuron retrogradely labeled from the cerebellar flocculus (purple).

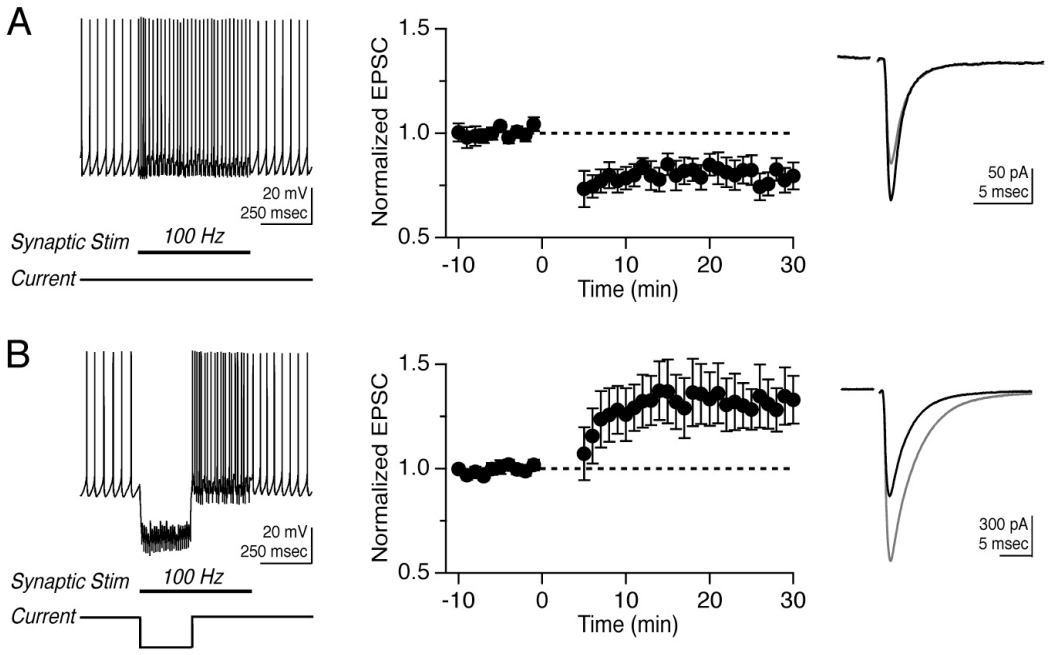

Fig. 4.2 Bidirectional, non-Hebbian plasticity of vestibular nerve synapses onto YFP-16 neurons in the MVN. (A) Representative response to protocol consisting of 100 Hz synaptic stimulation for 550 msec (left). Mean EPSC peak amplitude before and after protocol, which was applied at time= 0 min (middle, n=11). EPSC values are normalized to the mean baseline value in this and related figures. Representative EPSC before (black) and after (grey) LTD induction (right). (B) Representative response to protocol consisting of 100 Hz synaptic stimulation for 550 msec paired with 250 msec hyperpolarization (left). Mean EPSC peak amplitudes before and after protocol (middle, n=21). Representative EPSC before (black) and after (grey) LTP induction. In this and subsequent figures, error bars = SEM.

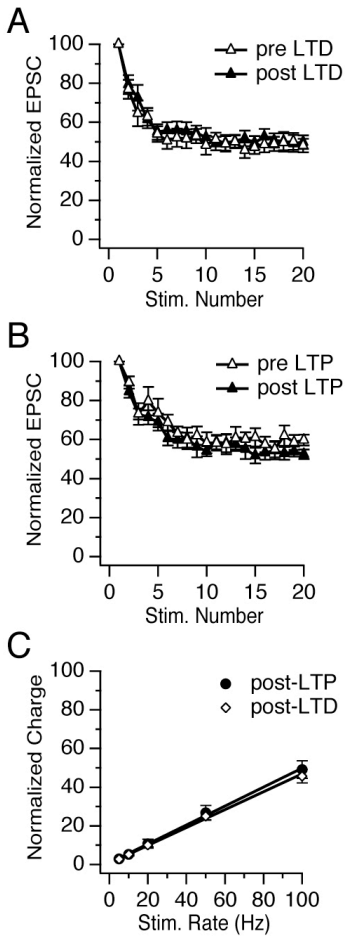

Fig. 4.3 Synaptic plasticity uniformly scales synaptic currents evoked by stimulus trains. (A) EPSCs measured during vestibular nerve stimulation at 10 Hz rapidly reach a steady-state plateau of 49 ± 4% ($EPSC_{11-20}$) of the EPSC amplitude response to a single stimulus ($EPSC_1$) before LTD induction and 50 ± 4% after. (B) Short-term synaptic dynamics also did not change following LTP, in which the steady-state plateau was 59 ± 4% before and 55 ± 3% after induction. (C) Steady-state EPSCs evoked during stimulus trains (5-100 Hz) were measured following LTD and LTP induction to assess short-term dynamics over the physiological range of the synapse. The total synaptic charge transfer per unit time increased linearly with vestibular nerve stimulation rate. Steady-state charge transfer was calculated as the integrated area under the average steady-state EPSC, normalized to the charge transfer of the first EPSC in the train.

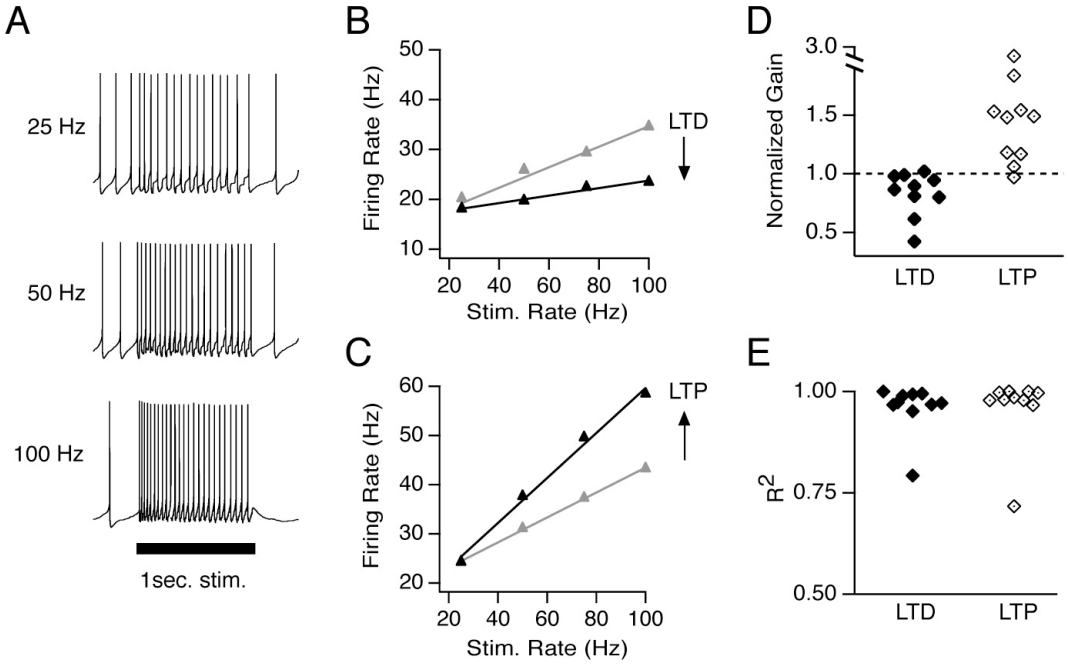

Fig. 4.4 LTD and LTP control the gain of synaptically-evoked postsynaptic firing. (A) Representative responses of a YFP-16 neuron to 1-sec stimulation of the vestibular nerve at 25, 50, and 100 Hz. (B) Example synaptic gain recorded in a YFP-16 neuron before (grey) and after (black) LTD induction, and (C) before (grey) and after (black) LTP induction. Data points in B and C are the average of 5 trials. Error bars are smaller than the symbols. (D) Summary of normalized firing response gains of synaptic transmission following LTD and LTP induction. (E) Summary of goodness of linear fits following LTD and LTP induction.

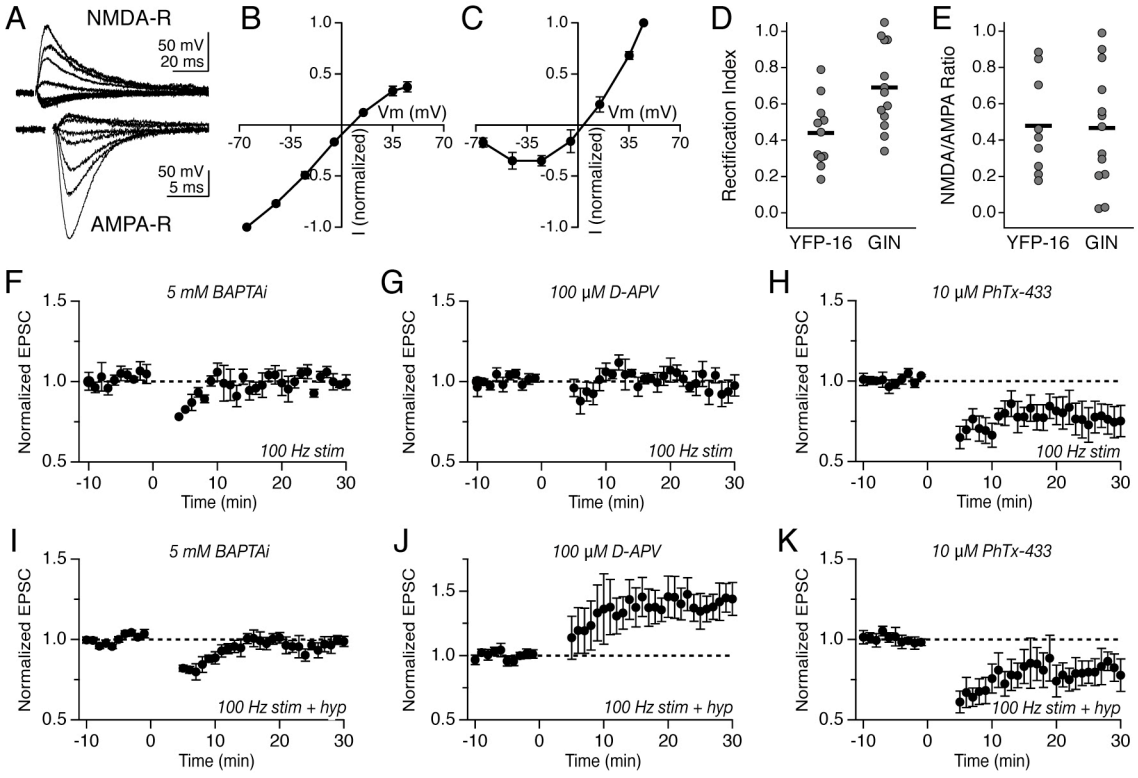

Fig. 4.5 LTD and LTP require postsynaptic calcium and distinct classes of ionotropic glutamate receptors. (A) Evoked vestibular nerve EPSCs measured at membrane potentials from -65 to +45 mV in the presence of 10 µM NBQX (top) or 100 µM D-APV (bottom). (B) Mean current-voltage relation of AMPA-R-mediated EPSCs in YFP-16 neurons, normalized to the amplitude at -65 mV (n=11). (C) Mean current-voltage relation of NMDA-R-mediated EPSCs in YFP-16 neurons, normalized to the amplitude at +45 mV (n=9). (D) Summary of rectification indices (+45/–45 mV) measured in individual YFP-16 and GIN neurons. (E) Summary of NMDA/AMPA ratio (+45/–65 mV) measured in YFP-16 and GIN neurons. (F) Inclusion of 5 mM BAPTA in the recording pipette abolished LTD and (I) LTP. (G) Bath application of 100 µM D-APV blocked LTD but (J) not LTP. (H) Bath application of 10 µM Philanthotoxin-433 did not affect LTD but (K) abolished LTP and unmasked an underlying LTD.

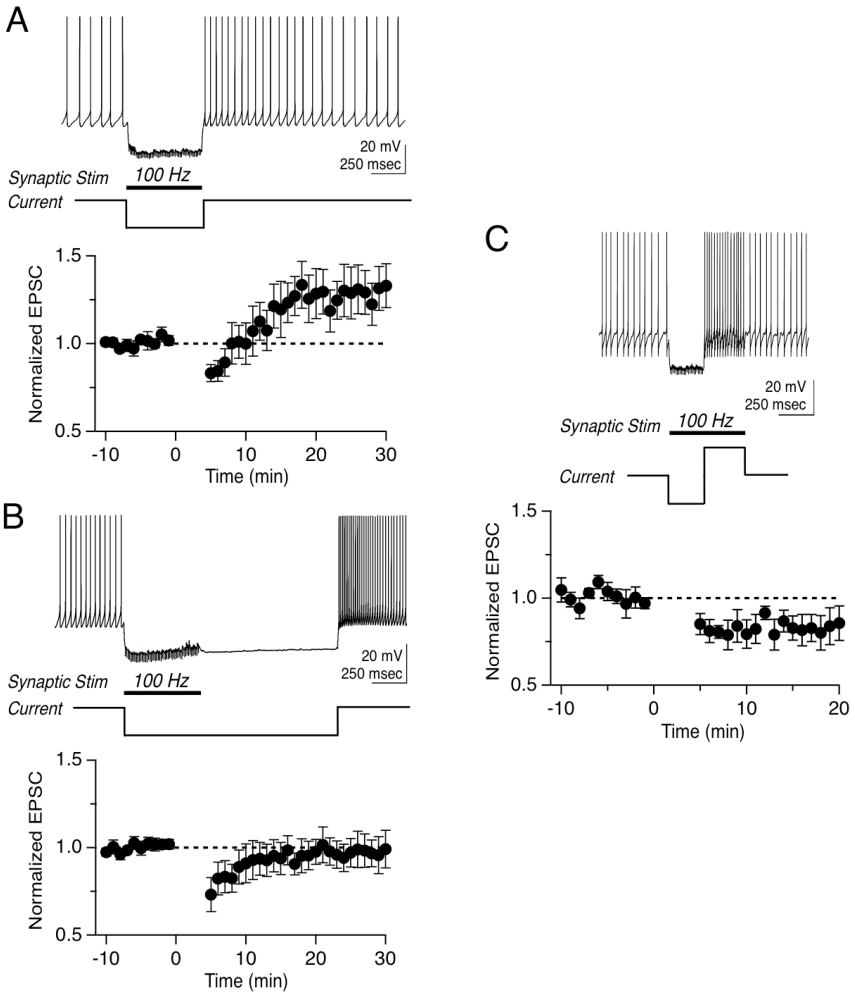

Fig. 4.6 LTP of synapses onto projection neurons depends on the relative timing of synaptic stimulation and hyperpolarization offset. (A) LTP is induced by pairing 550-msec, 100 Hz synaptic stimulation with coincident 550-msec hyperpolarization. (B) Extending the hyperpolarization step to 1550 msec, so that the rebound follows synaptic stimulation by 1 sec, prevented the induction of LTP. (C) In YFP-16 neurons lacking intrinsic post-hyperpolarization rebound firing, a modified 100 Hz stim plus hyperpolarization protocol was applied in which a 300-msec depolarizing current step was injected immediately following the hyperpolarizing step to mimic rebound. This protocol elevated the post-hyperpolarization firing rate by 35.2 ± 6.1 Hz but failed to induce LTP.

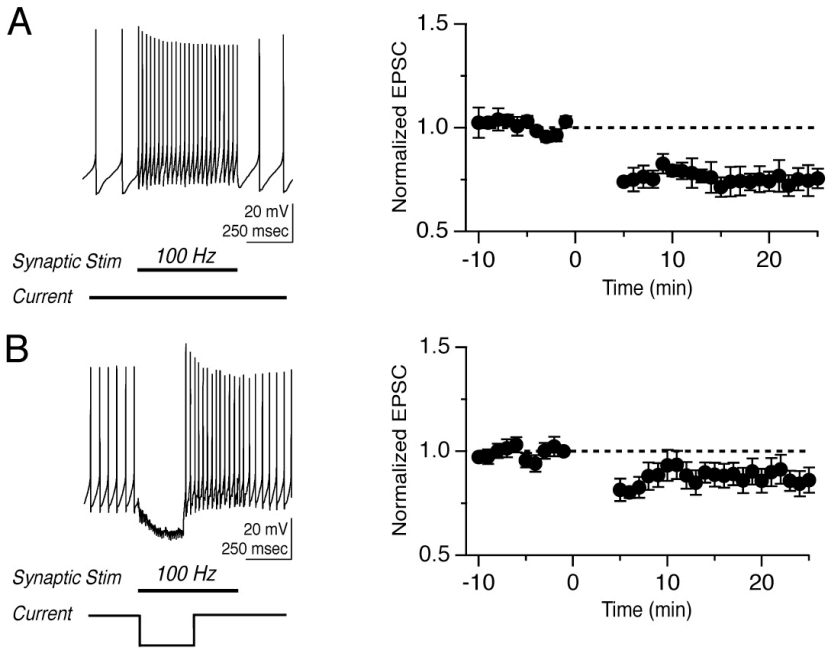

Fig. 4.7 Vestibular nerve synapses onto MVN interneurons exhibit LTD. (A) Representative response evoked by protocol consisting of 100 Hz synaptic stimulation for 550 msec (left). Mean EPSC amplitude before and after protocol (right). (B) Representative response evoked by protocol consisting of 100 Hz synaptic stimulation for 550 msec paired with 250 msec hyperpolarization (left). Mean EPSC amplitude before and after protocol (right).

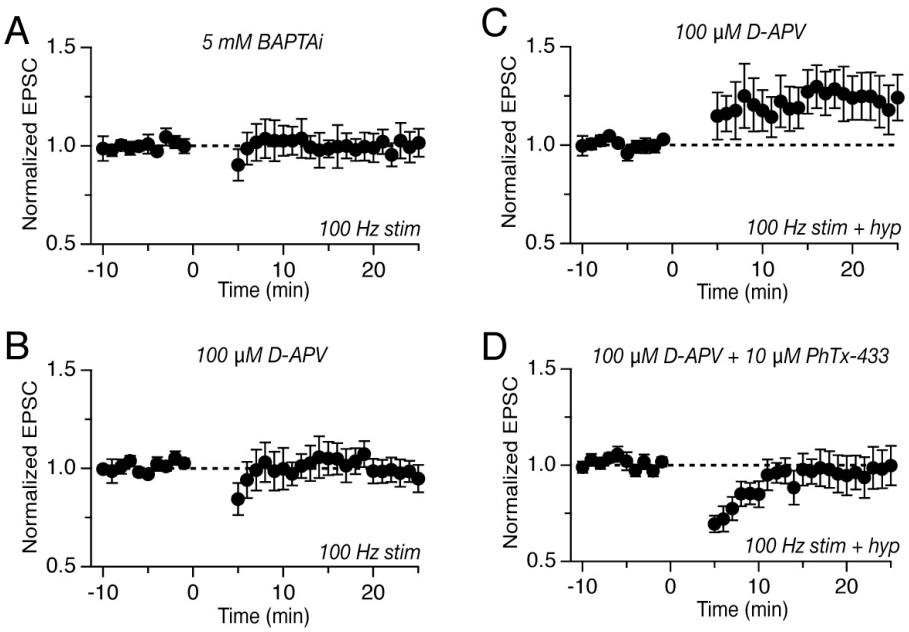

Fig. 4.8 Plasticity in interneurons is dominated by NMDA-R-mediated LTD. (A) Inclusion of 5 mM BAPTA in the recording pipette abolished LTD induced by the 100 Hz stim protocol, as did (B) bath application of 100 µM D-APV. (C) Bath application of 100 µM D-APV during the 100 Hz stim plus hyperpolarization protocol unmasked an underlying LTP. (D) 10 µM Philanthotoxin-433 blocked the unmasked LTP.

Table 4.1 Intrinsic characteristics of YFP-16 MVN neurons before and after synaptic plasticity induction protocols. Values indicate mean ± SEM.

	100 Hz Stim Protocol			**100 Hz Stim plus Hyperpolarization Protocol**		
	Pre	**Post**	***P* value**	**Pre**	**Post**	***P* value**
AP width (ms)	0.67 ± 0.05	0.67 ± 0.04	0.83	0.61 ± 0.03	0.61 ± 0.03	0.99
Threshold (mV)	-51.9 ± 1.3	-53.1 ± 1.2	0.08	-50.6 ± 1.0	-52.0 ± 1.2	0.09
Input res. (MΩ)	71.1 ± 15.6	71.5 ± 15.8	0.93	71.9 ± 12.5	74.2 ± 13.8	0.15
Gain (Hz/nA)	219 ± 32	212 ± 30	0.31	238 ± 24	238 ± 26	0.71

Chapter 5. Conclusions and future directions

The studies presented in this dissertation define several functional, anatomical, and molecular properties that underlie the faithful transmission of head motion signals by the vestibular nerve synapse. The preceding chapters describe key aspects of this synapse: (1) its unique linear filtering capacity, (2) the properties that underlie sustained transmission and regulate linearity across the wide behaviorally-relevant activity range, and (3) the activity patterns, cell-type specificity, and mechanisms that bidirectionally control synaptic strength over long timescales. Taken together, these studies demonstrate that the vestibular nerve synapse is well suited to mediate the excellent performance and plasticity of vestibular reflexes.

Linear transmission at the vestibular nerve synapse

In contrast to all previously studied central synapses, the vestibular nerve synapse operates as a linear filter. The results in Chapter 2 describe the unusual short-term synaptic plasticity that underlies this linearity. Repeated firing of vestibular afferents results in a short-lasting reduction in the amplitude of the synaptic current, which reaches a steady-state level after 10-15 action potentials. The remarkable feature of this short-term depression is that its magnitude does not depend on the firing rate across the entire physiological range (5 – 125 Hz). Thus, the vestibular nerve synapse is predicted to operate in a tonically depressed state *in vivo*, and the amplitude of the postsynaptic currents will be constant irrespective of the presynaptic firing rate. Vestibular nerve synapses contain fast AMPA-Rs and a relatively small NMDA-R contribution, which

prevents temporal summation of synaptic currents. Thus, the charge transfer, the current fluxed per unit time, at vestibular nerve synapses scales linearly with the presynaptic firing rate. This linear charge transfer provides postsynaptic vestibular nucleus neurons with an unambiguous signal about presynaptic firing rate and head velocity.

Both local and projection neurons in the vestibular nucleus transformed vestibular nerve synaptic inputs into linear increases in firing rate. This demonstrates that the intrinsic linearity of vestibular nucleus neurons (du Lac and Lisberger, 1995; Sekirnjak and du Lac, 2002; Straka et al., 2005) extends to their capacity for synaptic integration. Linear integration is likely enabled in part by the brief duration of postsynaptic action potentials, as well as the long, deep afterhyperpolarization that minimizes changes in the interspike membrane potential and, correspondingly, the synaptic driving force. Undoubtedly, the dendritic properties of vestibular nucleus neuron must be well tuned to avoid nonlinear filtering that can occur in other neurons (London and Hausser, 2005).

Linear transmission at the vestibular nerve synapse is extraordinary considering that all previously studied central synapses exhibit rundown during sustained transmission at high rates. To enhance synaptic strength, several synapse in the cerebellum minimize neurotransmitter uptake to allow spillover between individual connections (Carter and Regehr, 2000; DiGregorio et al., 2002; Telgkamp et al., 2004). Spillover promotes high-rate transmission by offsetting rundown, but it sacrifices temporal fidelity, which is essential for vestibular reflexes, which exhibit latencies of < 10 ms (Huterer and Cullen, 2002; Minor et al., 1999).

Another well-studied fast synapse, the Calyx of Held in the auditory brainstem, is optimized for fidelity via the capacity for each presynaptic spike to drive a postsynaptic

spike (Lorteije et al., 2009; von Gersdorff and Borst, 2002). This 1:1 firing relationship is a simple solution for implementing linear transmission because it permits fluctuations in synaptic current amplitude as long as each synaptic response drives an action potential. This solution demands less precision from synaptic machinery, but the fixed 1:1 relationship between action potentials in the pre- and postsynaptic neurons, while linear, does not allow for plasticity and the fine-tuning of synaptic function.

The vestibular system differs from the auditory system in that vestibular nucleus neurons not only integrate sensory signals but also directly drive motor responses. Therefore, the vestibular system likely requires the capacity to modify underlying synapses in order to calibrate sensory-motor transformations. As shown in Chapter 4, vestibular nucleus neurons do indeed express the necessary machinery to alter the strength of vestibular nerve synapses. Rate-independent short-term depression and linear postsynaptic integration mediate high-fidelity and linear synaptic transmission while permitting plasticity over long timescales.

Functional basis of vestibular nerve short-term dynamics

The findings described in Chapter 3 include results from electrophysiology, pharmacology, electron microcopy, and computational modeling studies. Together these results highlight a key strategy used by vestibular nerve synapses to sustain broadband linearity: greatly limiting the probability of neurotransmitter release allows individual release sites to operate at low rates. The unreliable contribution of individual release sites, on account of the low probability of release, is offset by a large number of release sites at each synaptic terminal, which functionally “take turns”. In vestibular nerve

afferent terminals, fast action potentials restrict calcium influx. This limits release probability at the earliest possible opportunity and reduces the challenge of high-rate transmission on downstream synaptic processes. Therefore, the reliable transmission of head motion signals to the central nervous system is not achieved through consistent individual release sites but through the collective function of multiple low-probability release sites.

The initially low release probability at the vestibular nerve synapse further decreases in response to repeated activity and causes short-term depression. While vestibular nerve afferents fire over the range 5 -125 Hz, we predict that individual release sites predominantly operate at 0.6 – 15 Hz in the steady-state and *in vivo*. Given that one of the greatest challenges for sustained transmission is vesicle availability, this reduced operating range advantageously minimizes the extreme temporal demands on the machinery responsible for the clearing release sites and the translocation, docking, and priming of new vesicles. Vesicle dynamics at the vestibular nerve synapse were estimated to be among the fastest in the central nervous system, which is necessary to ensure constant vesicle availability. Vesicle dynamics at cerebellar mossy fiber synapses are known to be similar to those at vestibular nerve synapses, however the relatively high release probability at the mossy fiber synapse leads to vesicle depletion at high rates (Saviane and Silver, 2006), which also occured at the vestibular nerve synapse when release probability was artificially raised.

We built a model of vestibular nerve synaptic transmission, which incorporated our experimental results. This model showed that the concerted function of several molecular and anatomical properties determine the range over which synaptic

transmission does not depend on prior activity. The model demonstrated that the probability of release and vesicle kinetics are the primary determinants of upper limit of the range of rate-independence. The lower limit is determined by the kinetics of recovery from depression. Recovery from short-term depression at the vestibular nerve synapse is unusual in that it occurs very slowly following ~500 ms of no recovery. Thus, at firing rates as low as 5 Hz, the recovery process does not interfere with the steady-state depression. In addition to these presynaptic properties, efficient glutamate uptake and desensitization-resistant AMPA-Rs were both critical for translating linear glutamate release into constant-amplitude postsynaptic currents. These results suggest that each aspect of the vestibular nerve synapse is refined to meet the computational and behavioral goal of the synapse.

Many properties have been demonstrated to influence short-term plasticity at other synapses, including release probability, vesicle depletion, calcium accumulation, synapse anatomy, and postsynaptic receptor sensitivity (Fioravante and Regehr, 2011; Jones and Westbrook, 1996; Xu-Friedman and Regehr, 2004; Zucker and Regehr, 2002). The functional interpretations of studies on short-term plasticity are generally limited, because the behavioral function of firing in pre- and postsynaptic neurons is often unknown. The clear relationship between the vestibular nerve synapse and behavior allows the functional and computational purpose of individual synaptic refinements to be assessed. Rather than a single refinement of the vestibular nerve synapse dominating its synaptic computation, this study demonstrates that the coordination of several synaptic properties underlies linear transmission across the behaviorally relevant range. It is possible that the ethological importance of stability and clear vision during animal motion

have refined the vestibular nerve synapse to a greater degree than other synapses. It is more likely that all synapses are similarly refined, but we do not yet have an adequate framework for interpreting the importance of "details" at other synapses.

The dependence of linearity on the coordination of several synaptic properties raises the question of how evolution optimized the vestibular nerve synapse. While this synapse is distinctive in its linear transmission, its genetic basis might be quite similar to other fast central synapses. For example, if the cerebellar mossy fiber synapse had a lower release probability and better glutamate uptake, it might be able to function linearly. Thus, the linearity of the vestibular nerve synapse might only require a few refinements beyond what is exhibited by other brainstem and cerebellar synapses. An advantage to the cellular strategy for linearity at the vestibular nerve synapse is its potential adaptability. Firing rates in the vestibular system vary across species, and the rates in primates are approximately double those in rodents (Goldberg and Fernandez, 1971; Yang and Hullar, 2007). To extend linear synaptic transmission to the broader primate range, it may be sufficient to tweak synaptic function by simply docking more vesicles.

In addition to the aspects of the vestibular nerve synapse described in this dissertation, many additional properties are certainly specialized for linearity. Of particular interest for future studies is the identification of the calcium sensor, given the extraordinary linear relationship between extracellular calcium concentration and neurotransmitter release. Molecular analyses of vestibular afferents are currently limited because their cell bodies are encased in bone, and there is no genetic marker of vestibular afferents. We are currently pursing a candidate transgenic mouse, in which the vestibular

afferents are likely to be fluorescently labeled. This mouse could facilitate the efficient identification of the molecular components of the synapse by permitting immunostaining of nerve terminals. Given the large size of the vestibular nerve boutons, direct patch clamp recordings of the boutons could also be pursued. The extensive myelination of the vestibular nuclei poses a challenge for the visualization of boutons, which the fluorescent labeling of the afferents would facilitate. Dual recordings from somatic terminals and postsynaptic targets would be a very powerful approach for further elucidating the processes underlying the rate-invariant release of neurotransmitter.

An additional, interesting aspect of linearity at the vestibular nerve synapse is its development. Results in Chapter 3 demonstrate the dependence of linearity on fast repolarizing potassium currents that minimize presynaptic calcium influx during the action potential. Because these potassium currents are not expressed early in development, we predicted the immature nerve synapse to exhibit rate-dependent transmitter release. In a study not included in this dissertation, we tested this hypothesis and confirmed that release is rate-dependent through the middle of the third postnatal week. To our surprise, however, the relationship between pre- and postsynaptic firing is still quite linear (R^2= 0.94, n=9). As has been reported at many other synapses, AMPA-R kinetics were significantly slower during development; EPSC fall times decrease from 4.9 ± 0.7 ms to 3.0 ± 0.3 ms during the third postnatal week. Remarkably, this rate-dependent temporal summation of slow AMPA-R currents perfectly offsets the rundown of release at high rates during development. Thus, linear transmission is implemented via a different set of requirements in immature synapses. These findings further illuminate the extent to which the vestibular nerve synapse is tuned to ensure linearity.

Long-term plasticity of synaptic gain

The results in Chapter 4 of this dissertation demonstrate that the vestibular nerve synapse is capable of long-term, activity-dependent plasticity and that the direction of the plasticity is biased by postsynaptic membrane potential. Vestibular nerve LTD and LTP are induced by non-Hebbian plasticity rules: paired pre- and postsynaptic activity induces NMDA-R-dependent LTD, whereas paired presynaptic activity with postsynaptic hyperpolarization induces calcium-permeable AMPA-R-dependent LTP. Synapses onto projection neurons exhibit both LTD and LTP, whereas synapses onto interneurons exhibit only LTD under normal conditions.

The induction of vestibular nerve synaptic plasticity is unusual in its bidirectional dependence on membrane potential. Given the high baseline firing rates in the vestibular system and the central role of GABAergic Purkinje cells in reflex calibration, it is unsurprising that plasticity mechanisms in the vestibular system differ from those in quiescent circuits. Non-Hebbian plasticity mechanisms are particularly common in fast-firing neurons and have been identified at many synapses in the cerebellum and in cerebellum-like circuits (Bender and Trussell, 2011; Jorntell and Hansel, 2006; Pugh and Raman, 2009). The differential dependence of LTD and LTP on AMPA and NMDA receptors suggests that the dynamic balance and timing of excitatory and inhibitory inputs to vestibular nucleus neurons can control the strength of vestibular nerve synapses.

The role of post-hyperpolarization rebound currents in LTP induction is distinctive. Rebound firing *in vivo* is likely to occur following disinhibition of the vestibular nucleus neurons targeted by Purkinje cells. Pronounced disinhibition could be caused by reduced synchrony among converging Purkinje cells or by a complex spike-

induced pause in Purkinje cell simple spikes, which have both been proposed as relevant motor learning signals (De Zeeuw et al., 2011; Medina and Mauk, 1999; Steuber et al., 2009; Wetmore et al., 2008).

The lack of LTP in the ~29% of YFP-16 neurons that did not express rebound firing suggests these neurons are fundamentally different from the YFP-16 neurons capable of rebound firing. Is there an anatomical basis? Adaptation of the VOR alters the firing responses of the subset of vestibular nucleus neurons that directly receive Purkinje cell inhibition (Lisberger et al., 1994; Partsalis et al., 1995). While <1% of the neurons in the medial vestibular nucleus have been reported to be extensively targeted by Purkinje cells (Sekirnjak et al., 2003), recent evidence demonstrates that Purkinje cells inhibit ~85% of YFP-16 neurons (Shin et al., in press). This dense innervation of YFP-16 neurons contrasts with the finding that Purkinje cells target only ~16% of GIN neurons, which also lack LTP under normal conditions. Considering these recent anatomical findings, it is possible that vestibular nerve synapses specifically onto Purkinje-cell-target neurons undergo bidirectional plasticity. A recently developed mouse, in which Purkinje cells express the fast variant of channelrhodopsin, will facilitate experiments to determine whether those neurons targeted by Purkinje cells express LTP and whether/how Purkine cell activity induces LTP.

What are the consequences of vestibular nerve synaptic plasticity on circuit function? Because vestibular nerve afferents fire tonically *in vivo,* we extended our analyses from synaptic currents evoked by single stimuli to responses evoked by stimulus trains. Our results demonstrate that the induction of LTD and LTP resulted in the uniform scaling of synaptic efficacy throughout stimulus trains, and the amplitude of steady-state

synaptic currents did not depend on stimulus rate. This finding is most consistent with the interpretation that postsynaptic AMPA-R removal and insertion underlie LTD and LTP. Most studies of long-term synaptic plasticity do not examine the effects of LTD or LTP on short-term synaptic plasticity. However, the role of short-term plasticity in shaping synaptic computations suggests such experiments would be generally informative (Abbott and Regehr, 2004). In the case of the vestibular nerve synapse, the analysis of long-term and short-term plasticity together was essential for identifying the effects of long-term plasticity within the behaviorally relevant activity range.

For long-term synaptic plasticity to influence behavior, it must ultimately alter firing in postsynaptic neurons. Synaptic strength is known to influence evoked postsynaptic firing (Bliss and Lomo, 1973; Fetz and Gustafsson, 1983; Mittmann and Hausser, 2007; Reyes and Fetz, 1993; Smith and Otis, 2005; Walter and Khodakhah, 2006), but it is unknown how bidirectional long-term synaptic plasticity impacts postsynaptic firing under physiological conditions. The results in Chapter 3 indicate that vestibular nerve synapse LTD and LTP result in linear scaling of postsynaptic firing responses. The transformation of synaptic inputs into postsynaptic action potentials depends on many differentially expressed conductances, and the consequences of LTD and LTP on postsynaptic firing likely differ greatly across different synapse and cell types. Vestibular nucleus neurons differ from pyramidal cells in the hippocampus and cortex in the wide range of firing rates over which spike generation is linear (Sekirnjak and du Lac, 2002; Serafin et al., 1991). Whether synaptic plasticity scales postsynaptic firing responses in other neurons that exhibit linear spike generation, such as

hippocampal, cortical, and basal ganglia interneurons, as well as other brainstem and cerebellar neurons, remains to be examined.

LTD and LTP of vestibular nerve synapses are well suited to underlie the consolidation of VOR adaptation given their sensitivity to postsynaptic membrane potential and linear effects on postsynaptic firing rates. Several types of plasticity likely influence motor learning in the vestibular system (Boyden et al., 2006; Boyden and Raymond, 2003; De Zeeuw et al., 2011; Miles and Eighmy, 1980). Vestibular nucleus neurons express activity-dependent plasticity of intrinsic excitability, which also has been proposed to play a role in VOR adaptation (Nelson et al., 2005; Nelson et al., 2003). One advantage to plasticity at the vestibular nerve synapse is the specificity of its effects on head motion signal processing. While the vestibular nerve is the dominant input to vestibular nuclei, vestibular nucleus neurons integrate inputs from other modalities, including visual and proprioceptive signals (Angelaki and Cullen, 2008). Intrinsic excitability would increase the responsiveness of vestibular nucleus neurons to all excitatory inputs. Therefore, intrinsic plasticity might be an optimal response to the loss of inner ear function, a type of sensory deprivation in the vestibular system. In this scenario, the loss of excitatory vestibular nerve excitation would be predicted to decrease the postsynaptic firing rate and, correspondingly, calcium concentration, which is the known trigger of intrinsic excitability plasticity (Nelson et al., 2005). Intrinsic plasticity could provide a global activity boost to restore function to the deafferented network. Plasticity at the vestibular nerve synapse provides complementary mechanisms that specifically modify the strength of head motion signals without altering the speed or linearity of the circuit.

Determining whether VOR adaptation requires vestibular nerve LTD or LTP is an exciting future direction. Because these mechanisms rely on distinct types of glutamate receptors, altering the function of NMDA-R and calcium-permeable AMPA-R would be informative. NMDA-Rs contribute minimally to the evoked firing responses of vestibular nucleus neurons. Thus, perfusing the vestibular nuclei with the NMDA-R antagonist D-APV during learning is predicted to block LTD without altering VOR performance. Additional experiments would be needed, however, to identify whether a behavioral effect depended on LTD of synapses onto projection neurons or interneurons. Pharmacologically blockade of calcium-permeable AMPA-Rs *in vivo* would impair VOR performance and thus complicate all training paradigms, because calcium-permeable AMPA-Rs contribute significantly to evoked firing in vestibular nucleus neurons. An alternative approach to testing the role of LTP could be the overexpression of mRNA for the GluR2 subunit. If this subunit were appropriately incorporated into receptors that were delivered to synapses, the AMPA-R calcium influx could be minimized without drastically reducing synapse strength and baseline VOR performance. If the downstream mechanisms of LTD or LTP were known, additional, more specific manipulations could be considered.

Taken together, the studies contained in this dissertation define many of the essential properties and mechanisms that control synaptic transmission at the gateway to the vestibular system. The simple computational and behavioral goals of the vestibular nerve synapse allow synaptic mechanisms to be addressed within a functional context. Together with the exceptional intrinsic properties of vestibular nucleus neurons (du Lac and Lisberger, 1995; Gittis and du Lac, 2007, 2008; Sekirnjak and du Lac, 2002), the

vestibular nerve synapse beautifully demonstrates the tuning of cellular and molecular diversity to the demands of animal behavior.

References

Abbott, L.F., and Regehr, W.G. (2004). Synaptic computation. Nature *431*, 796-803.

Angelaki, D.E., and Cullen, K.E. (2008). Vestibular system: the many facets of a multimodal sense. Annu Rev Neurosci *31*, 125-150.

Bender, K.J., and Trussell, L.O. (2011). Synaptic plasticity in inhibitory neurons of the auditory brainstem. Neuropharmacology *60*, 774-779.

Boyden, E.S., Katoh, A., Pyle, J.L., Chatila, T.A., Tsien, R.W., and Raymond, J.L. (2006). Selective engagement of plasticity mechanisms for motor memory storage. Neuron *51*, 823-834.

Boyden, E.S., and Raymond, J.L. (2003). Active reversal of motor memories reveals rules governing memory encoding. Neuron *39*, 1031-1042.

Carter, A.G., and Regehr, W.G. (2000). Prolonged synaptic currents and glutamate spillover at the parallel fiber to stellate cell synapse. J Neurosci *20*, 4423-4434.

De Zeeuw, C.I., Hoebeek, F.E., Bosman, L.W., Schonewille, M., Witter, L., and Koekkoek, S.K. (2011). Spatiotemporal firing patterns in the cerebellum. Nat Rev Neurosci *12*, 327-344.

DiGregorio, D.A., Nusser, Z., and Silver, R.A. (2002). Spillover of glutamate onto synaptic AMPA receptors enhances fast transmission at a cerebellar synapse. Neuron *35*, 521-533.

du Lac, S., and Lisberger, S.G. (1995). Membrane and firing properties of avian medial vestibular nucleus neurons in vitro. J Comp Physiol A *176*, 641-651.

Fioravante, D., and Regehr, W.G. (2011). Short-term forms of presynaptic plasticity. Curr Opin Neurobiol.

Gittis, A.H., and du Lac, S. (2007). Firing properties of GABAergic versus non-GABAergic vestibular nucleus neurons conferred by a differential balance of potassium currents. J Neurophysiol *97*, 3986-3996.

Gittis, A.H., and du Lac, S. (2008). Similar properties of transient, persistent, and resurgent Na currents in GABAergic and non-GABAergic vestibular nucleus neurons. J Neurophysiol *99*, 2060-2065.

Goldberg, J.M., and Fernandez, C. (1971). Physiology of peripheral neurons innervating semicircular canals of the squirrel monkey. I. Resting discharge and response to constant angular accelerations. J Neurophysiol *34*, 635-660.

Huterer, M., and Cullen, K.E. (2002). Vestibuloocular reflex dynamics during high-frequency and high-acceleration rotations of the head on body in rhesus monkey. J Neurophysiol *88*, 13-28.

Jones, M.V., and Westbrook, G.L. (1996). The impact of receptor desensitization on fast synaptic transmission. Trends Neurosci *19*, 96-101.

Jorntell, H., and Hansel, C. (2006). Synaptic memories upside down: bidirectional plasticity at cerebellar parallel fiber-Purkinje cell synapses. Neuron *52*, 227-238.

Lisberger, S.G., Pavelko, T.A., and Broussard, D.M. (1994). Neural basis for motor learning in the vestibuloocular reflex of primates. I. Changes in the responses of brain stem neurons. J Neurophysiol *72*, 928-953.

London, M., and Hausser, M. (2005). Dendritic computation. Annu Rev Neurosci *28*, 503-532.

Lorteije, J.A., Rusu, S.I., Kushmerick, C., and Borst, J.G. (2009). Reliability and precision of the mouse calyx of Held synapse. J Neurosci *29*, 13770-13784.

Medina, J.F., and Mauk, M.D. (1999). Simulations of cerebellar motor learning: computational analysis of plasticity at the mossy fiber to deep nucleus synapse. J Neurosci *19*, 7140-7151.

Miles, F.A., and Eighmy, B.B. (1980). Long-term adaptive changes in primate vestibuloocular reflex. I. Behavioral observations. J Neurophysiol *43*, 1406-1425.

Minor, L.B., Lasker, D.M., Backous, D.D., and Hullar, T.E. (1999). Horizontal vestibuloocular reflex evoked by high-acceleration rotations in the squirrel monkey. I. Normal responses. J Neurophysiol *82*, 1254-1270.

Nelson, A.B., Gittis, A.H., and du Lac, S. (2005). Decreases in CaMKII activity trigger persistent potentiation of intrinsic excitability in spontaneously firing vestibular nucleus neurons. Neuron *46*, 623-631.

Nelson, A.B., Krispel, C.M., Sekirnjak, C., and du Lac, S. (2003). Long-lasting increases in intrinsic excitability triggered by inhibition. Neuron *40*, 609-620.

Partsalis, A.M., Zhang, Y., and Highstein, S.M. (1995). Dorsal Y group in the squirrel monkey. I. Neuronal responses during rapid and long-term modifications of the vertical VOR. J Neurophysiol *73*, 615-631.

Pugh, J.R., and Raman, I.M. (2009). Nothing can be coincidence: synaptic inhibition and plasticity in the cerebellar nuclei. Trends Neurosci *32*, 170-177.

Saviane, C., and Silver, R.A. (2006). Fast vesicle reloading and a large pool sustain high bandwidth transmission at a central synapse. Nature *439*, 983-987.

Sekirnjak, C., and du Lac, S. (2002). Intrinsic firing dynamics of vestibular nucleus neurons. J Neurosci *22*, 2083-2095.

Sekirnjak, C., Vissel, B., Bollinger, J., Faulstich, M., and du Lac, S. (2003). Purkinje cell synapses target physiologically unique brainstem neurons. J Neurosci *23*, 6392-6398.

Steuber, V., Schultheiss, N.W., Silver, R.A., De Schutter, E., and Jaeger, D. (2009). Determinants of synaptic integration and heterogeneity in rebound firing explored with data-driven models of deep cerebellar nucleus cells. J Comput Neurosci.

Straka, H., Vibert, N., Vidal, P.P., Moore, L.E., and Dutia, M.B. (2005). Intrinsic membrane properties of vertebrate vestibular neurons: function, development and plasticity. Prog Neurobiol *76*, 349-392.

Telgkamp, P., Padgett, D.E., Ledoux, V.A., Woolley, C.S., and Raman, I.M. (2004). Maintenance of high-frequency transmission at purkinje to cerebellar nuclear synapses by spillover from boutons with multiple release sites. Neuron *41*, 113-126.

von Gersdorff, H., and Borst, J.G. (2002). Short-term plasticity at the calyx of held. Nat Rev Neurosci *3*, 53-64.

Wetmore, D.Z., Mukamel, E.A., and Schnitzer, M.J. (2008). Lock-and-key mechanisms of cerebellar memory recall based on rebound currents. J Neurophysiol *100*, 2328-2347.

Xu-Friedman, M.A., and Regehr, W.G. (2004). Structural contributions to short-term synaptic plasticity. Physiol Rev *84*, 69-85.

Yang, A., and Hullar, T.E. (2007). Relationship of semicircular canal size to vestibular-nerve afferent sensitivity in mammals. J Neurophysiol *98*, 3197-3205.

Zucker, R.S., and Regehr, W.G. (2002). Short-term synaptic plasticity. Annu Rev Physiol *64*, 355-405.